

University of Verona

DEPARTMENT OF COMPUTER SCIENCE
Master Degree in Computer Science and Engineering

**Model-based design of
at-the-edge heterogeneous Robotics Applications
based on ROS**

Candidate:
Simone Girardi

Thesis advisor:
Prof. Nicola Bombieri
Research supervisor:
Prof. Franco Fummi

Abstract

Developing distributed robotics applications on embedded devices, we have to deal with the diversity of the applications and the different platforms where these applications run. At the state of the art there are some solutions that allow us to develop robotics applications and deploy them on embedded boards. The problem is that none of these solutions allows us to be sufficiently accurate to guarantee the functioning of the entire system, especially if we want to increase its complexity. To solve the problem we must take account of the necessary resources to run the applications and the constraints imposed by the limits of the devices.

Contents

Abstract	i
1 Introduction	1
1.1 Thesis outline	1
2 Deep Learning	3
2.1 Background	3
2.2 Measurement	5
2.3 Frameworks	5
2.4 Challenges	5
2.5 Discussion	5
3 Edge Computing	7
3.1 System description	7
3.2 Stability	8
3.3 Passivity	10
3.4 Teleoperation without delay	12
3.4.1 The Four Channel Architecture	12
3.5 Teleoperation with constant delay	13
3.5.1 PD and passivity terms	14
3.6 Teleoperation with time varying delay	16
3.6.1 PSPM	16
3.6.2 The Two Layer Algorithm	18
3.7 Discussion	22

4 Robotics Applications	23
4.1 A model for the teleoperation system	23
4.1.1 The port-Hamiltonian description	23
4.1.2 Port-Hamiltonian system with energy tank	24
4.1.3 A port-Hamiltonian formulation for the tank-based tele-operation system	26
4.2 Improvements on the Two-Layer	29
4.2.1 Energy evaluation in task space	29
4.2.2 Energy scaling	32
4.3 Implemented teleoperation schemes	34
4.3.1 Position - Position (P-P)	35
4.3.2 Position - Force (P-F)	37
4.4 Discussion	40
5 Robotics Platforms	41
5.1 Manipulators	41
5.1.1 Phantom Omni	41
5.1.2 WAM	42
5.1.3 ATI Nano 17	43
5.2 Software Architecture	45
5.2.1 ROS	47
5.2.2 Frame Mapper	48
5.2.3 WAM control	48
5.2.4 Phantom Omni control	49
5.2.5 Network Simulator	50
5.2.6 Neft node	50
5.2.7 Virtual visualizer	50
5.2.8 Setup limitations	51
6 Case Study	53
6.1 Position-Position	55
6.1.1 Without Delay	56
6.1.2 Constant Delay	69
6.2 Position-Force	81

CONTENTS

v

6.2.1	Without Delay	82
6.2.2	Constant Delay	94
6.3	Discussion	106
Conclusions		109
Bibliography		111

List of Figures

2.1 DNN example	4
3.1 Block representation of the bilateral teleoperation	8
3.2 The Four Channel Architecture	13
3.3 Lee-Spong PD dissipative approach	14
3.4 PSPM teleoperation schema	17
3.5 TwoLayer teleoperation schema	19
4.1 The implemented P-P architecture	35
4.2 The implemented P-F architecture	38
5.1 The WAM and Phantom Omni	43
5.2 The needle holder assembly	44
5.3 The cryoablation needle holder	44
5.4 Architecture overview	46
5.5 ROS nodes and topics	47
5.6 The visualizer	51
6.1 Position tracking in free motion. P-P architecture without delay.	57
6.2 Orientation tracking in free motion. P-P control architecture without delay.	58
6.3 Force tracking in free motion. P-P control architecture without delay.	59
6.4 Position tracking with 90° insertion approach. P-P control architecture without delay.	61
6.5 Orientation tracking with 90° insertion approach. P-P control architecture without delay.	62

6.6	Force tracking with 90° insertion approach. P-P control architecture without delay.	63
6.7	Position tracking with 45° insertion approach. P-P control architecture without delay.	66
6.8	Orientation tracking with 45° insertion approach. P-P control architecture without delay.	67
6.9	Force tracking with 45° insertion approach. P-P control architecture without delay.	68
6.10	Position tracking in free motion. P-P control architecture with 0.2s RTT delay.	70
6.11	Orientation tracking in free motion. P-P control architecture with 0.2s RTT delay.	71
6.12	Force tracking in free motion. P-P control architecture with 0.2s RTT delay.	72
6.13	Position tracking with 90° insertion approach. P-P control architecture with 0.2s RTT delay.	74
6.14	Orientation tracking with 90° insertion approach. P-P control architecture with 0.2s RTT delay.	75
6.15	Force tracking with 90° insertion approach. P-P control architecture with 0.2s RTT delay.	76
6.16	Position tracking with 45° insertion approach. P-P control architecture with 0.2s RTT delay.	78
6.17	Orientation tracking with 45° insertion approach. P-P control architecture with 0.2s RTT delay.	79
6.18	Force tracking with 45° insertion approach. P-P control architecture with 0.2s RTT delay.	80
6.19	Position tracking in free motion. P-F control architecture without delay.	83
6.20	Orientation tracking in free motion. P-F control architecture without delay.	84
6.21	Orientation tracking in free motion. P-F control architecture without delay.	85
6.22	Position tracking with 90° insertion approach. P-F control architecture without delay.	87

6.23 Orientation tracking with 90° insertion approach. P-F control architecture without delay.	88
6.24 Force tracking with 90° insertion approach. P-F control architecture without delay.	89
6.25 Position tracking with 45° insertion approach. P-F control architecture without delay.	91
6.26 Orientation tracking with 45° insertion approach. P-F control architecture without delay.	92
6.27 Force tracking with 45° insertion approach. P-F control architecture without delay.	93
6.28 Position tracking in free motion. P-F control architecture with 0.2s RTT delay.	95
6.29 Orientation tracking in free motion. P-F control architecture with 0.2s RTT delay.	96
6.30 Force tracking in free motion. P-F control architecture with 0.2s RTT delay.	97
6.31 Position tracking with 90° insertion approach. P-F control architecture with 0.2s RTT delay.	99
6.32 Orientation tracking with 90° insertion approach. P-F control architecture with 0.2s RTT delay.	100
6.33 Force tracking with 90° insertion approach. P-F control architecture with 0.2s RTT delay.	101
6.34 Position tracking with 45° insertion approach. P-F control architecture with 0.2s RTT delay.	103
6.35 Orientation tracking with 45° insertion approach. P-F control architecture with 0.2s RTT delay.	104
6.36 Force tracking with 45° insertion approach. P-F control architecture with 0.2s RTT delay.	105

List of Tables

5.1	WAM D-H parameters	44
5.2	ATI Nano 17 calibration	45
5.3	The custom ROS message structure	46
6.1	Tresholds	54
6.2	P-P parameters	55
6.3	P-F parameters	81

Chapter 1

Introduction

1.1 Thesis outline

This thesis is organised as follows: Chapter 2 is an overview over the research contribution in the field of percutaneous procedures, focusing on modelling the action and presenting some robotic system designed for them. In Chapter 3 the key concepts of a teleoperation system and some of the teleoperation schemas developed in the recent years are presented. In Chapter 4 is presented the port-Hamiltonian representation of the investigated teleoperation algorithm and proved its passivity and the passivity of the two improvements proposed. In Chapter 5 is discussed the implementation of this architecture on a physical setup, lastly in Chapter 6 the experimental results are showed and discussed.

Chapter 2

Deep Learning

Deep learning has recently been highly successful in machine learning across a variety of application domains, including computer vision, natural language processing, and big data analysis, among others. For example, deep learning methods have consistently outperformed traditional methods for object recognition and detection in the ISLVRC Computer Vision Competition since 2012 [12]. However, deep learning’s high accuracy comes at the expense of high computational and memory requirements for both the training and inference phases of deep learning. Training a deep learning model is space and computationally expensive due to millions of parameters that need to be iteratively refined over multiple time epochs. Inference is computationally expensive due to the potentially high dimensionality of the input data (e.g., a high-resolution image) and millions of computations that need to be performed on the input data.

2.1 Background

As described in [6], the modern term “deep learning” goes beyond the neuroscientific perspective engineering applications on the current breed of machine learning models. It appeals to a more general principle of learning *multiple levels of composition*, which can be applied in machine learning frameworks that are not necessarily neurally inspired. A deep learning prediction algorithm, consists of a number of layers, as shown in Fig. 2.1.

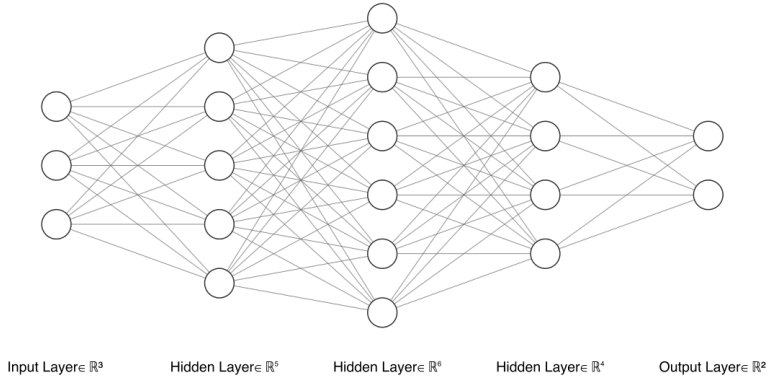


Figure 2.1: DNN example with image classification

In deep learning *inference*, the input data pass through the node's layers in sequence, and each layer performs matrix multiplications on the data. The output of a layer is usually the input to the subsequent layer. After data are processed by the final (fully connected) layer, the output is either a feature or a classification value. When the model contains many layers in sequence, the neural network is known as a deep neural network (DNN). When the matrix multiplications include convolutional filter operations, the model is named convolutional neural networks (CNNs), which is common for image and video processing contexts. There are also DNNs designed especially for time series prediction; these are called recurrent neural networks (RNNs), which have loops in their layer connections to keep state and enable predictions on sequential inputs.

In deep learning *training*, the computation proceeds in reverse order. Given the ground-truth training labels, multiple passes are made over the layers to optimize the parameters of each layer of matrix multiplications, starting from the final layer and ending with the first layer. The algorithm used is typically stochastic gradient descent (SGD). In each pass, a randomly small subset of N input data ("mini-batch") from the training data set, is

selected and used to update the gradients in the direction that minimizes the training loss (where the training loss is defined as the difference between the predictions and the ground truth). One pass through the entire training data set is called a training epoch [11].

There are some considerations to take into account: the first is that there are a large number of parameters in the matrix multiplications, resulting in many computations being performed and thus the latency issues that we see on end devices. The second is that there are many choices (hyper-parameters) on how to design the DNN models (e.g., the number of parameters per layer, and the number of layers), which makes the model design more of an art than a science. Different DNN design decisions result in tradeoffs between system metrics; for example, a DNN with higher accuracy likely requires more memory to store all the model parameters and will have higher latency because of all the matrix multiplications being performed. On the other hand, a DNN model with fewer parameters will likely execute more quickly and use less computational resources and energy, but it may not have sufficient accuracy to meet the application's requirements.

2.2 Measurement

How can we evaluate the performance of a neural network?

2.3 Frameworks

2.4 Challenges

2.5 Discussion

Needle insertion is a complex procedure that involves a non-trivial effect, needle's bending, which is also non-trivial both to model and control. When performing this action the clinician relays on kinesthetic feedback and visual feedback. The former provides information on the moment of puncturing and the tissue type, the latter gives a feedback on the target and also on tissues

type. The needle bending could be exploited especially by robotic procedures to provide a more precise target reaching and to avoid obstacle on the insertion path.

In order to design a fully automated system a precise model of the forces acting on the needle, a clear identification of puncturing stages (pre, post and puncturing) and a predictive model of tissue deformation are needed to develop control strategies and path planning. The system also need a feedback that should provide needle and target tracking, and information on the environment like the interaction forces. Engineering and integrating such a system is really challenging. Because of the surgeon expertise with challenging task and unexpected situations the preferred clinical solution is to develop a robotic assisted device that assists the operator in the positioning phase but demands to the clinician the insertion phase.

Telerobotics could be a valuable solution to put clinician's expertise in the loop while enhancing the procedure's precision. However it has to deal with the classical teleoperation trade off between stability and transparency as we will discuss in the following chapter. In particular for the puncturing action the main issue is the abrupt change in the force at the puncturing time which may induce in the operator an unwanted reflection feedback that breaks the transparency.

Chapter 3

Edge Computing

This chapter will focus on bilateral teleoperation. It will introduce what a bilateral teleoperation is and what the goals of a good teleoperation system are.

3.1 System description

A bilateral teleoperation system has the purpose to allow an operator to interact remotely with an environment. The system, generally speaking, is made of three main blocks:

master robot on which the operator physically acts, generating commands for the slave and perceiving feedbacks received from the slave.

slave robot that interacts with the environment executing the received command and transmit to the master a feedback (ex. force, position, velocity).

communication channel on which the control signal flows forward, from the master to the slave, and backward, from the slave to the master.

A block representation could be found in Figure3.1.

At each side, master and slave, a local controller is implemented that combines local and remote information to create a bilateral coupling: the operator actuates the slave while feeling a force feedback from the remote site.

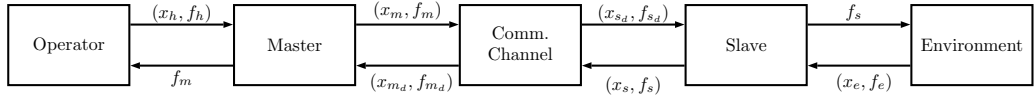


Figure 3.1: Block representation of the bilateral teleoperation.

The communication channel could be affected by delays: this means that a command sent from the master at time t is received by the slave at time $t + \tau_{m2s}$, where τ_{m2s} is the amount of time required to transmit the information in the feed forward channel.

Consequently a feedback produced by the slave at time t is received at the master at time $t + \tau_{s2m}$, with τ_{s2m} the amount of time required to transmit the information in the feedback channel. The sum of τ_{m2s} and τ_{s2m} is denoted as *round-trip time* delay.

A good bilateral teleoperation system should ensure the operator a transparent and stable interface with the environment, allowing safe and immediate responses to any event both known and unknown.

From a theoretical point of view, the two main properties for a bilateral teleoperation system are:

Stability The system should maintain the stability of the closed control loop independently of operator's or environment's behaviour. Stability of the whole system is hard and complex to prove, thus this property is more easily investigate with the passivity theory.

Transparency Is the capability of the system to provide to the operator the sense of telepresence while interacting with the remote environment.

3.2 Stability

There is no single concept of stability, and many different definitions are possible. The following are fundamental statements for stability:

Definition 3.2.1. An equilibrium state $x = 0$ is said to be:

- (a) **Stable** if for any positive scalar ε there exists a positive scalar δ such that $\|x(t_0)\| < \delta$ implies $\|x(t)\| < \varepsilon$ for all $t \geq t_0$.

(b) **Asymptotically stable** if it is stable and if in addition $x(t) \rightarrow 0$ as $t \rightarrow \infty$

(c) **Unstable** if it is not stable.

The definition (a) is often called “stability in the sense of Lyapunov” (stability i.s.L.) after the Russian mathematician Aleksandr M. Lyapunov (1857- 1918), whose important work features prominently in current control theory. Asymptotic stability in the large implies that all motions are bounded. Generally,

Definition 3.2.2. An equilibrium state $x = 0$ is said to be **bounded** (or Lagrange stable) if there exists a constant M , which may depend on t_0 and $x(t_0)$, such that $\|x(t)\| \leq M$ for all $t \geq t_0$.

To provide a proof of passivity the aim is to determine the stability nature of the equilibrium state (at the origin) of system Σ without obtaining the solution $x(\cdot)$. This could be done with the so called *direct method of Lyapunov* in relation to the (initialized) nonlinear autonomous dynamical system Σ given by

$$\dot{x} = F(x), \quad x(0) = x_0 \in \mathbb{R}^n; \quad F(0) = 0 \quad (3.1)$$

Modifications needed to deal with the (non autonomous) case

$$\dot{x} = F(t, x), \quad x(t_0) = x_0$$

are possible.

The essential idea is to generalize the concept of energy V for a conservative system in mechanics, where a well-known result states that an equilibrium point is stable if the energy is minimum.

Thus V is a positive function which has \dot{V} negative in the neighbourhood of a stable equilibrium point.

More generally,

Definition 3.2.3. We define a Lyapunov function $V : \mathbb{R}^n \rightarrow \mathbb{R}$ as follows :

- V and all its partial derivatives $\frac{\partial V}{\partial x_i}$ are continuous

- V is positive definite; that is, $V(0) = 0$ and $V(x) > 0$ for $x \neq 0$ in some neighbourhood $\{x \mid \|x\| \leq k\}$ of the origin

A Lyapunov function V for the system (3.1) is said to be

- **strong** if the derivative \dot{V} is negative definite;
that is, $\dot{V}(0) = 0$ and $\dot{V}(x) < 0$ for $x \neq 0$ such that $\|x\| \leq k$.
- **weak** if the derivative \dot{V} is negative semi-definite;
that is, $\dot{V}(0) = 0$ and $\dot{V}(x) \leq 0 \forall x$ such that $\|x\| \leq k$.

The statements of the two theorems of Lyapunov are :

Theorem 3.2.1. Lyapunov's First Theorem

Suppose that there is a strong Lyapunov function V for system Σ . Then system Σ is asymptotically stable.

Theorem 3.2.2. Lyapunov's Second Theorem

Suppose that there is a weak Lyapunov function V for system Σ . Then system Σ is stable.

3.3 Passivity

One method derived from control theory to ensure stability of the whole teleoperation system, even in presence of delays, is by designing each component in a way that it is passive.

By the definition found in [10], a system $G(s)$ is passive if and only if a finite amount of energy can be extracted from it; or, in other words, the energy that can be extracted by a passive system is always less or at most equal to the amount inserted. Intuitively, a passive teleoperation system cannot increase the amount of energy inserted in it by the operator and/or by the environment.

To introduce the required formulation of passivity, the following definition of extended measurable functions is needed:

Definition 3.3.1. Let $\mathcal{L}_2(\mathbb{R}^n)$ be the space of all measurable function $f : \mathbb{R} \rightarrow \mathbb{R}^n$ for which

$$\int_{-\infty}^{+\infty} \|f(t)\|^2 dx < \infty \quad (3.2)$$

Definition 3.3.2. *The space $\mathcal{L}_{2e}(\mathbb{R}^n)$, $\mathcal{L}_2(\mathbb{R}^n)$ extended, is defined as the space of all measurable function $f : \mathbb{R} \rightarrow \mathbb{R}^n$ for which*

$$f_T \in \mathcal{L}_2(\mathbb{R}^n) \quad \forall T \in [-\infty, +\infty] \quad (3.3)$$

where f_T is the truncated version of f . Then the passivity definition, as in [3], is the following:

Definition 3.3.3. *If the input in the time domain is described as $u(t) \in \mathcal{L}_{2e}(\mathbb{R}^n)$ and the output $y(t) \in \mathcal{L}_{2e}(\mathbb{R}^n)$,*
a system

$$G : \mathcal{L}_{2e}(\mathbb{R}^n) \rightarrow \mathcal{L}_{2e}(\mathbb{R}^n) \quad u \rightarrow v = G(u)$$

is passive if there exist a constant $\beta > 0$ such that

$$\int_0^t y^T(\tau)u(\tau)d\tau \geq -\beta \quad \forall t \geq 0, \forall u(\cdot) \quad (3.4)$$

The combination of two passive systems, connected in a feedback or parallel configuration, is a passive system as well. The connection of passive systems in a series configuration may not result in a passive system.

To show that passivity implies stability, we recall the definition of stability for a linear, time-invariant system $G(s)$ performed by the analysis of poles and zeroes of the system's transfer function in the Real and Imaginary plane.

Definition 3.3.4. *A linear, time-invariant system $G(s)$ is defined **stable** if and only if it does not present any pole in \mathbb{R}^+ plane and the poles in \mathbb{R}^0 are simple.*

The previous considering the imaginary axis and excluding $\mathbb{R}^+ \cup \mathbb{R}^0$ plane result in the **asymptotical stability** definition. The following theorem conveys these formulations for passivity and stability, proving that the former implies the latter:

Theorem 3.3.1. *Let $G(s)$ be the transfer function of a linear, time-invariant (LTI), single input/single output (SISO) system. $G(s)$ is passive if and only if*

- $G(s)$ has no pole in the \mathbb{R}^+ plane

- $\operatorname{Re}G(j\omega) \geq 0, \quad \forall \omega \in [-\infty, +\infty]$ such that $j\omega$ is not a pole for $G(s)$
- if $j\omega_0$ is a pole of $G(s)$, then it must be simple and the residual be greater than 0

$$\lim(s - j\omega_0)G(s) \geq 0$$

3.4 Teleoperation without delay

Most teleoperation algorithms has been designed to be robust even in an environment were communication delays occur. Despite that, some critical applications require absolute stability and high reliable network conditions.

3.4.1 The Four Channel Architecture

A solution, namely *The Four channel Architecture* was proposed by Lawrence [7].

It's a PF-PF (Position Force) architecture using forces and velocities as reference signals.

The teleoperation system is completely transparent if the operator feels that is directly interacting with the remote environment: this implies equality between forces ($F_m = F_s$) and velocities ($V_m = V_s$).

Transparency requires that the transmitted impedance Z_t is equal to the environment impedance $Z_e = F_s$. According to the block diagram in Figure3.2 the controllers $C_s, C_m, C_1, \dots, C_4$ have to be designed in such a way that the hybrid matrix H

$$\begin{bmatrix} F_m(s) \\ V_m(s) \end{bmatrix} = \underbrace{\begin{bmatrix} H_{11}(s) & H_{12}(s) \\ H_{21}(s) & H_{22}(s) \end{bmatrix}}_{\triangleq H} \begin{bmatrix} V_s(s) \\ F_s(s) \end{bmatrix} \quad (3.5)$$

is equal to $\begin{bmatrix} 0 & I \\ I & 0 \end{bmatrix}$.

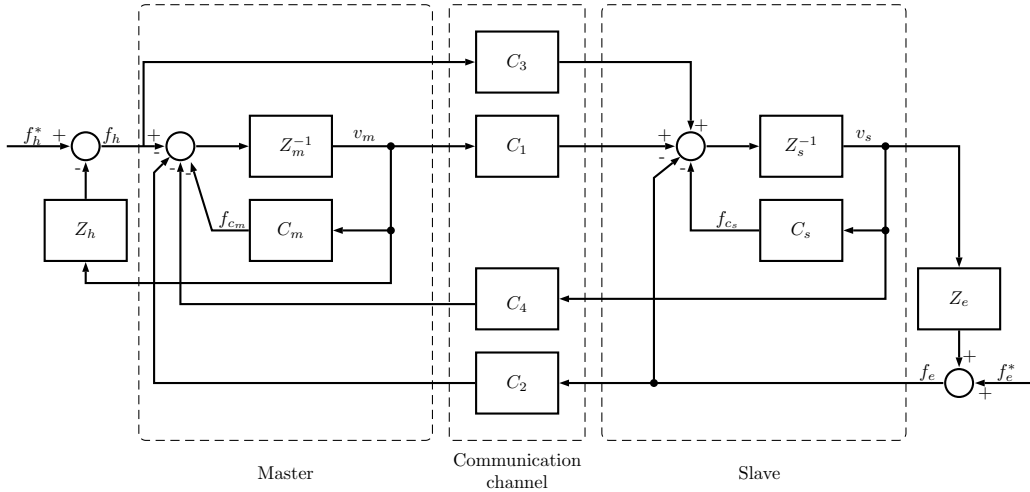


Figure 3.2: The Four Channel Architecture.

That implies

$$Z_t = \frac{F_m}{V_m} = (H_{11} - H_{12}Z_e)(H_{21} - H_{22}Z_e)^{-1} = Z_e \quad (3.6)$$

To achieve the goal of transparency, it is necessary to have a very accurate model both of master and slave robots. A good transparency is required mainly at low frequencies, where mathematical models are more accurate, in order to provide a good feedback at frequencies the operators work on. In his work, Lawrence proposes to associate the abstract notion of passivity derived from the mathematical representation of positive real transfer functions to a more physical measure of passivity that describes how the covariant variables at each port must be in phase in order to maintain a positive energy flow to the system.

3.5 Teleoperation with constant delay

The transmission of power variables over a communication channel affected by delays, is the reason for which bilateral teleoperation models may become unstable. Consider a basic control system structure, the mathematical description clearly shows the effect of the delays over the communication channel. Considering an input and output $X(s), Y(s)$ in the Laplace domain

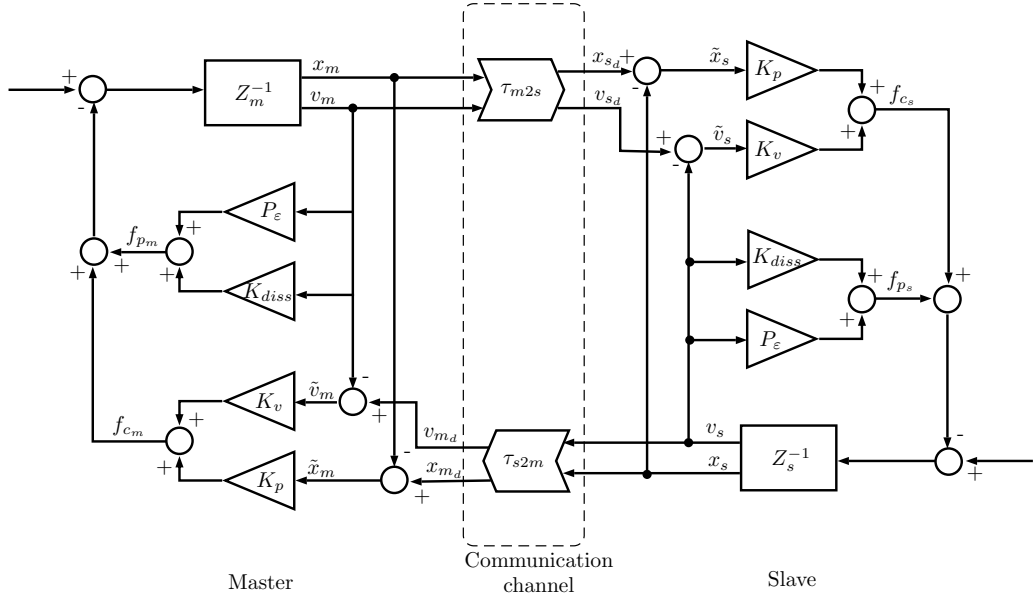


Figure 3.3: Lee-Spong PD dissipative approach

variable s , a plant $P(s)$, a controller $C(s)$ and a feedback delay of T seconds, the transfer function of $G(s)$ is:

$$G(s) = \frac{Y(s)}{X(s)} = \frac{e^{sT} P(s) C(s)}{1 + e^{sT} P(s) C(s)} \quad (3.7)$$

The term e^{sT} that appears at denominator is the cause of the performance loss. Increasing the value of T , the system loses phase margin, thus the system could become unstable.

With a passivity based analysis the communication channel could be separated from the master and slave blocks allowing the demonstration of system's stability by passivating the channel.

3.5.1 PD and passivity terms

Lee and Spong [8] provides a solution for the teleoperation with constant time delay. It guarantees the stability of a position-position bilateral teleoperator by adding a dissipative term to the PD controller at each side of the architecture. Figure 3.3 shows the block-schema of this architecture. This solution does not suffer of position drift between master and slave, which is

the major drawback of scattering-based solutions due to the extraction of velocity from the communicated scattering variables [8].

The explicit position feedback enables to guarantee the asymptotic master-slave position coordination. This approach passifies the combination of the communication and control blocks all together, in contrast to scattering approach, where the delayed communication block is passified in such a way that the closed-loop teleoperator becomes an interconnection of passive sub-modules. Stability is guaranteed by an over estimation of the round-trip time delay $\bar{\tau}_{RTT} \geq \tau_{RTT}$.

Representing a manipulator with:

$$M(q)\ddot{q}(t) + C(q, \dot{q})\dot{q} = T(t) + F(t) \quad (3.8)$$

where $q \in \mathbb{R}^m$ is the configuration, $F \in \mathbb{R}^n$ is the interacting force, $T \in \mathbb{R}^n$ the control, $M(q) \in \mathbb{R}^{m \times m}$ the symmetric and positive-definite inertia matrix and $C(q, \dot{q}) \in \mathbb{R}^{m \times m}$, the control terms for master and slave could be written as function of local and remote delayed informations as follow:

$$T_m(t) := T_m(q_m(t), \dot{q}_m(t), q_s(t - \tau_s), \dot{q}_s(t - \tau_s)) \in \mathbb{R}^m \quad (3.9)$$

$$T_s(t) := T_s(q_s(t), \dot{q}_s(t), q_m(t - \tau_m), \dot{q}_m(t - \tau_m)) \in \mathbb{R}^m \quad (3.10)$$

The goal is to design the control terms T_s and T_m to achieve

- **master-slave position coordination** if $(F_m, F_s) = 0$, then

$$q_{error}(t) := q_m(t) - q_s(t) \rightarrow 0, \quad t \rightarrow 0 \quad (3.11)$$

- **static force reflection** if $(\dot{q}_m(t), \dot{q}_s(t), q_m(t), q_s(t)) \rightarrow 0$, then

$$F_m(t) \rightarrow -F_s(t) \quad (3.12)$$

- **energetic passivity** of the closed loop teleoperation system. If there exists a finite constant $d \in \mathbb{R}^m$ such that

$$\int_0^t [F_m^T(\theta)\dot{q}_m(\theta) + F_s^T(\theta)\dot{q}_s(\theta)] d\theta \geq d^2 \quad \forall t \geq 0 \quad (3.13)$$

meaning that the maximum extractable energy from the two-port closed-loop teleoperator is always bounded.

In order to fulfil (3.11), (3.12) and (3.13) the design of master and slave controls $T_m(t)$ and $T_s(t)$ in (3.9) and (3.10) is:

$$T_m(t) = \underbrace{-K_p((q_m(t) - q_s(t - \tau_m)) - K_v(\dot{q}_m(t) - \dot{q}_s(t - \tau_m))}_{\substack{\text{delayed P-action} \\ F_{mc}}} - \underbrace{(K_d + P_\varepsilon)(\dot{q}_m(t))}_{\substack{\text{dissipation} \\ F_{mp}}} \quad (3.14)$$

$$T_s(t) = \underbrace{-K_p((q_s(t) - q_m(t - \tau_s)) - K_v(\dot{q}_s(t) - \dot{q}_m(t - \tau_s))}_{\substack{\text{delayed P-action} \\ F_{sc}}} - \underbrace{(K_d + P_\varepsilon)(\dot{q}_s(t))}_{\substack{\text{dissipation} \\ F_{sp}}} \quad (3.15)$$

where $K_d = \frac{\bar{\tau}_{RTT}}{2}K_p$ and P_ε is an additional damping ensuring master-slave coordination.

3.6 Teleoperation with time varying delay

The occurrence of time-varying delays makes the energy handling in the communications channel a challenging problem. Even the most stable and transparent architecture is susceptible to that.

The simpler solution is the use of buffers at each side to re-order information and absorb the variation by releasing packets with a constant rate. The drawbacks of this approach are the increased RTT because of the time spent for store each packet in the buffer and the dynamic growing of the buffer if the delay increases.

3.6.1 PSPM

The Passive Set-Position Modulation (PSPM) is P-P teleoperation architecture proposed by Lee [9] that addresses teleoperation with time-variant

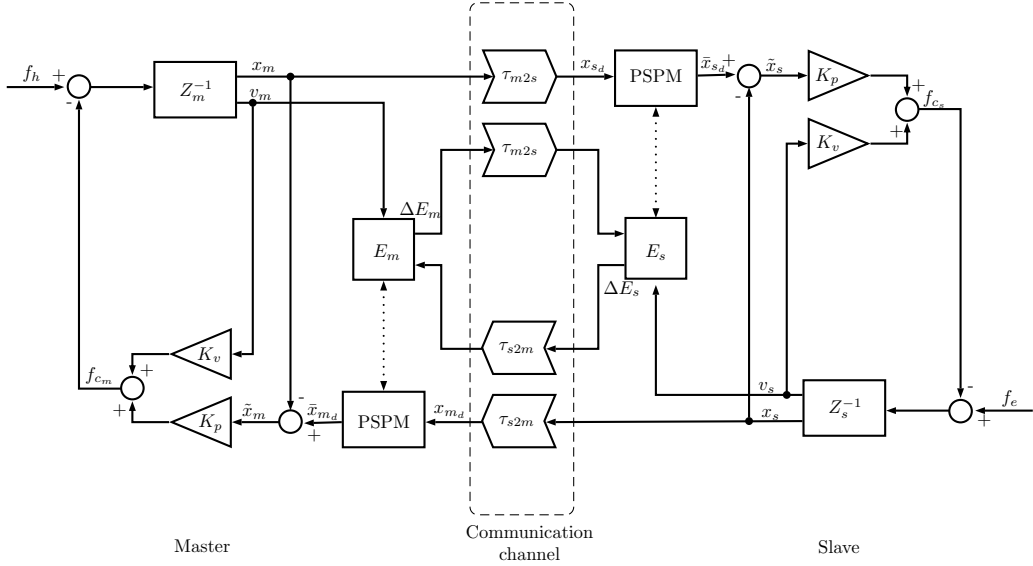


Figure 3.4: PSPM teleoperation schema

delay.

A representation is available in Figure 3.4. The input signal $y(k)$ is a discrete-time input sequence of sparse or slowly updating set position, possibly non uniformly received at time t_k .

This signal is applied to a spring-damper model $K_P(x(t) - y(k)) + K_d v(t)$ where $x(t)$ and $v(t)$ are the continuous time values of manipulator position and velocity. The approach consider the possible passivity breaking due to the spring's energy jump at switching instances by solving the minimisation problem

$$\|x(t) - y(k)\| \quad \text{s.to} \quad E(k+1) + \Delta E_{in}(k) + D(k-1) - \Delta \bar{P}(k) \geq 0 \quad (3.16)$$

into the PSPM block each time the reference signal is updated. $E(k+1)$ is the local energy reserve, $\Delta E_{in}(k)$ is the energy received at time t_k from the counterpart (*energy-shuffling*), $D(k-1)$ is the causal approximation of the damping dissipation (*energy re-harvesting*), namely $\frac{1}{2}K_d v^2(t)$, that is position-only dependent to avoid the sequence of numerical differentiation and integration that will introduce noise contamination into the signal. Fi-

nally $-\Delta\bar{P}(k)$ is the spring energy jump

$$-\Delta\bar{P}(k) = \frac{1}{2} \|x(t_k) - \bar{y}(k)\|_{K_p}^2 - \frac{1}{2} \|x(t_k) - \bar{y}(k-1)\|_{K_p}^2 \quad (3.17)$$

The resulting $\bar{y}(k)$ signal is modulated in such a way that it is as close as possible to the original $y(k)$ yet only to the extent that the use of $\bar{y}(k)$ for the spring coupling K_p is permissible by the passivity constraint.

The *virtual energy reservoir* is a mechanism to improve performance by the use of *energy reharvesting*. It recaptures and deposits in the *energy reservoir* a portion of the otherwise wasted energy due to the damper and through the *energy shuffling/ceiling*. The latter limits the accumulation of virtual energy by setting an upper shorthold to the reservoir and sending the exceeding energy to the counterpart.

This approach should accommodate a variety of communication/data-update imperfections of $y(k)$, including variable-rate update, varying delay, packet loss, and even time-swapping.

3.6.2 The Two Layer Algorithm

This algorithm proposed by Franken *et al.* [5] implements a hierarchical two-layer approach: a top *transparency layer* and a bottom *passivity layer*. The main idea is that, without making any assumption about on type of controller implemented, in the former layer a control algorithm is in charge of displaying the desired behaviour and achieving transparency. The only requirement is that the algorithm implemented in this layer computes the control forces τ_{TL} to be applied to the manipulator.

The passivity layer on the bottom monitors and enforces the energy balance in the system ensuring that no virtual energy is generated. With this approach, the strategy used to obtain transparency is independent of the one to obtain passivity, thus enabling the possibility to adopt in the transparency layer strategies known to be non passive e.g. most filtering techniques.

Two two-way communication channels enable the communication between master and slave: one is dedicated to communicate energy exchange information between the passivity layers, the other relays the information required by the algorithm in the transparency layer. In contrast with other approaches,

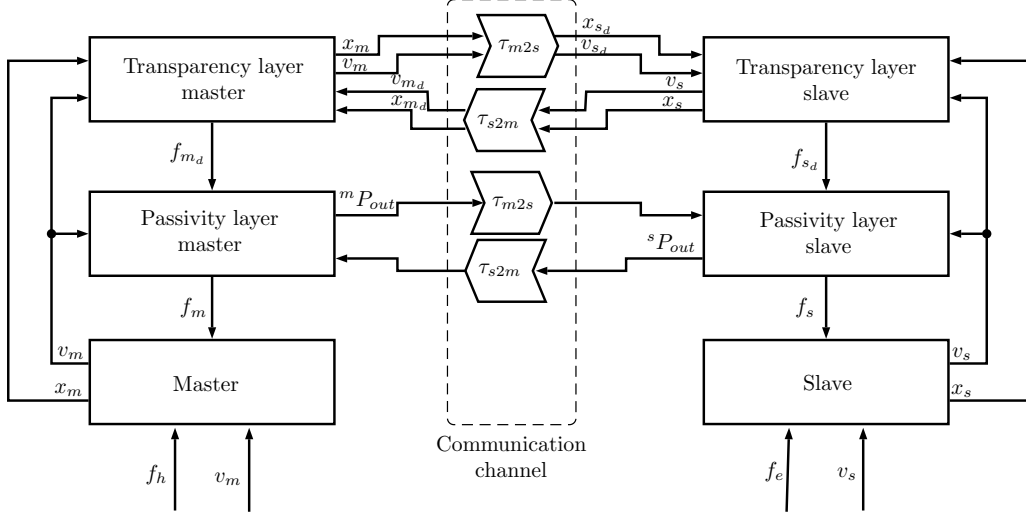


Figure 3.5: TwoLayer teleoperation schema. F_{m_d}, F_{s_d} are master and slave τ_{TL} , while f_m, f_s are the two τ_{PL}

the passivity is achieved after the computation of the commands and not before. This architecture is summarized in Figure 3.5.

The passivity layer requires impedance causality both for master and slave (i.e. velocities as input and forces as output).

The latter layer acts as follows: at first, the energy exchange between the discrete time controller and physical world is evaluated as:

$$\begin{aligned} \Delta H(k) &= \int_{(k-1)\Delta T_s}^{(k)\Delta T_s} \tau_r(k) \dot{q}(t) dt \\ &= \tau_r(k)(q(k) - q(k-1)) \\ &= \tau_r(k)\Delta q(k) \end{aligned} \quad (3.18)$$

where $\tau_r(k)$ is the torque exerted by the actuators at sample k , $\dot{q}(k)$ the velocity vector of the actuators and $q(k)$ their sampled position.

At the same time the energy received from the counterpart is taken into account:

$$H_+(k) = \sum_{i \in Q(k)} H(i) \quad (3.19)$$

where Q is the queue which stores all the packets received between two time instants and $H(i)$ is the i_{th} packet in the queue. Then the energy level in the

local tank is updated:

$$H(k) = H(\bar{k}) + H_+(k) - \Delta H(k) \quad (3.20)$$

where $H(\bar{k})$ is the state of the tank at the previous sampling time.

An energy quantum $H_-(k) < H(k)$ could be transferred to the tank on the other side of the teleoperation system according to the transport protocol that has been implemented. $H_-(k)$ is then extracted from the tank. The energy available during the next sampling period $H(\overline{k+1})$ becomes

$$H(\overline{k+1}) = H(k) - H_-(k) \quad (3.21)$$

The available energy is then used to ensure the stability of the system.

An approach could be to allow the command τ_{TL} only if the tank stores enough energy

$$\tau_{max1}(k) = \begin{cases} 0, & \text{if } H(\overline{k+1}) \leq 0 \\ \tau_{TL}, & \text{otherwise} \end{cases}$$

or to compute an upper bound for the command in order to guarantee the stability of the teleoperated system

$$\tau_{max2}(k) = \frac{H(\overline{k+1})}{\dot{q}(\bar{k})\Delta Ts}.$$

The combination of multiple approaches allows more advanced passivation strategy by allowing e.g. the minimum value from a set of conditions

$$\tau_{max}(k) = \min(\tau_{max1}(k), \tau_{max2}(k), \dots)$$

Then the torques τ_{PL} are a bounded version of the ones requested by the transparency layer

$$\tau_{TL}(k) = sgn(\tau_{TL}) \min(\tau_{PL}, \tau_{max}(k)). \quad (3.22)$$

To maintain the energy level above a minimum threshold, usually at master side, a Tank Level Controller (TLC) is implemented. When the energy goes below the threshold H_D , an extra variable damping is injected to extract an extra amount of energy

$$\tau_{TLC}(k) = -d(k)\dot{q}(k) \quad (3.23)$$

with $d(k)$

$$d(k) = \begin{cases} \alpha(H_D - H(\bar{k}+1)), & \text{if } H(\bar{k}+1) < H_D \\ 0, & \text{otherwise} \end{cases} \quad (3.24)$$

Thus the command to be applied to the device during the sample period $k+1$ becomes

$$\tau_r(k+1) = \tau_{TL}(k) + \tau_{TLC}(k) \quad (3.25)$$

Looking at the communication channel, the change of energy in the channel $\Delta H_C(k)$ at sample k is

$$\begin{aligned} H_C(k) &= \sum_{i=1}^k \Delta H_C(i) \\ &= \sum_{i=1}^k H_{-M}(i) - H_{+M}(i) + H_{-S}(i) + H_{+S}(i) \end{aligned} \quad (3.26)$$

and due to time delays and packet loss in the channel

$$\begin{aligned} H_{-S}(i) &= H_{+M}(i + d_{SM}(i)) \\ H_{-M}(i) &= H_{+S}(i + d_{MS}(i)) \end{aligned} \quad (3.27)$$

where $d_{MS}(i) \geq 0$ and $d_{SM}(i) \geq 0$ takes into account nondeterministic time delays. Therefore

$$\begin{aligned} \sum_{i=0}^k H_{-M}(i) &\geq \sum_{i=0}^k H_{+S}(i) \\ \sum_{i=0}^k H_{-M}(i) &\geq \sum_{i=0}^k H_{+S}(i) \end{aligned} \quad (3.28)$$

so that

$$H_C(k) \geq 0 \quad \forall k \quad (3.29)$$

meaning that the communication channel can never produce energy as long as packets duplication is prevented.

We can now write the total energy $H_T(k)$ in the control system at instant k as

$$H_T(k) = H_M(k) + H_C(k) + H_S(k) \cdot \quad (3.30)$$

Finally the passivity condition for the system is

$$H_T(k) \geq 0 \quad (3.31)$$

and the condition that ensure a passive interconnection of the entire system to the physical world is

$$\dot{H}_T(k) \leq P_M(k) + P_S(k) \quad (3.32)$$

where $\dot{H}_T(k)$ is the rate of the energy balance of the system, $P_M(k)$ and $P_S(k)$ are respectively the power of master and slave flowing between the robot and it's respective controller.

3.7 Discussion

In this chapter the problem of teleoperation has been addressed and some of the possible solutions to overcome the problem of delay in the communication and keep the system passive have been presented. Teleoperation have two main goals: stability and transparency. The former is mandatory and ensured by the passivity of the system, the latter is responsible for a good haptic feedback and for the precision while performing a task.

The strategy adopted to achieve the goal of passivity could reduce the level of transparency in the system. A flexible and robust approach between the one presented is the Two-Layer algorithm.

Chapter 4

Robotics Applications

This chapter will present the improvements of the Two-Layer teleoperation architecture developed within the i-Sur European project [4] for a needle insertion task. First we present the teleoperation system modelled as a port-Hamiltonian system [4], then we demonstrate both the equivalence between energy computation in task and joint space, and that a proper energy scaling between master and slave keeps the whole teleoperation system passive. Finally we describe the two teleoperation schemas, a Position-Position and a Position-Force architecture. Both control architectures are endowed with *pilot mode* for insertion assistance.

4.1 A model for the teleoperation system

The port Hamiltonian framework is a generalization of standard Hamiltonian mechanics, where energetic characteristics and power exchange between subsystems are clearly identified.

4.1.1 The port-Hamiltonian description

The most common representation of a port-Hamiltonian system is

$$\begin{cases} \dot{x} = [J(x) - R(x)] \frac{\partial H}{\partial x} + g(x)u \\ y = g^T(x) \frac{\partial H}{\partial x} \end{cases} \quad (4.1)$$

where $x \in \mathbb{R}^n$ is the state vector and $H(x) : \mathbb{R}^n \rightarrow \mathbb{R}$ is the lower bounded Hamiltonian function representing the amount of energy stored in the system, $J(x) = -J(x)^T$ and $R(x) \geq 0$ are the matrices that represent the internal energetic interconnections and the dissipation of the port-Hamiltonian system, and $g(x)$ is the input matrix. The input u and output y are dual variables and their product is (generalized) power. The pair (u^T, y) represents the power exchanged by the system with the external world. It can be shown that the following equality holds:

$$\dot{H}(x) + \frac{\partial^T H}{\partial x} R(x) \frac{\partial H}{\partial x} = u^T(t) y(t) \quad (4.2)$$

This means that the power supplied to the system is either stored or dissipated, thus that a port-Hamiltonian system is passive with respect to the pair (u, y) .

Let

$$D(x) = \frac{\partial^T H}{\partial x} R(x) \frac{\partial H}{\partial x} \geq 0 \quad (4.3)$$

be the power dissipated by the system. $D(x)$ represent the *passivity margin*: the larger $D(x)$, the higher the passivity of the system. A large passivity margin allows the system to absorb more energy generated by non passive actions while preserving its passivity.

4.1.2 Port-Hamiltonian system with energy tank

The Two-Layer framework exploits the passivity margin by using of energy tank framework. The energy dissipated by the system is stored in a (virtual) energy tank and can be used for implementing any desired control action in a passivity preserving way as described in Section 3.6.2.

The model for a port-Hamiltonian system endowed with a tank is given by

$$\begin{cases} \dot{x} &= [J(x) - R(x)] \frac{\partial H}{\partial x} + g(x)u \\ \dot{x}_t &= \frac{\sigma}{x_t} D(x) + \frac{1}{x_t} (\sigma P_{in} - P_{out}) + u_t \\ y_1 &= \begin{pmatrix} y \\ y_t \end{pmatrix} \end{cases} \quad (4.4)$$

where x_t is the state associated with the energy storing tank, and

$$T(x_t) = \frac{1}{2}x_t^2 \quad (4.5)$$

is the energy stored in the tank. $P_{in} \geq 0$ and $P_{out} \geq 0$ are the incoming and outgoing power flows that the tank can exchange with other tanks. The pair (u_t, y_t) is the power port the tank can use to exchange energy with the external world and $y_t = \frac{\partial T}{\partial x_t} = x_t$. The parameter $\sigma \in \{0, 1\}$ allows to upper bound the amount of energy stored in the tank.

The power balance for the tank is derived from the (4.4):

$$\dot{T} = \sigma D(x) + \sigma P_{in} - P_{out} + u_t^T y_t \quad (4.6)$$

which means that, if $\sigma = 1$, the tank stores the power dissipated by the system $D(x)$ and the incoming power flow P_{in} , while the outgoing power flow P_{out} is released. Furthermore the power can be injected and extracted from the tank via the power port (u_t, y_t) .

In order to avoid singularities, ($x_t = 0$ in (4.4)) a small amount of energy must always be present in the tank, thus we chose an arbitrary small threshold $\varepsilon > 0$ representing the minimum amount of energy we want stored into it. The tank has to be initialize and managed in such a way that $T(x_0) > \varepsilon$ and energy extraction is not allowed if $T(x_0) \leq \varepsilon$. It is also necessary to set the upper bound σ mentioned before. In fact, if there is no bound, the energy available can become very large as time increases and it would be possible to implement behaviour that are unstable in practice, even if the system remain passive for a while. Thus, σ is set with the following policy:

$$\sigma = \begin{cases} 1, & \text{if } T(x_t) \leq \bar{T} \\ 0, & \text{otherwise} \end{cases} \quad (4.7)$$

where \bar{T} is an application dependent upper bound on the energy that can be stored in the tank.

The energy stored in the tank can be exploited for passively implementing any desired input $w \in \mathbb{R}^n$ to the port-Hamiltonian system with the tank is associated, by connecting the power port of the system (u, y) with the power

port of the tank (u_t, y_t) through the following preserving interconnection:

$$\begin{cases} u &= \frac{w}{x_t} y_t = \frac{w}{x_t} x_t = w \\ u_t &= \frac{-w^t}{x_t} y \end{cases} \quad (4.8)$$

that implies the balance

$$u^T y = -u_t^T y_t \quad (4.9)$$

meaning that the energy supplied to/extracted from the port-Hamiltonian system for implementing the desired input is the same extracted from/supplied to the tank, consequently no energy is generated in the whole interconnected system.

4.1.3 A port-Hamiltonian formulation for the tank-based teleoperation system

The master and slave manipulators in a teleoperation system not affected by communication delays can be represented with the formalism with $i = m, s$

$$\begin{cases} \begin{pmatrix} \dot{x}_i \\ \dot{p}_i \end{pmatrix} &= \begin{pmatrix} 0 & I \\ -I & R_i \end{pmatrix} \begin{pmatrix} \frac{\partial H_i}{\partial x_i} \\ \frac{\partial H_i}{\partial p_i} \end{pmatrix} + \begin{pmatrix} 0 \\ I \end{pmatrix} F_{ext,i} + \begin{pmatrix} 0 \\ I \end{pmatrix} F_i \\ \dot{x}_{t_i} &= \frac{\sigma_i}{x_{t_i}} D_i(x) + \frac{1}{x_{t_i}} (\sigma^i P_{in} - {}^i P_{out}) + u_{t_i} \\ y_i &= \begin{pmatrix} v_i \\ y_{t_i} \end{pmatrix} \end{cases} \quad i = m, s \quad (4.10)$$

where $x_{t_i}, y_{t_i} = x_{t_i}$, and $T_i = \frac{1}{2}x_{t_i}^2$ are the state of the tank, the output associated to the tank, and the energy stored in the tank respectively, D_i represents the energy dissipated by the robot possibly increased by inserting a local damping injection (e.g. TLC) and ${}^i P_{in}$ and ${}^i P_{out}$ are the power flows that can be exchanged with the tank. $F_{ext,i}$ are the external forces acting on the system and F_i are the command provided by the passivity layer.

The coupling forces $F_{d,i}$ provided by the transparency layer are implemented using the energy available in the tanks by the following power preserving

interconnection between the tank power port (u_{t_i}, y_{t_i}) and the robot power port (F_i, v_i) :

$$\begin{cases} F_i &= \frac{F_{d,i}}{x_{t_i}} y_{t_i} = \frac{F_{d,i}}{x_{t_i}} x_{t_i} = F_{d,i} \\ u_{t_i} &= -\frac{F_{d,i}^T}{x_{t_i}} v_i \end{cases} \quad i = m, s \quad (4.11)$$

With this interconnection the command $F_{d,i}$ provided by the transparency layer is implemented by exchanging energy with the tank: if $F_{d,i} > 0$, it means that some amount of energy is necessary for implementing the desired input and should be extracted from the tank. If $F_{d,i} < 0$, it means that the desired action is dissipative, thus the dissipated energy is stored in the tank. The provided input could be passively achieved if and only if the tank is full enough, otherwise it could be either modulated by some passivation strategy or completely cut off as explained in Section 3.6.2.

If the tank goes below the threshold $T(x_{t_i}) \leq \varepsilon_i$, energy extraction is forbidden and the coupling force implemented is $F_{d,i} = 0$. This ensure the passivity and a stable behaviour of the teleoperation system but, it negatively affects its transparency.

It is then necessary to ensure that, both at the master and slave side, the level of the tank is kept much higher than a more conservative minimum level. There are two methods for increasing the local tank level: transfer energy from the remote tank and extract it from the local robot by damping injection (TLC). The former should be preferred over the latter as it does not affect the dynamic of the system and does not affect either the feedback perceived by the user, as well.

The energy transfer strategy acts as follows: when the energy is below the more conservative minimum threshold ${}^i T_{req}$, an *energy quantum* is requested from the other tank. If at the other side the fill level of the tank is high enough, namely it is greater than a threshold ${}^i T_{ava}$, an *energy quantum* is sent. This *availability* threshold helps to keep the energy balanced through the two sides. Furthermore, if the tank is already full, all the energy dissipated by the local robot is sent to the other side in order to recover it. Formally the

request signal is:

$${}^i E_{req} = \begin{cases} 1, & \text{if } T_i(x_{t_i}) < {}^i T_{req} \\ 0, & \text{otherwise} \end{cases} \quad i = m, s \quad (4.12)$$

and the whole energy transfer strategy could be described as

$$\begin{cases} {}^m P_{out} = (1 - \sigma_m) D_m + {}^s E_{req} \beta_m \bar{P}_m = {}^s P_{in} \\ {}^s P_{out} = (1 - \sigma_s) D_s + {}^m E_{req} \beta_s \bar{P}_s = {}^m P_{in} \end{cases} \quad (4.13)$$

where, as discussed in Section 4.1.2, if the tank is already full we send to the other tank the energy dissipated by the robot setting $\sigma_i = 0$.

The variable $\beta_i \in \{0, 1\}$ enables/disables the transfer of the energy from the tank, and its value is given by

$$\beta_i = \begin{cases} 1, & \text{if } T_i(x_{t_i}) \geq {}^i T_{ava} \\ 0, & \text{otherwise.} \end{cases} \quad (4.14)$$

$\bar{P}_i > 0$ is the rate of energy flowing from one tank to the other and it's a design parameter. The bigger \bar{P}_i , the faster the energy transfer.

All these thresholds are also application dependent, and the following constrain must be satisfied: $\varepsilon_i < {}^i T_{req} < {}^i T_{ava} < \bar{T}_i$, for $i = m, s$

This teleoperation schema is passive with respect to the environment, i.e. it is passive with respect to the pair $\left((F_h^T, F_e^T)^T, (v_m^T, v_s^T)^T \right)$

Proof. [4] Consider the total energy of the teleoperation system as a storage function:

$$H(t) = H_m(t) + H_s(t) + T_m(t) + T_s(t) \quad (4.15)$$

Using (4.10) we obtain that

$$\begin{aligned} \dot{H}(t) = & -D_m(t) + F_m^T v_m + \sigma_m D_m(t) + \sigma_m {}^m P_{in} - {}^m P_{out} \\ & - D_s(t) + F_s^T v_s + \sigma_s D_s(t) + \sigma_s {}^s P_{in} - {}^s P_{out} \\ & + u_{t_m} y_{t_m} + F_h^T v_m + u_{t_s} y_{t_s} + F_e^T v_s \end{aligned} \quad (4.16)$$

Since the tanks and the robots are interconnected with the power preserving interconnection (4.11), we have that $F_i^T v_i = -u_{t_i} y_{t_i}$, where $i = m, s$ thus the

(4.16) can be rewritten as

$$\begin{aligned}\dot{H}(t) = & - (1 - \sigma_m)D_m(t) - (1 - \sigma_s)D_s(t) \\ & - (1 - \sigma_m)^m P_{in} - (1 - \sigma_s)^s P_{in} \\ & + F_h^T v_m + F_e^T v_s\end{aligned}\tag{4.17}$$

Finally using (4.13), we have that

$$\begin{aligned}\dot{H}(t) = & - (1 - \sigma_m)D_m(t) - (1 - \sigma_s)D_s(t) \\ & - (1 - \sigma_m)^s P_{out} - (1 - \sigma_s)^m P_{out} \\ & + F_h^T v_m + F_e^T v_s\end{aligned}\tag{4.18}$$

and since $\sigma_i \in \{0, 1\}$, ${}^i P_{out}$, $D_i \geq 0$ for $i = m, s$ it follows that

$$\dot{H}(t) \leq F_h^T v_m + F_e^T v_s\tag{4.19}$$

thus (3.32) holds, which proves our statement. \square

Augmenting the local damping, via the TLC approach, is a passivity preserving technique. For a formal proof the port-Hamiltonian model should be rewritten with a variable damping matrix and the previous proof is similar.

4.2 Improvements on the Two-Layer

The Two Layer approach is a really versatile and powerful tool for the development of a passive bilateral teleoperation system. Although there is some space to exploit it, giving even more flexibility and control to the designer in order to better manage transparency, thus preserving passivity, even neglecting the dynamic model of the two manipulators involved.

4.2.1 Energy evaluation in task space

Both in the i-Sur project and in the original paper from Frankel *et. all* [5], energy computation and the passification strategy are performed in the joint space. For a single DoF device it is less challenging to develop a passification strategy and analyse how the transparency of the system is affected. But for a

multi DoF device the passification strategy could heavily affect transparency: a uniform action between the joints could, due to the kinematics mapping, results in a dangerous behaviour in the task space.

Take needle insertion as an example: for ensuring the safety of the patient, when no needle steering techniques are involved, the path executed must follow the needle's main z axis. It is desirable that also the passivity strategy could, in a way, act preserving, as much as possible, transparency in the task space to ensure the patient safety. In this example could be a good idea splitting the task into two subtasks with different degrees of transparency priority.

An high degree of priority task should ensure the correct $x - y$ position and orientation of the needle tip, the other one, which could afford more safely a lower degree of transparency, performs the puncturing action along the z axis. In fact if there is not enough energy for performing the full action, the system will puncture with less force but the needle will not injure neighbour tissues.

This approach requires only minimal changes into the passivity layer: in fact the notion of transparency affects only the strategy on how τ_{max} is computed in (3.22). The development of a task-oriented passivity approach requires energy evaluation in the task space. Furthermore, this approach for energy evaluation allows the designer to work in a well known spatial domain, thus better understand the behaviour of the system, where to act and how to tune the parameters of the system to achieve a more stable behaviour.

Theorem 4.2.1. Energy equivalence between joint and task space
The amount of energy required in task space to perform a task is equal to the one in joint space.

The proof of this statement requires the notion of Jacobian and Static Wrench Transmission.

The Jacobian matrix $J(q)$ allows the solution to the forward instantaneous kinematics problem for a serial chain manipulator, where the total velocity of the end effector has to be found given the the position and velocity of all members of the chain joints

$${}^k v_N = J(q)\dot{q} \quad (4.20)$$

where ${}^k v_N$ is the spatial velocity of the end effector expressed in the frame k , $\dot{q}(t)$ the n -dimensional vector composed of the joints rates and $J(q)$ is a $6 \times n$ matrix whose elements are, in general, non-linear function of q and is expressed relative to the same coordinate frame as the spatial velocity ${}^k v_N$ [13].

The static wrench transmission establishes the relationship between wrenches applied to the end effector and forces/torques applied to the joints. Exploiting the principle of virtual work, the relationship between wrenches applied to the end effector and force/torques applied to the joints can be shown to be

$$\tau = J^T f \quad (4.21)$$

where τ is the n -dimensional vector of applied joint forces/torques for an n -Dof manipulator and f is the spatial wrench vector

$$f = \begin{bmatrix} f \\ o \end{bmatrix} \quad (4.22)$$

in which o and f are the vectors of torques and forces, respectively, applied to the end-effector, both expressed in the coordinate frame where the Jacobian is expressed. The Jacobian maps the joint rates into the spatial velocity of the end-effector, its transpose maps the wrenches applied into the end-effector into joint forces/torques [13]. The formalization for Theorem 4.2.1 is:

$$E = \int \tau^T(t) \dot{q}(t) dt = \int f^T(t) \dot{x}(t) dt \quad (4.23)$$

and can be proved as follows

Proof. Consider the formulation of energy in joint space

$$E_\tau = \int \tau^T(t) \dot{q}(t) dt \quad (4.24)$$

thus we can write the elementary work in joint space as

$$dW_\tau = \tau^T(t) dq \quad . \quad (4.25)$$

The energy in task space is

$$E_f = \int f^T(t) \dot{x}(t) dt \quad (4.26)$$

and the elementary work in task space is

$$dW_f = f^T(t)dx \quad . \quad (4.27)$$

Using (4.20) we end up will

$$dW_f = f^T(t)J(q)dq \quad (4.28)$$

Manipulators are time independent system with holonomic constraints: their pose depends only on joints positions, meaning that virtual displacements match physicals ones.

By this consideration we can write

$$\delta W_\tau = \tau^T(t)\delta q \quad (4.29)$$

$$\delta W_f = f^T(t)J(q)\delta q \quad (4.30)$$

and for the principle of virtual works

$$\delta W_f = \delta W_\tau \quad \forall \delta q \quad (4.31)$$

Now using (4.21) in (4.28)

$$\begin{aligned} dW_f &= f^T(t)J(q)dq \\ &= \tau^T(t)J^T(q)J(q)dq \\ &= \tau^T(t)dq \\ &= dW_\tau \end{aligned} \quad (4.32)$$

□

For a redundant manipulator in (4.21) the Jacobian pseudoinverse has to be addressed instead of J^T .

4.2.2 Energy scaling

When dealing with a pair of the similes manipulator, jointly coupled, performing the commanded task at the slave side will require the same amount of energy supplied at the master side. This is not true when dealing with

manipulators that are mechanically different. Performing the same task require different amount of energy, even if the Cartesian motion is exactly the same. This is due to the different dynamical model of the two manipulators. Furthermore manipulator friction is another energy dissipative unknown variable to deal with. When adopting an energy based approach for enforcing the passivity of the interconnected teleoperation system, all these effects produce an energy leakage.

With the purpose to balance the different energy requirement between the two manipulators, we introduce a couple of constants α and γ such that

$$\alpha\gamma = 1 \quad \alpha, \gamma > 0 \quad (4.33)$$

When performing the energy transmission between the two tanks, the master, which have a low inertia, send to the slave, which have a greater inertia, a properly scaled up quantum of energy to compensate the energy requirement between the two manipulator. The slave do the same but scaling down the value of the quantum of energy. In other words, if we set in e.g. $\alpha = 10$, then $\gamma = \frac{1}{10}$, it means that an action performed on the master requires ten times more energy to be replicated on the slave, at the same time a feedback from the slave require one tenth of the original energy to be executed on the master.

This idea clearly affects the energy transmission strategy that, with the introduction of energy scaling, becomes

$$\begin{cases} \alpha^m P_{out} = \alpha ((1 - \sigma_m) D_m + {}^s E_{req} \beta_m \bar{P}_m) = {}^s P_{in} \\ \gamma {}^s P_{out} = \gamma ((1 - \sigma_s) D_s + {}^m E_{req} \beta_s \bar{P}_s) = {}^m P_{in} \end{cases} \quad (4.34)$$

This enhancement preserves the passivity of the whole teleoperation system. The proof can be shown looking at the whole architecture either from the master, or from the slave side. Interdependently of the choice, each side sees the energy at the other side proportionally scaled by its scale factor.

Proof. Slave side

Let focus on the slave side. The storage function that represent the energy in the system is

$$\hat{H}_s(t) = \alpha H_m(t) + H_s(t) + \alpha T_m(t) + T_s(t) \quad (4.35)$$

Using (4.10) we obtain that

$$\begin{aligned}\dot{\hat{H}}_s(t) = & -\alpha D_m(t) + \alpha F_m^T v_m + \sigma_m \alpha D_m(t) + \alpha (\sigma_m {}^m P_{in} - {}^m P_{out}) \\ & - D_s(t) + F_s^T v_s + \sigma_s D_s(t) + (\sigma_s {}^s P_{in} - {}^s P_{out}) \\ & + \alpha u_{t_m} y_{t_m} + \alpha F_h^T v_m + u_{t_s} y_{t_s} + F_e^T v_s\end{aligned}\quad (4.36)$$

Since the tanks and the robots are interconnected with the power preserving interconnection (4.11), we have that $F_i^T v_i = -u_{t_i} y_{t_i}$, where $i = m, s$.

Substituting (4.34) we have

$$\begin{aligned}\dot{\hat{H}}_s(t) = & -(1 - \sigma_m) \alpha D_m(t) - (1 - \sigma_s) D_s(t) \\ & \sigma_m \alpha \gamma {}^s P_{out} - {}^s P_{out} + \sigma_s \alpha {}^m P_{out} - \alpha {}^m P_{out} \\ & + \alpha F_h^T v_m + F_e^T v_s\end{aligned}\quad (4.37)$$

Rearranging terms, we end up with

$$\begin{aligned}\dot{\hat{H}}^s(t) = & -(1 - \sigma_m) D_m(t) - (1 - \sigma_s) D_s(t) \\ & -(1 - \sigma_m) {}^s P_{out} - (1 - \sigma_s) \alpha {}^m P_{out} \\ & + \alpha F_h^T v_m + F_e^T v_s\end{aligned}\quad (4.38)$$

and since $\sigma_i \in \{0, 1\}$, ${}^i P_{out}$, $D_i \geq 0$ for $i = m, s$ it follows that

$$\dot{\hat{H}}_s(t) \leq \alpha F_h^T v_m + F_e^T v_s . \quad (4.39)$$

Thus (3.32) holds, which proves our statement. \square

The same could be done from the master point of view by considering the storage function $\hat{H}_m(t)$

$$\hat{H}_m(t) = H_m(t) + \gamma H_s(t) + T_m(t) + \gamma T_s(t) \quad (4.40)$$

instead of (4.35).

4.3 Implemented teleoperation schemes

The effectiveness of this approach has been evaluated with two different control schemes implemented within the transparency level: a position-position (PP), for bilateral motion synchronism and a position-force (PF) for better force reflection.

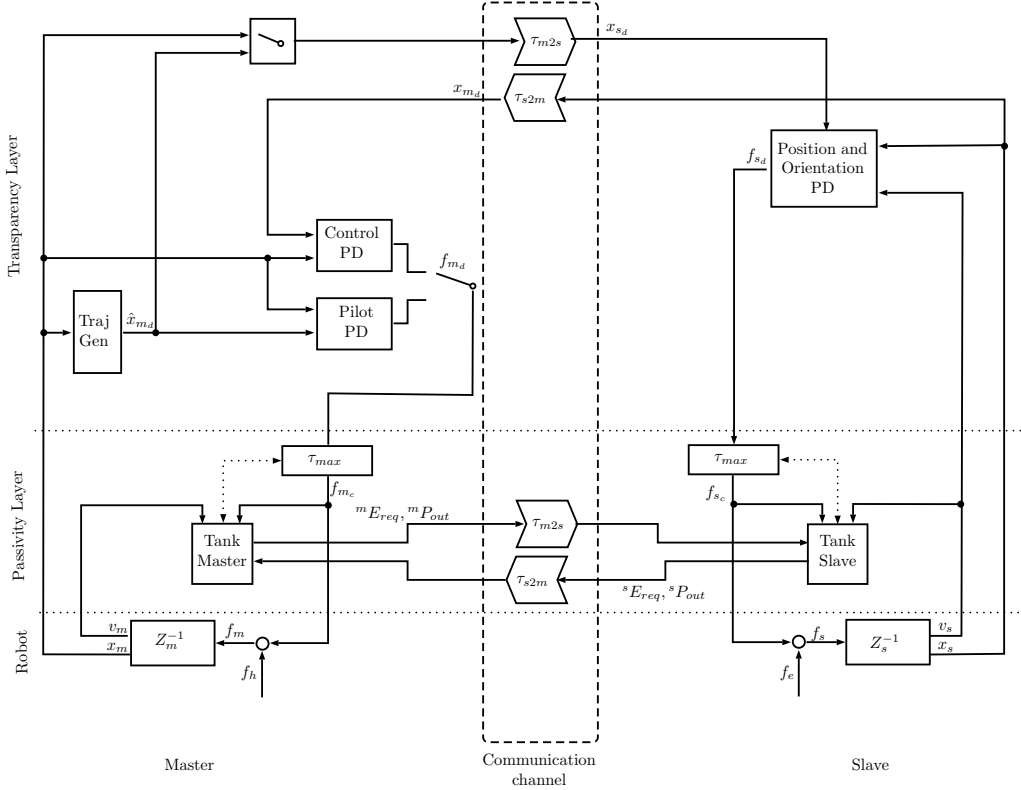


Figure 4.1: The implemented position-position architecture

4.3.1 Position - Position (P-P)

As shown in Figure 4.1, the first teleoperation schema implemented in the transparency layer is a simple Position-Position. The main goal of such schema is to achieve a synchronism between the two manipulator poses.

Master pose is sent to the slave on which a PD controller is in charge of tracking the commanded Cartesian position and orientation. Slave pose is sent back to the master and used as a feedback signal that tells the operator if the slave robot is moving in free space or if it is in contact with the environment. This is possible thanks to the virtual spring-damper coupling operated by the PD controller. In fact the virtual displacement between the two manipulator produces a force acting at both side.

When the slave is in free motion, at master side the error between the desired pose, imposed by the operator, and the feedback one is small. The slave can

freely follow the pose commanded by the master, reducing the tracking error. The operator feels this little tracking displacement as a sort of inertia.

When the slave is in contact, the tracking displacement increases. At master side the error between the desired pose and the feedback one also increases, providing a stronger reaction force that acts as a kinaesthetic feedback.

Because of the P-P architecture the error displacement is the same at both sides, thus the kinaesthetic feedback induced at master side is mainly proportional to the force being applied at master side through the relationship between $K_{p_{master}}$ and $K_{p_{slave}}$. The remaining force is due to the presence of a damping factor K_d acting on the error derivative.

The slave PD pose controller is made by two separate PD controllers that works in parallel. The former acts on the Cartesian position and performs a linear control on the position error in task space. Its outputs are the control Cartesian forces, expressed in the slave's base frame, commanded to the robot.

The position error in task space is

$$e_{pos} = (x_{pos_d} - x_{pos}) \quad (4.41)$$

where x_{pos_d} is the vector of Cartesian position commanded by the master and x_{pos} the vector of current slave position

The position PD controller is formulated as

$$\mathbf{f}(t) = K_{p_{pos}} e_{pos}(t) + K_{d_{pos}} \frac{de_{pos}(t)}{dt} \quad (4.42)$$

where $K_{p_{pos}}$ and $K_{d_{pos}}$ are 3×3 diagonal matrices of the position control gains. The latter acts on Cartesian orientation and performs a linear control action on the orientation error in task space. Its output are the control Cartesian torques, expressed in the slave's base frame, commanded to the robot. The orientation error in task space is

$$e_{ang} = (x_{ang_d} - x_{ang}) \quad (4.43)$$

where x_{ang_d} and x_{ang} are the Cartesian orientation commanded by the master and the current slave orientation respectively.

The orientation PD controller is formulated as

$$\mathbf{o} = K_{p_{ang}} e_{ang}(t) + K_{d_{ang}} v_{ang}(t) \quad (4.44)$$

where $K_{p_{ang}}$ and $K_{d_{ang}}$ are 3×3 diagonal matrices of the position control gains, and $v_{ang}(t)$ is the slave's Cartesian angular velocity vector. The stronger damping action on the orientation controller helps the system stability.

The two components of the Cartesian wrench command, forces f and torques o are then passivated by the passivity layer (τ_{max}) and then mapped into joints torque through the Jacobian Pseudo-inverse. This mapping is performed by the robot itself.

At master side, when performing the standard bilateral P-P teleoperation, acts the same PD controller presented for the slave, tuned with proper values for $K_{p_{pos}}$, $K_{d_{pos}}$, $K_{p_{ang}}$ and $K_{d_{ang}}$.

Before performing the puncturing, the clinician could switch from this controller to a specialized one, previously mentioned as *pilot mode*, designed to help the operator to perform a more precise puncture along the needle's z axis direction.

A trajectory generator holds the values of the master orientation and $x - y$ position relative to the end-effector reference frame at switching time. The z position, instead, is always the current one.

This new conditioned command, \hat{x} , is provided both as a reference for the slave and as a reference value for the local PD controller.

In order to provide a different kind of feedback when in this mode, the PD controller is replicated thus we could use different gains.

The operator feels a constrain force that guides him moving only along z , in this direction the coupling between the master and the slave is preserved together with the feedback.

This controller switching ability is clearly a non passive solution. However we can safely apply such strategy because of the Two-Layer architecture guarantees the passivity of the system.

4.3.2 Position - Force (P-F)

The latter teleoperation scheme implemented is a simple Position-Force, an illustration is available in Figure 4.2, The main goal of such scheme is providing a more effective force feedback to the operator.

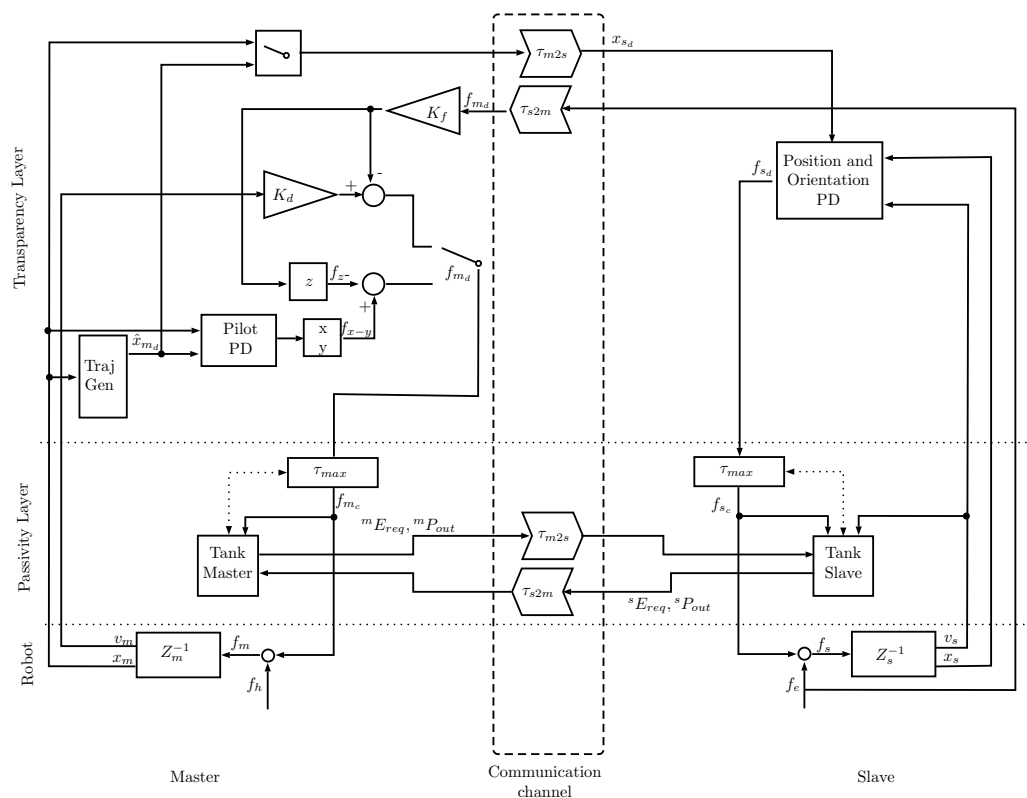


Figure 4.2: The implemented position-force architecture

Master pose is sent to the slave on which, the same PD controller of the previous scheme is in charge to track the commanded Cartesian position and orientation. The feedback signal f_{slave} from the slave is the interaction wrench provided by a force sensor. At the master side this signal could be scaled down by the K_f gain which is, again, a 6×6 diagonal matrix of gains. Because of the two layer algorithm, we have to produce some amount of energy to perform actions at slave side while in free motion (if there are no interaction forces, the commanded force on the master is null and consequently the instantaneous power is zero). This is achieved introducing a small and constant damping. The wrench applied to the master and thus perceived by the operator is

$$\mathbf{f}(t) = K_f f_{slave}(t) - K_d v_m(t) \quad (4.45)$$

where K_d is a 6×6 diagonal matrix of damping gains and v_m is the master velocity.

Even in this architecture, the clinician before performing the puncturing could switch to the specialized controller. The purpose is the same from the P-P architecture: provide a tool to help the operator to perform a more precise puncture along the needle's z axis direction.

To achieve this goal the *pilot mode* for this schema is a hybrid position-force controller. It acts as PD controller for orientation and for the position along $x - y$ axes while keeping the original slave force feedback along z .

The trajectory generator holds the values of the master orientation and $x - y$ position relative to the end-effector frame of reference at switching time. This conditioned signal, \hat{x} , is provided both as a reference for the slave and as reference value for the local PD controller. The operator feels a constrain force that forces him moving only along the master tool z axis, in this direction the operator feels the corresponding force feedback from f_{slave} modulated through K_f gain. This controller switching ability is clearly a non passive solution. However we can safely apply such strategy because of the Two-Layer architecture guarantees the passivity of the system.

4.4 Discussion

In this chapter with the Two-Layer teleoperation architecture modelled as a port-Hamiltonian system, we showed that energy evaluation is equivalent in task and in joint space. A proper energy scaling strategy has been proposed to allow the coupling, in a passive way, of very different manipulators. Finally we described the two teleoperation schemas implemented upon this formulation of Two-Layer algorithm.

Chapter 5

Robotics Platforms

In this chapter we present the experimental setup on which the proposed architecture has been developed, implemented and tested. First we will present the master and slave robots, then the general architecture is explained and finally we discuss on the impact that the limits of such setup have on the implementation.

5.1 Manipulators

This bilateral teleoperation setup is based upon two of the manipulators available in the Altair laboratory of the University of Verona. The master console is a Sensable Phantom Omni (recently rebranded as 3D-System Touch). The slave device is a Barret WAM in the 7-DoF configuration.

5.1.1 Phantom Omni

The Phantom Omni is a commercial, portable haptic device with six Degrees of Freedom (DoF) with the three translational degrees of freedom actuated, developed by Sensable Technologies. It is based on a serial architecture, which means that the handle is connected to the housing by a single serial chain. The device evolved from research done by Thomas Massie and Dr. Kenneth Salisbury at MIT.

The workspace of the Phantom Omni is $16\text{cm} \times 12\text{cm} \times 7\text{ cm}$ ($\text{W} \times \text{H} \times \text{D}$) and can provide a peak force feedback up to 3.3 N. Thanks to its six

DoFs and a nominal position resolution of around 0.055 mm the device is used in various professional environments. The Phantom Omni is currently sold by 3D-System under the product name Touch. The models available in the lab are the firewire and USB ones, both lacks of driver support for modern Linux distributions. Thus a Windows machine is a mandatory requirement to adopt the Phantom Omni in this setup.

The device ships with its SDK, OpenHaptics, designed for a simple control of the device. It provides two abstraction levels: namely HU and HD. The former it's oriented to provides haptic feedbacks from a virtual graphics scenario, the latter is close tight to the hardware and provides the Phantom's status information like stylus pose, stylus velocity and pressed buttons.

The available data vary upon the availability of actuated DoF on device in use: for the Omni model the API does not provide either angular velocity or the evaluated geometric Jacobian. The pose frame of reference, which is not clearly addressed in the documentation, has been empirically found in the middle of the Cartesian workspace. Finally, this is another unclear point from the available documentation, the pose provided by the HD API refers not to the stylus tip, but to the middle point of the gimbal. These are useful information when dealing with the virtual model of the device. A custom version of the urdf model [1] enables the correct visualization of the pose from HD API into the RVIZ visualizer.

5.1.2 WAM

The robotic arm used in this setup as slave robot is called WAM, from Barrett Techonology. The WAM is a manipulator available in two main configurations, 4 and 7-DoF, both with human-like kinematics. The manipulator available at the Altair laboratory has the seven degrees of freedom configuration, which offers better adaptability and dexterity and is shown in Figure 5.1b.

The uniqueness of the WAM arm lies in its backdriven cable drives, similar to human tendons. This kind of design concentrates the weight at its base and makes the whole arm light enough to have little brake time together with high acceleration and flexibility. Moreover, its lightness translates into

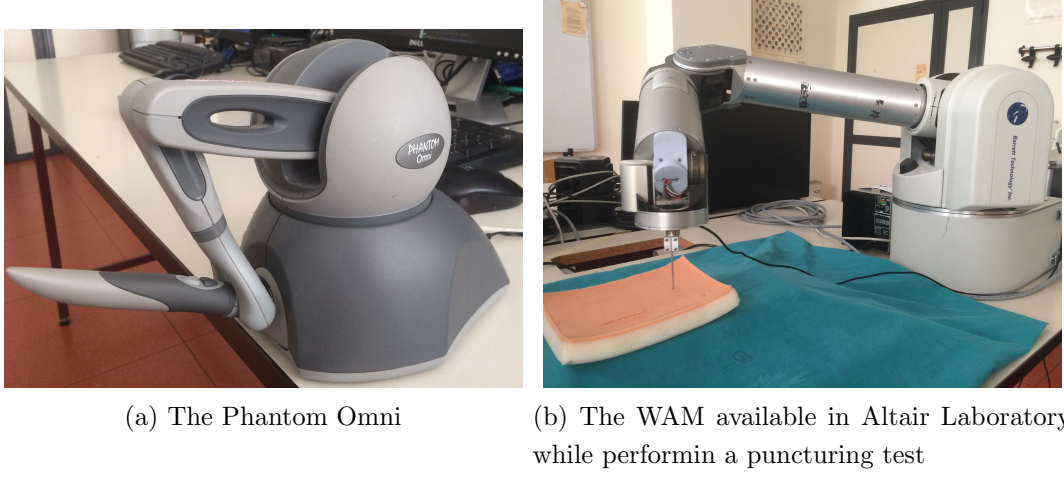


Figure 5.1: The two manipulators

power saving. Table 5.1 its the *Denavit-Hartenberg* parameters of the Barrett Wam's arm.

For the purpose of this work, a needle with its holder has been mounted at the end effector. The assembly includes a force sensor, the ATI Nano 17, that provides the external interaction forces in the Position - Force teleoperation schema. The whole assembly, from its base to the needle's tip, could be seen as a unique static transformation that could be added at the end of the WAM's kinematic chain (the last line in Table 5.1). Figure 5.2 shows the WAM end-effector.

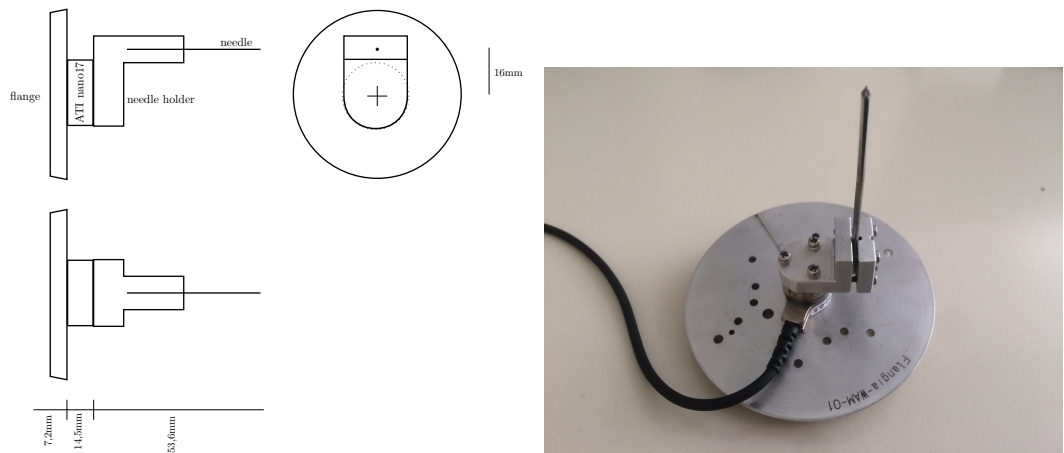
In this thesis we are focusing on the feasibility of the teleoperation architecture thus we are not interest on dealing with needle bending. Because of that, we applied to the needle holder a nail that represent an acceptable trade-off for our intent. However, with a different needle holder shown in Figure 5.3 that has been designed in the meanwhile, in future we will be able to evaluate the system with a real crioablation needle.

5.1.3 ATI Nano 17

The ATI Nano 17 is the force sensor attached between the WAM tool flange and the needle holder. It's a small six axis force/torque sensor with silicon strain gages. The one available in Altair Laboratory has the SI-50-0.5

	θ	d	a	α
<i>Robot</i>	θ_1	0	0	$-\pi/2$
	θ_2	0	0	$\pi/2$
	θ_3	0,55	0,045	$-\pi/2$
	θ_4	0	-0,045	$\pi/2$
	θ_5	0,3	0	$-\pi/2$
	θ_6	0	0	$\pi/2$
	θ_7	0,06	0	0
<i>End-Effector</i>	$-0, 16\pi$	0,085	0,08	0

Table 5.1: D-H parameters of the WAM manipulator with needle holder as end-effector



(a) Schematics of the whole needle holder assembly

(b) The end-effector

Figure 5.2: The needle holder assembly

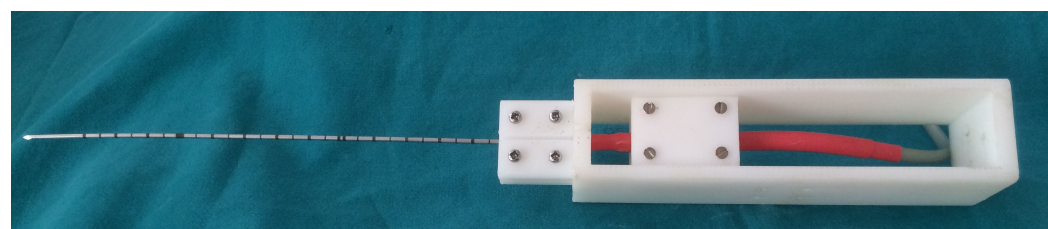


Figure 5.3: The crioablation needle holder

	Sensing ranges	Resolution
F_x	50N	1/80N
F_y	50N	1/80N
F_z	70N	1/80N
T_x	500Nmm	1/16Nmm
T_y	500Nmm	1/16Nmm
T_z	70Nmm	1/16Nmm

Table 5.2: ATI Nano 17 SI-50-0.5 calibration data

calibration whose sensing range and resolution has been reported in Table 5.2. By supplying the transformation between the sensor and the needle tip, the software in its data acquisition *NetBox* provides the measured wrenches correctly applied at the needle tip frame.

5.2 Software Architecture

The teleoperation schema has been implemented on three machines: two Linux machine and a Windows machine. The communication relays on the ROS framework and on a custom made socket. The socket acts as a bridge between the ROS environment and the windows machine. Two nodes that control the two manipulators, implementing respectively the master's and slave's Two-Layer controller, are connected through a couple of network simulator node. In the middle a *frame mapper* node maps the frame reference between the two manipulators.

The communication between the nodes relays on a custom ROS message which embeds all the information required both by the Two-Layer algorithm and the teleoperation strategy implemented at the transparency level. The message structure is reported in Table 5.3 while the software architecture is sketched in Figure 5.4. Finally in Figure 5.5 we show an overview of the ROS nodes and topics involved. They will be explained within this section.

Message type	Name
std_msgs/Header	header
geometry_msgs/Pose	pose
geometry_msgs/Twist	twist
geometry_msgs/Wrench	wrench
std_msgs/Float64	energy_request
std_msgs/Float64	power_send

Table 5.3: The custom ROS message structure

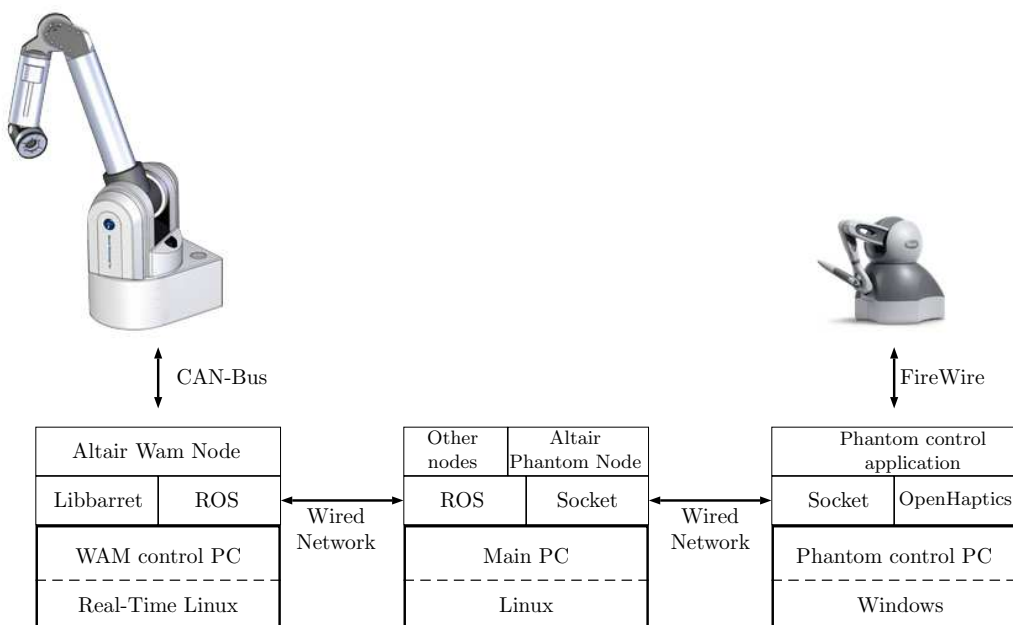


Figure 5.4: Hardware/Software overview of the teleoperation architecture

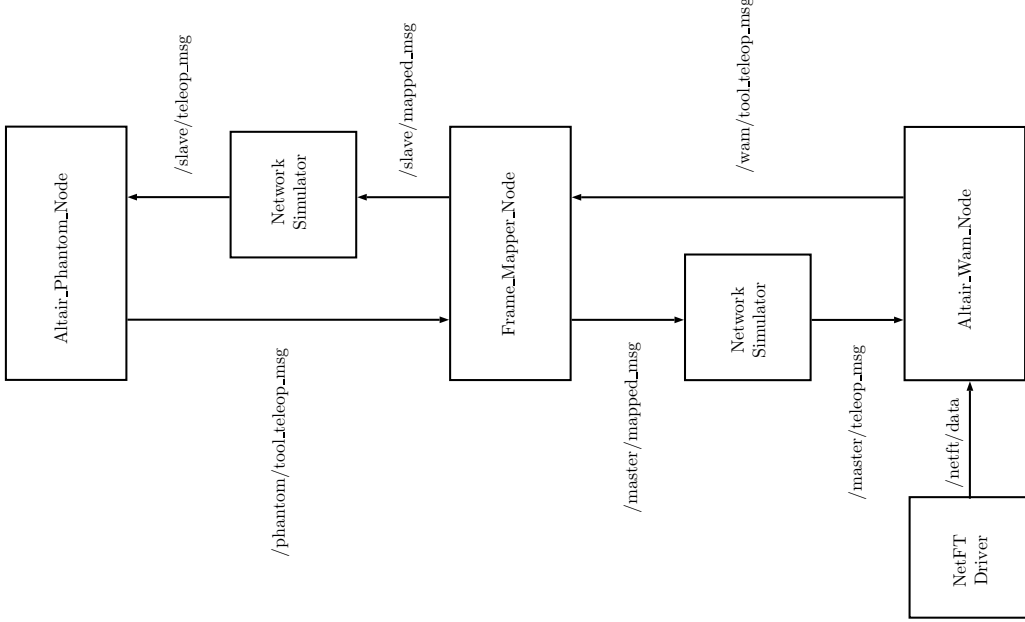


Figure 5.5: Nodes and topics in the implemented architecture

5.2.1 ROS

The Robot Operating System (ROS) [2] is a open-source framework based on the component-based software engineering paradigm that provides the middleware for inter-process communication. Initially developed by the Stanford Artificial Intelligence Laboratory its development continued at Willow Garage, a robotics research institute, and now it's maintained and improved under the action of the ORSF foundation [2].

As a meta-operating system, ROS offers features such as hardware abstraction, low-level device control, implementation of commonly used functionalities, message communication between processes and package management. It uses an asynchronous publish/subscribing mechanism made possible by message standardisation and encapsulation that make the external interface of every node as general as possible, allowing quick nodes exchange and, thus, great architectural flexibility. Each independent block, called *node*, executes a particular task of a process and can communicate with other nodes through *topics*. This allows to create complex architectures by aggregating many simpler entities and simplifies the use of different tasks or different

methods for the same task.

Additionally to the message-passing system, the core ROS component, called *roscore*, maintains a global execution time for the nodes to achieve synchronisation. Each node executes separately with its own internal clock driven by the set execution rate. At every message sent/received, containing the internal time information, the core component updates the global time by following the execution status provided by these messages.

5.2.2 Frame Mapper

The frame mapper node is fully transparent to the application and acts by matching both pose and force reference between the two manipulators. To keep the developed architecture and each node inside it as general and modular as possible with the purpose of reusability of the developed master and slave nodes, we develop this node in a such a way it could match any pair of manipulators by providing, in its configuration, the transformation between the master and the slave base frame.

When launched, the node computes the difference between the two initial poses, then applies the proper transformation in both directions.

It could operate with any custom message type, the only requirements is the definition of a pose message inside the custom generated message.

5.2.3 WAM control

The WAM control node (`Altair_Wam_Node`) runs on the first machine, which execute the Ubuntu Linux 14.04.1 distribution patched with real time Xenomai co-Kernel. This node is build on top of the Libbarret SDK. It continuously streams the status of the robot to the ROS infrastructure by publishing a set of topics with ROS standard messages. It provides the following informations:

- **End-effector position** referred both to the base and the tool frame of reference.
- **End-effector twist.**

- End-effector wrench.
- Joints position.

It offers some convenient ROS services to exploit simple actions like autonomous reaching of a desired configuration or the ability of idleing the robot (means the robot is gravity compensated and free to move by hand). On the basis of the ROS message received, the node engages the proper controller among the implemented ones.

This is possible by sending the control message to the proper control topic from the set of the topics the node subscribe itself. There are eight controller available right now: Cartesian position, Cartesian orientation, Cartesian pose (which is the combination of the two previous ones), Cartesian velocity, Cartesian wrench, joint position, joint velocity and finally the Two-Layer controller developed for this work.

The Two-Layer controller provides the implementation of the passivity layer, as described in Section 4.2, with the only difference that each threshold is designed as a range (a bottom and top thresholds) without violating the constraints between these variables, as explained in Section 4.10.

The transparency level implements the control strategy. For this work it's a position PD controller, which is the same for the two teleoperation schemas tested and implemented. It also provides the ability to filter the incoming control position, in order to smooth the control action when the input signal is noisy, as it happen with the measurements received from the Phantom Omni. The output of the node, the passivated control torque in task space, is passed to the underlying Libbarret real-time subsystem in charge of the low level control of the robot.

5.2.4 Phantom Omni control

Because of the lack of support for the modern Linux kernel, either for the old firewire model, and for the latest USB model, the Phantom Omni is physically attached and controlled on a Windows machine. The interface with the ROS environment is ensured through a custom designed network socket connection.

The Phantom control node (`Altair_Phantom_Node`) runs on another Linux machine, and it could establish a bidirectional communication with the Windows machine up to 1kHz. The design of the control node provides an abstraction of the Phantom manipulator in such a way that the socket interconnection could be easily replaced by a native device communication, through the OpenHaptics API, when the proper device driver will be available. In fact on the Windows machine, the software simply receives commands from the remote controller and send back the Phantom status.

On top of this device abstraction, a general, abstract *Phantom controller* has been designed. It's a partially implemented class which defines the standard *Phantom controller* interface and implements a common thread that streams to the ROS network the device status in the same way the WAM control node does. With this design, each specialization of the Phantom controller could be simply loaded into the Phantom ROS node and managed inside it in a standard way. For this work, two specializations of the Phantom Controller have been written: one for the position-position architecture and one for the position-force architecture. These specializations share the passivity layer implementation and most of the controller design with the WAM control node.

5.2.5 Network Simulator

This node has the purpose to simulate a real network environment. It could provide constant and time-varying delay with packet losses. A couple of this node provides the communication delay in both direction.

5.2.6 Neft node

This node simply reads the wrench value from the ATI Nano 17 NetBox and streams it to the ROS network.

5.2.7 Virtual visualizer

The setup includes a virtual visualizer, based upon RVIZ, where a model of both the manipulators could be seen in a 3D environment. This tool

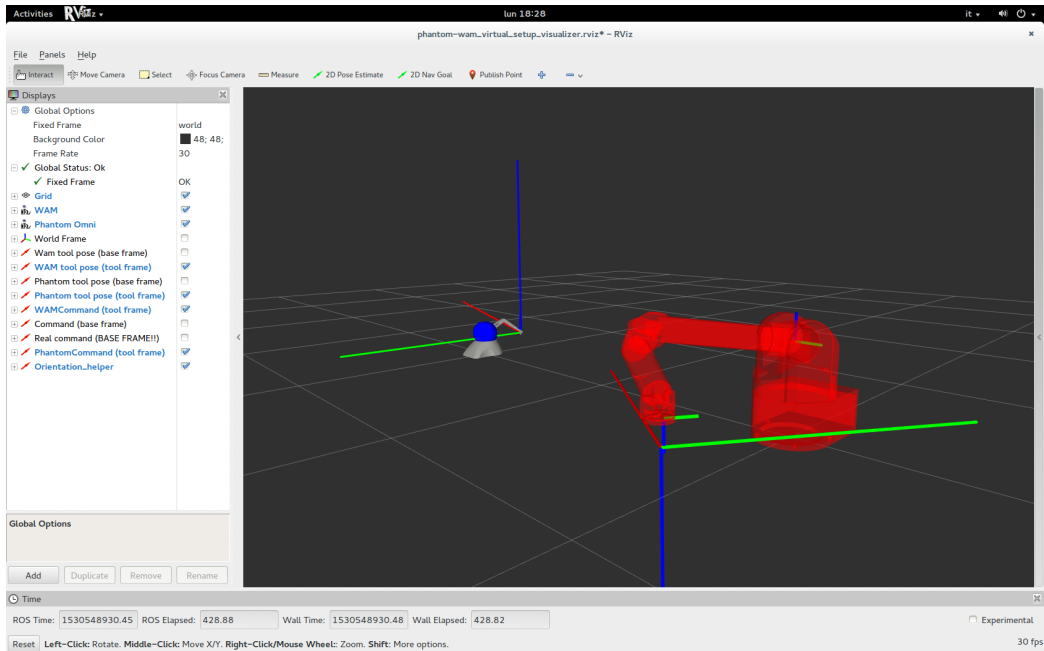


Figure 5.6: Screenshot of the visualizer in action

is useful for a pre-operative check on the correctness of the transformation applied to the commanded pose for each manipulator.

5.2.8 Setup limitations

Because of the only three translational degrees of freedom actuated on the Phantom Omni, this setup implements only a translational bilateral coupling. This means that also the energy computation, both at master and slave sides, is performed only on translation.

The energy evaluated is the one flowing from the controller to the robot. The lack of actuation means that no torque is exerted on the master and consequentially the instantaneous power is always equal to zero.

Because we cannot control the orientations, for them we have to rely on a unilateral teleoperation schema.

Unfortunately we cannot measure the real interaction force with the operator, but only the commanded one. However when the force on one axes exceeds the maximum values that the Phantom Omni could render, its APIs crops the value to 3.3N. This limits the transparency of the system so we set K_f

looking for a trade off to achieve a good transparency, meaning that the operator is still able to distinguish the insertion stage from the free motion.

Chapter 6

Case Study

In order to prove the effectiveness of the variation implemented on the Two-Layer framework and the feasibility of the two teleoperation schemas proposed to perform a puncturing, a set of tests has been conducted.

For each teleoperation schema we collected the result from a test scenario in which a synthetic double-layer tissue is punctured with two different angles of approach, namely 90° and 45° , demonstrating the stability of the control architecture applied to this procedure. Then, because of taking into account the case of multiple puncturing site a free motion test has been also carried out.

For each teleoperation schema the system parameters are the same for all the experiments. This choice goes in the opposite direction of showing the best possible results. Instead of tuning the system to achieve its best performance for each experiment, we want to investigate also its flexibility by performing different type of experiment with the same tuning. We believe that with this choice we will be able to better understand also the limits of our system with the purpose of enhance it in a near future.

The full set of tests has been carried out both in a undelayed scenario and with 0,1s of constant channel delay (which means a 0,2s round-trip-time delay). That is reasonable in our scenario.

In the plots that we will be shown below (from Figure 6.1 to Figure 6.36) the correspondence between the threshold names and the legend of the plots is reported in Table 6.1.

Thesis	Plots
T_{ava}	Eava
T_{req}	Ereq
$T_{TLC_{top}}$	TLC top
$T_{TLC_{bot}}$	TLC bott
ε_{top}	Emin
ε_{bot}	is the grey area

Table 6.1: Thresholds names in plots

For clarity the parameter H_d in Section 3.6.2 has been renamed T_{TLC} and, as mentioned in Section 5.2.3, the threshold has been implemented as a range. The TLC gain factor α that appears in Section 3.6.2 is now called K_{TLC} .

Because the two manipulators express their pose in their frame of reference, and the linking between them is provided through the *Frame Mapper*, we choose to show the results as follows. For each experiment we will show how the slave robot tracks the command received from the master side by showing the position of the slave with respect the master's position both expressed in the slave reference frame. The same is done for the orientation. Because we are interested in the force feedback provided to the operator, we show the forces applied in the master reference frame with respect of the tool.

		Slave	Master	Master _{pilot}
Position PD	$K_{p_{pos}}$	500.0	50.0	50.0
	$K_{d_{pos}}$	5.0	0.15	0.15
Orientation PD	$K_{p_{ang}}$	6.0	0.0	0.0
	$K_{d_{ang}}$	0.06	0.0	0.0
Passivity Layer	\bar{T}	1000.0	1000.0	
	T_{ava}	550	400	
	T_{req}	450	300	
	$T_{TLC_{top}}$		400	
	$T_{TLC_{bot}}$		300	
	ε_{top}	200	150	
	ε_{bot}	100	100	
	\bar{P}	1.0	0.5	
	K_{TLC}		0.03	
	Scale Factor (α/γ)	1/6	6.0	

Table 6.2: System's parameters for the Position-Position architecture

6.1 Position-Position

The first set of experiments we are going to show is about the Position-Position architecture. The experimental setup has been tuned with the parameter listed in Table 6.2 which are described in Sections 4.1.3 and 3.6.2. Because of the P-P architecture, in which the wrench applied by the controller is mostly proportional to the error displacement between the coupled pose of the two manipulators, we choose to scale the slave force down by a factor 10

$$\frac{s K_{p_{pos}}}{m K_{p_{pos}}}$$

to show how the command forces are tracked at both sides. In fact the PD controller embeds also a derivative term, $K_{d_{pos}}$, that operates on the variation of the error displacement. Its influence is less prominent than the proportional term which has the greater impact on the control action.

6.1.1 Without Delay

Free motion

The free motion test of the slave robot with the environment (Figures 6.1 to 6.3) shows the behaviour of the system when no interaction occurs. In Figure 6.1 we can see a good position tracking between the two manipulators.

The orientation tracking, as shown in Figure 6.2, is less precise than expected. This is due to a limits of the slave robot, i.e. the WAM manipulator, that manifests some undesired mechanical coupling between the fifth and the sixth joint, whose also tends to move in jerks specially for small movements.

The energy balance in the system is assured and the master is able to provide enough energy to the slave without draining its tank.

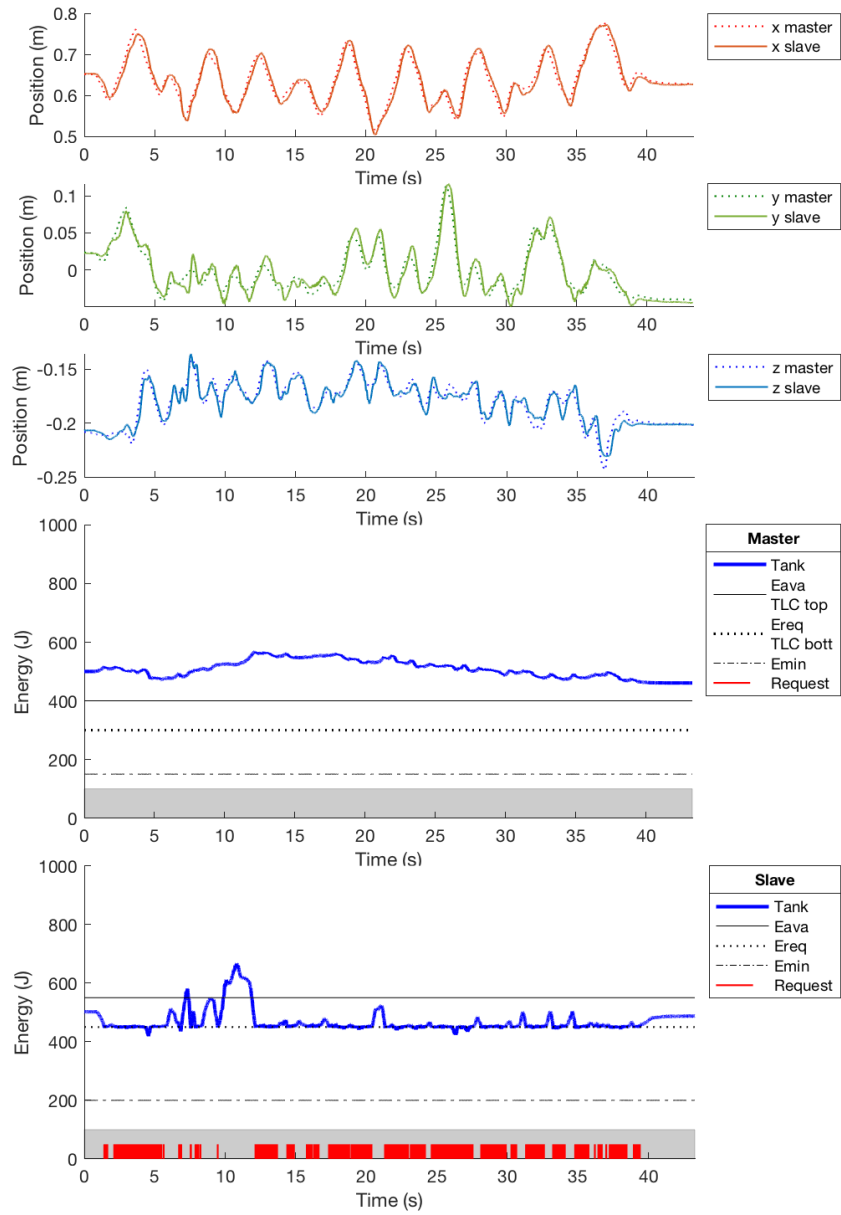


Figure 6.1: Position tracking in free motion. P-P architecture without delay.

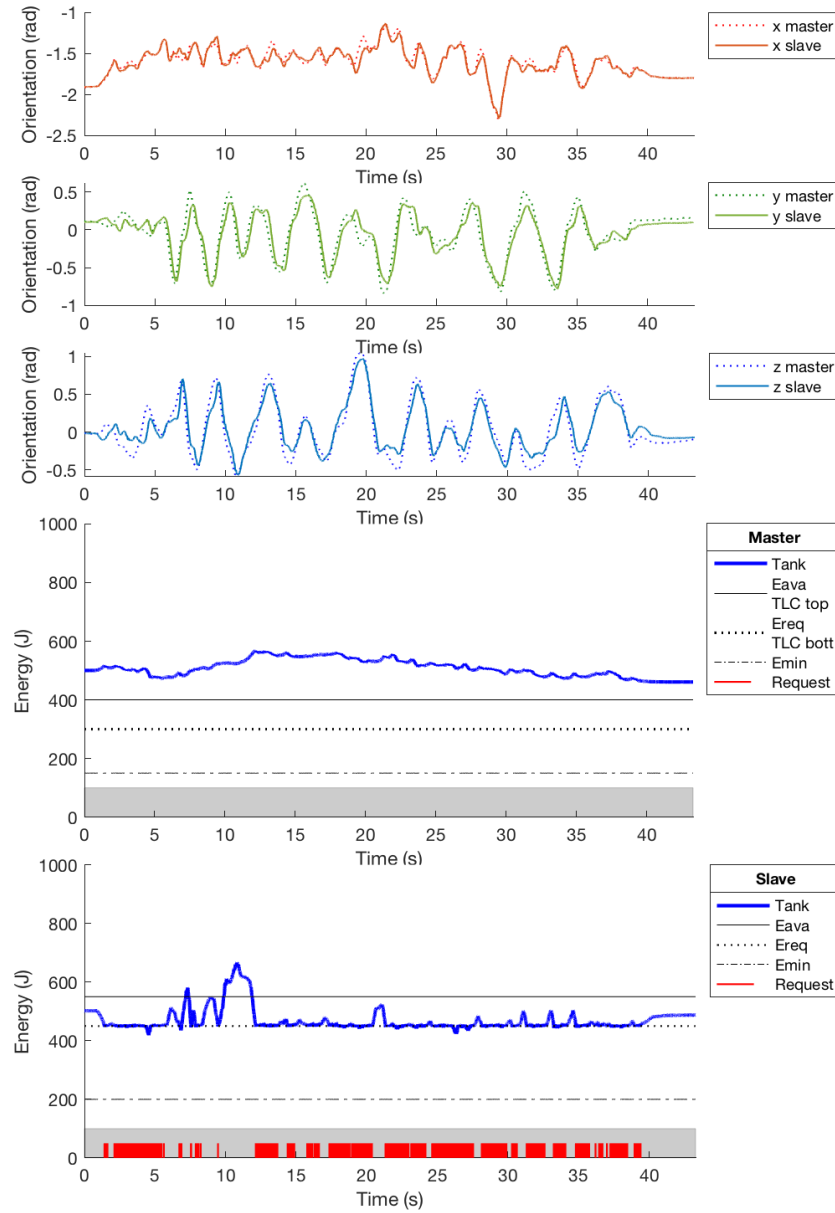


Figure 6.2: Orientation tracking in free motion. P-P control architecture without delay.

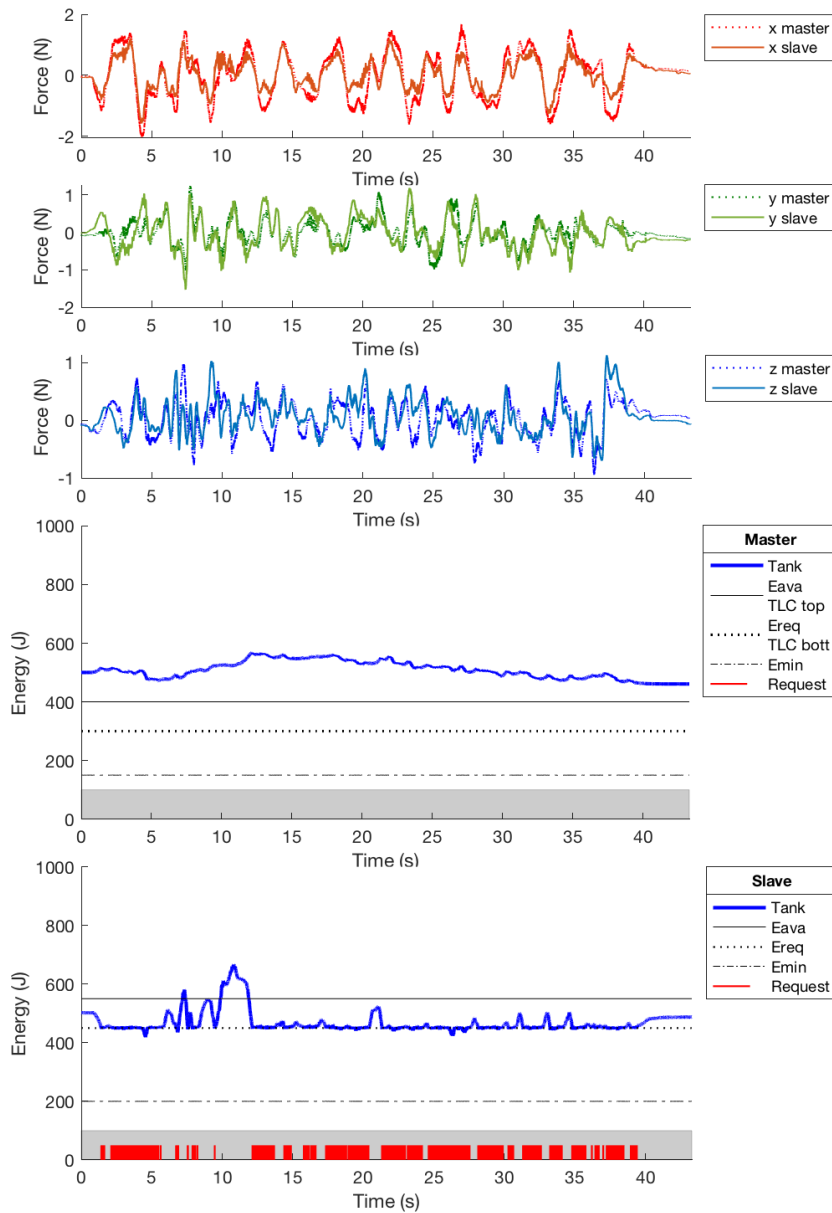


Figure 6.3: Force tracking in free motion. P-P control architecture without delay.

Insertion with 90° approaching angle

In this test (Figures 6.4 to 6.6) the first two punctures have been done within the *Pilot Mode*, described in Section 4.3.1, and the other two with the standard controller.

With this switch of controller we want to show the benefit of the *Pilot Mode* for the insertion procedure. The change of controller at time 38.8s is highlighted by a vertical line.

The motion along of the $x - y$ reference from the master in Figure 6.4 is due to it's not perfect 90° orientation with respect to the plane when starting the test (the desired motion is along the z axis, orthogonal to the tissue or the $x - y$ plane). This happens because, without actuation on the three orientation DoF on the master, it is challenging to keep the correct starting position and orientation by hand.

The *pilot mode* provides a feasible insertion trajectory thus, when we perform an insertion with this feature enabled, the energy in the system is well balanced. When the insertion is performed with the standard controller, we experienced some issues due to the lack of feedback on the orientation. In fact on the orientation the teleoperation is unilateral: when the needle sinks inside the tissue a small change in the tip orientation involves a large movements at the needle base and along its shaft.

When inside the tissue, the needle shaft is constrained in its movements by the tissue itself. If we change the orientation while performing the puncturing, the tissue exert a reaction force on the needle shaft that we are unable to provide to the operator.

We see the side effect of this force as an increased energy consumption while performing the task. When the energy consumption becomes too high, the value chosen for energy scale factor (α/γ) cannot balance the increased energy needs from the slave.

The final tracking error along z between the master and the slave is due to the fact that the needle base reaches the top of the tissue. This is a common factor of all the test.

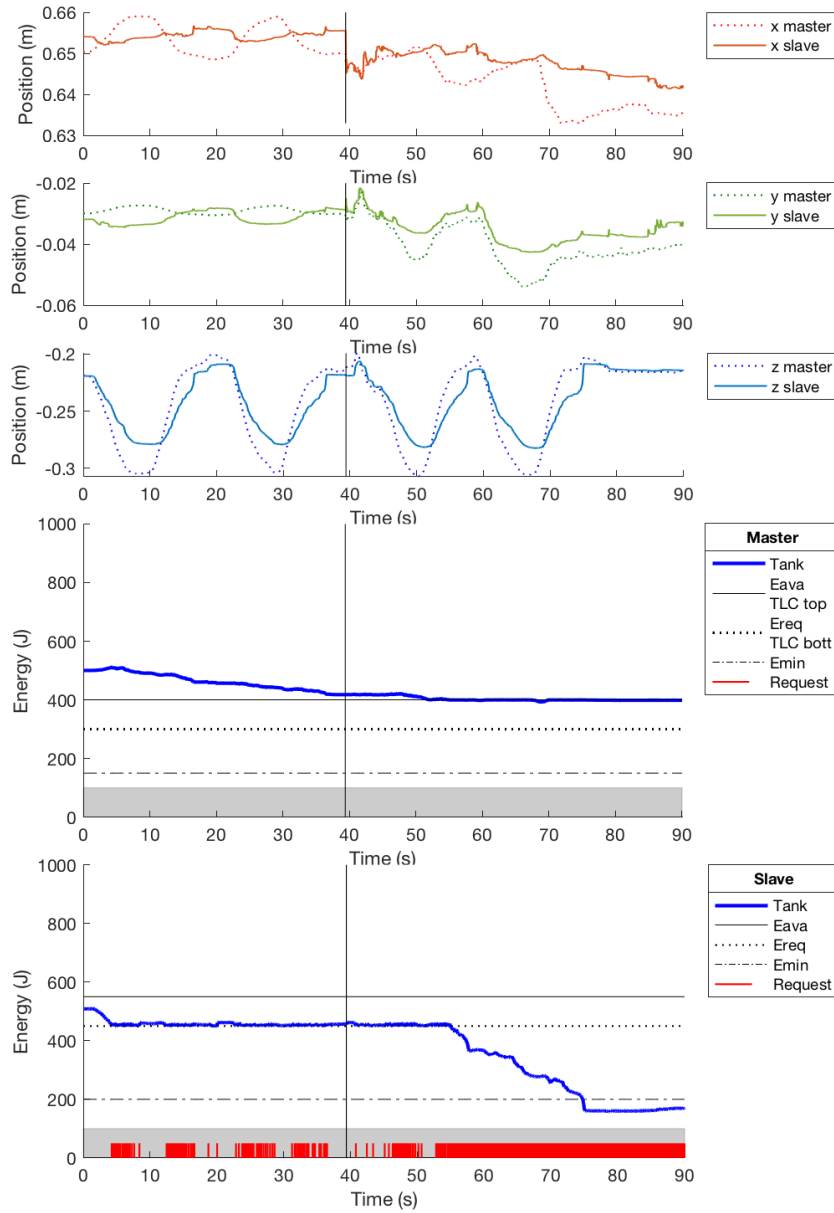


Figure 6.4: Position tracking with 90° insertion approach. P-P control architecture without delay.

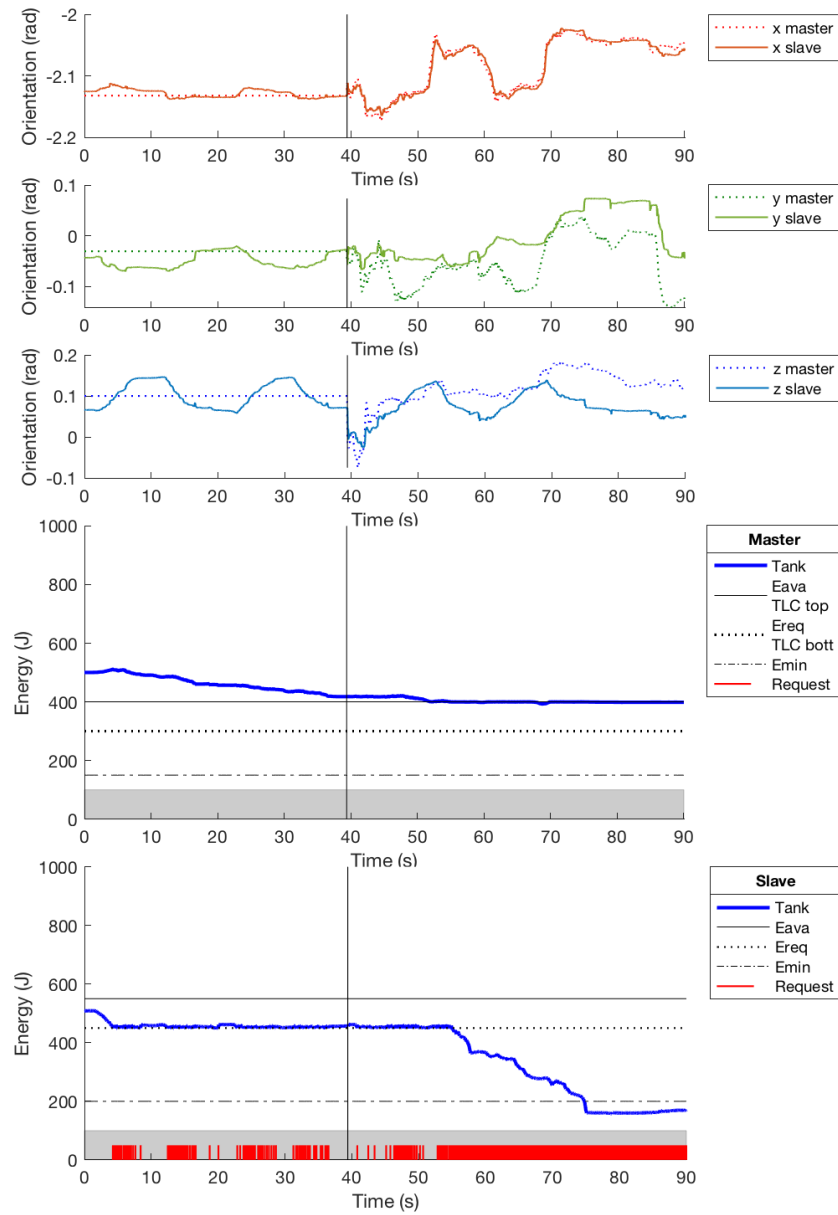


Figure 6.5: Orientation tracking with 90° insertion approach. P-P control architecture without delay.

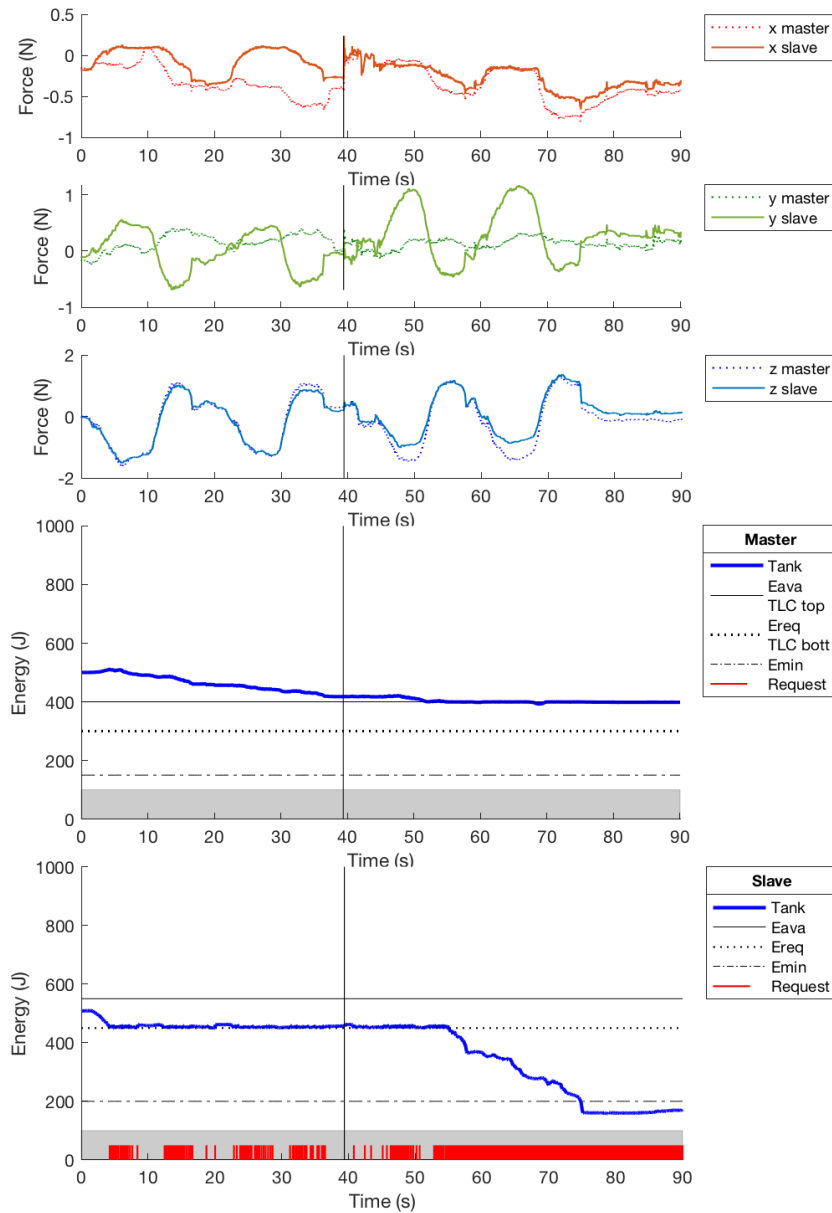


Figure 6.6: Force tracking with 90° insertion approach. P-P control architecture without delay.

Insertion with 45° approaching angle

In this test (Figure 6.7 to 6.9) the first two punctures have been executed within the *Pilot Mode* and the other two with the standard controller. The change of controller at time 30.4s is highlighted by a vertical line. The system is more stable when the insertion is artificially controlled, thus the inserting direction causes the tissue to exert a greater force on the ($x - y$) needle axes. This means that the slave requires more energy than in the previous experiment. When the operator is free to move, the slave reaches the minimum value of energy that the tank must keep at time 53s, thus it does not apply the controller commands.

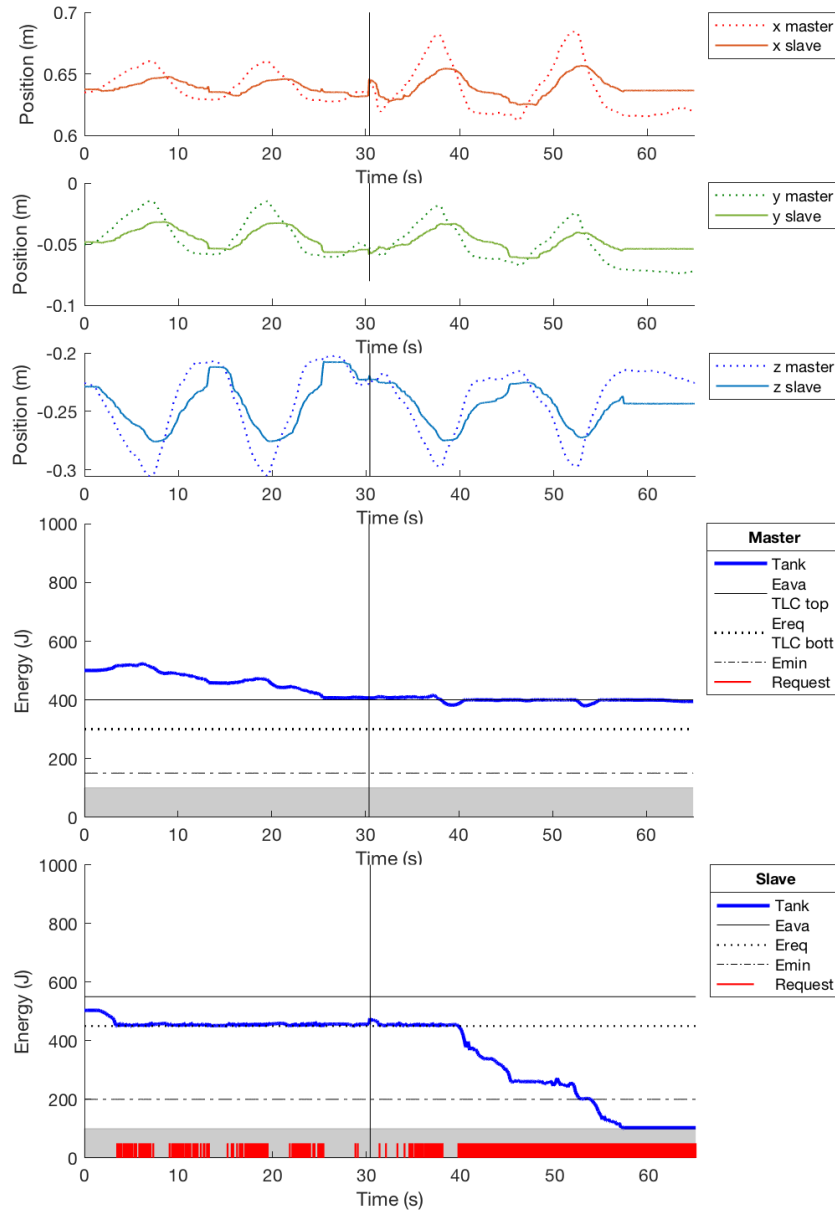


Figure 6.7: Position tracking with 45° insertion approach. P-P control architecture without delay.

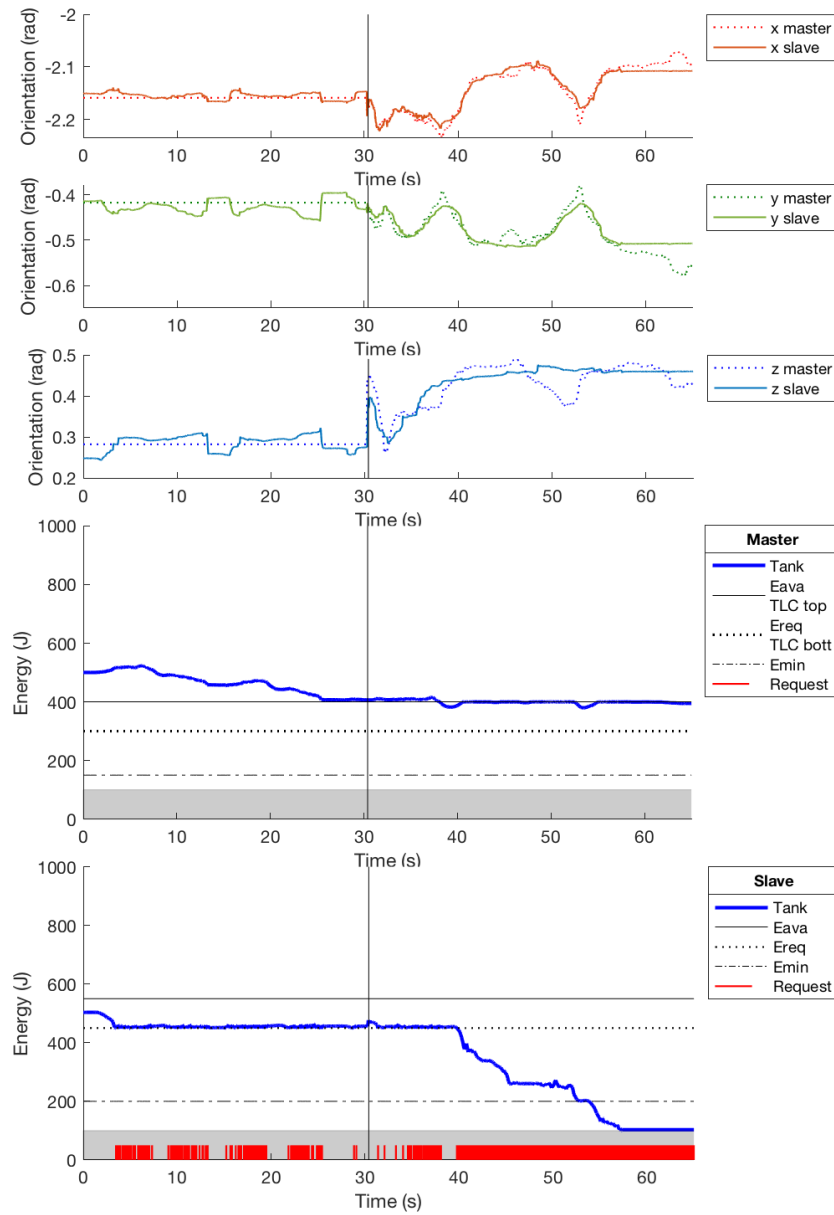


Figure 6.8: Orientation tracking with 45° insertion approach. P-P control architecture without delay.

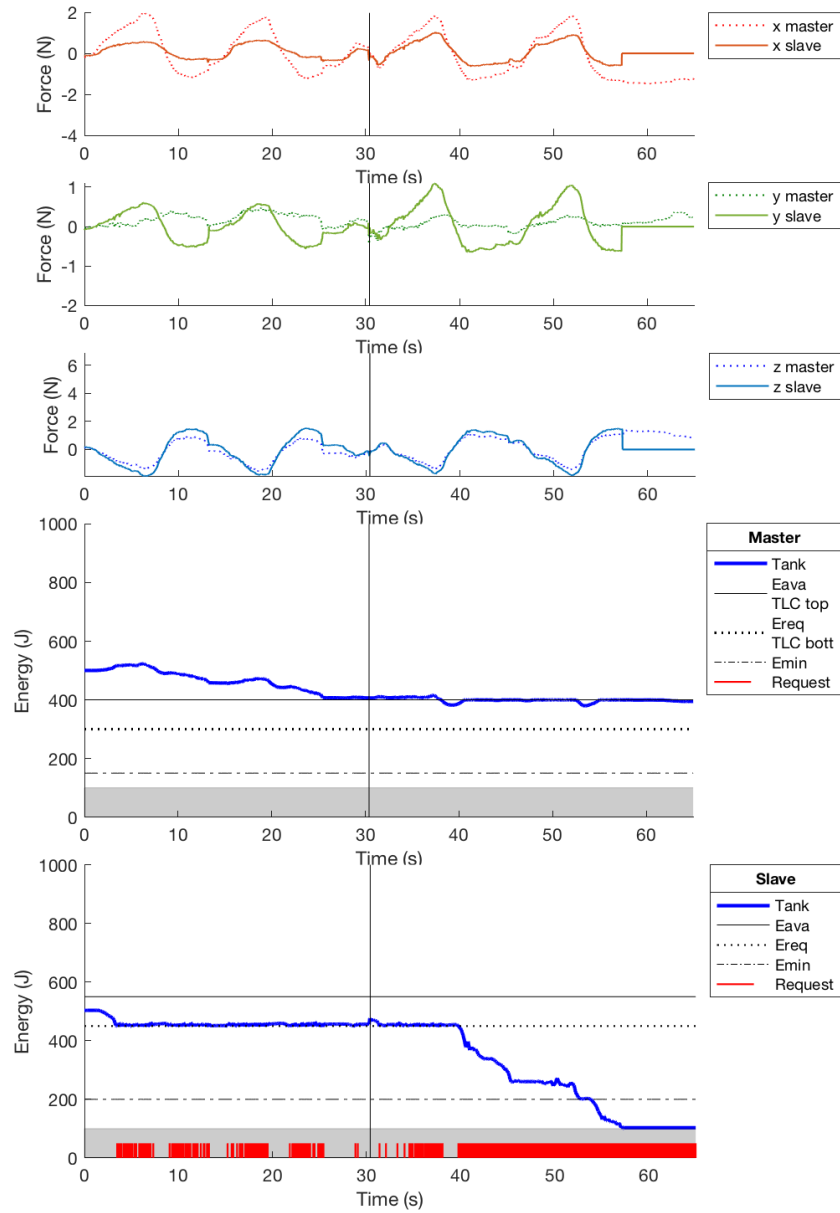


Figure 6.9: Force tracking with 45° insertion approach. P-P control architecture without delay.

6.1.2 Constant Delay

Free motion

The free motion tests have been repeated introducing a constant delay into the communication channel (Figures 6.10 to 6.12). It's interesting looking at the energy level in the tanks. Due to the delay the position tracking error increases especially when there are changes in the motion direction. This is felt by the operator as a larger force to overcome. Thus the operators provides more energy to the system. In this free motion scenario the position changes quite fast, as shown in Figure 6.10, thus the damping coefficient clearly shows its effects at the master side in Figure 6.12. The energy level in the slave tank increases and decreases really fast. This is due to the delay: in fact the system not only sees the energy requests delayed in time but, when the tank that is performing the request reaches the desired level of energy stored inside it, a RTT is needed to stop the incoming energy flow.

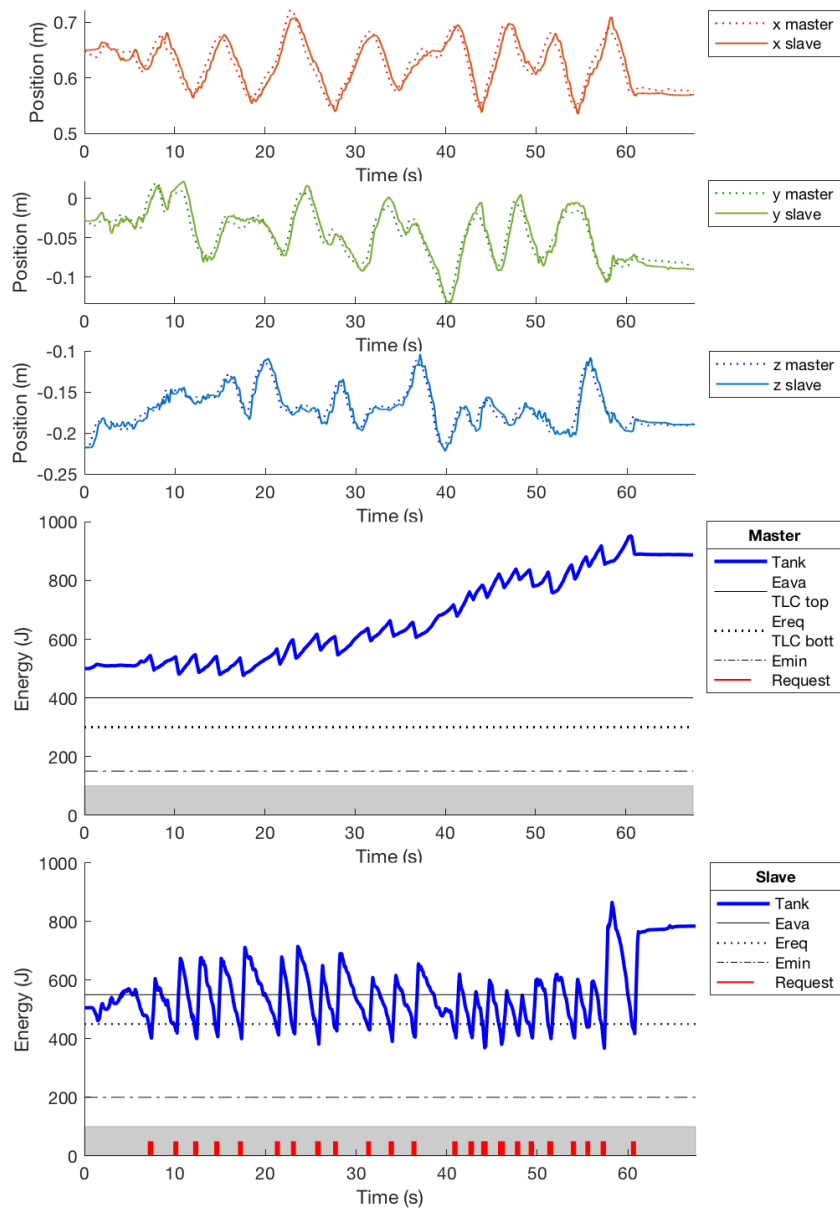


Figure 6.10: Position tracking in free motion. P-P control architecture with 0.2s RTT delay.

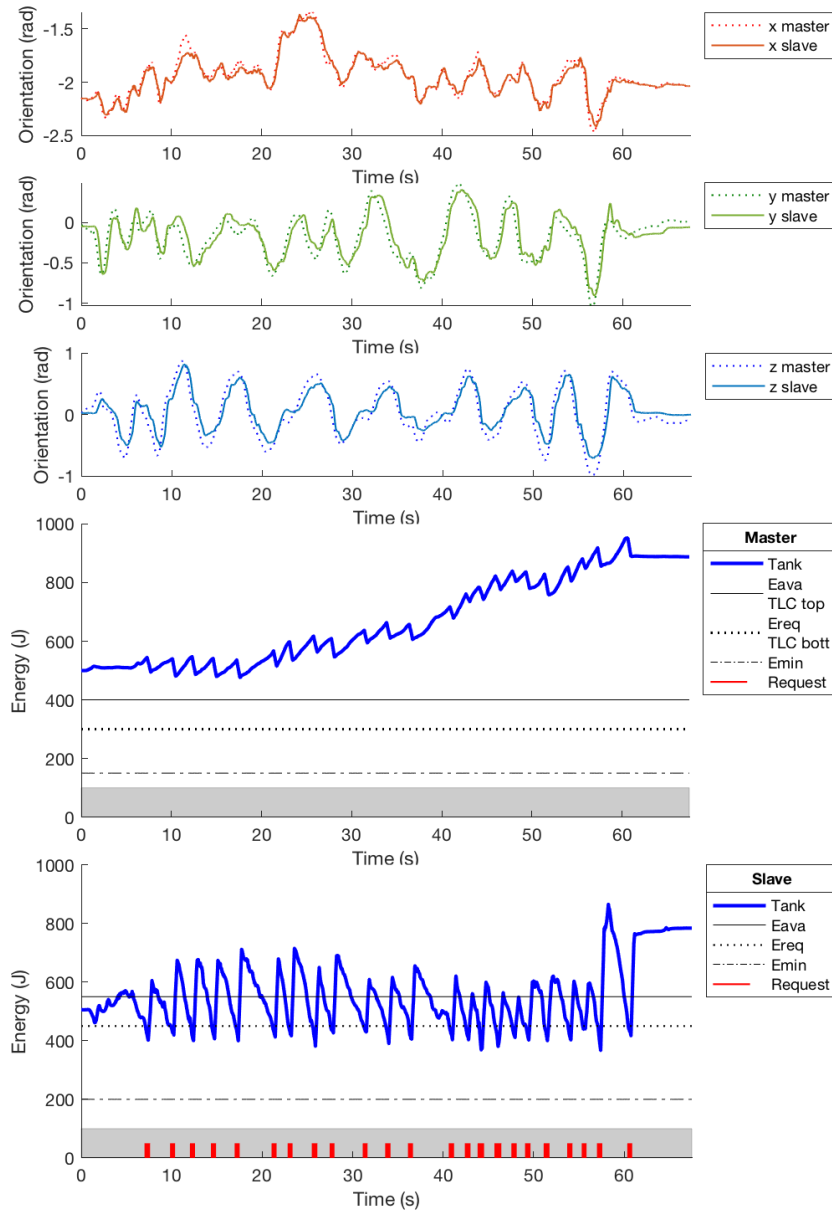


Figure 6.11: Orientation tracking in free motion. P-P control architecture with 0.2s RTT delay.

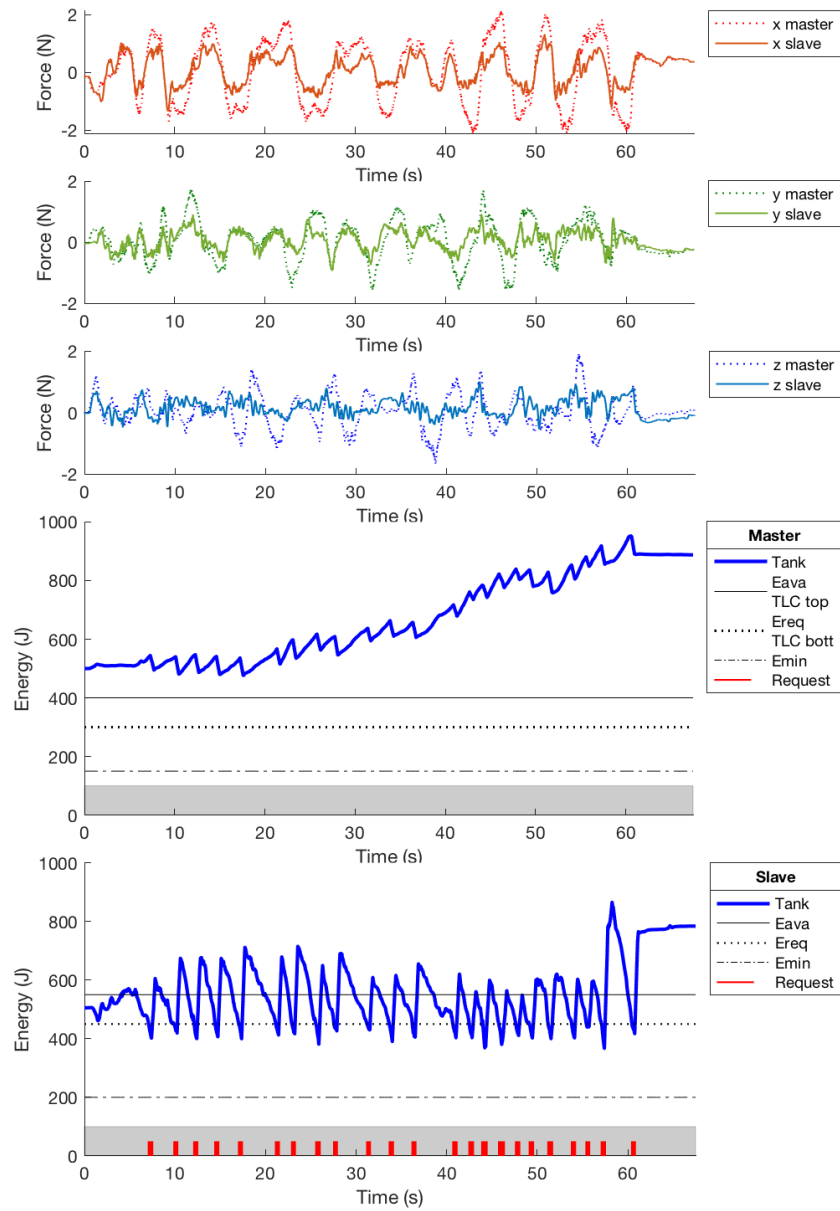


Figure 6.12: Force tracking in free motion. P-P control architecture with 0.2s RTT delay.

Insertion 90° approaching angle

In this test (Figures 6.13 to 6.15) the first two punctures have been done within the *Pilot Mode* and the other two with the standard controller. The change of controller at time 38.8s is highlighted by a vertical line. The behaviour of the position and orientation tracking is likely the same as in the no delayed version of the experiment. We can see again a non perfect initial positioning at the master side that causes the unexpected command along the $x - y$ axis. The energy balance is preserved while using the *Pilot Mode* as discussed in Section 6.1.1.

Regards the tank level, we can see the behaviour discussed in the free motion with delay test. The energy level in the slave tank increases and decreases really fast. This behaviour is due to the delay and to the RTT needed to start/stop the incoming energy flow. When there is not enough energy at the master side to fulfil the slave requirements the behaviour is the same as the undelayed test.

The difference between the force behaviour in x between master and slave that we can see in Figure 6.15 is due to the fact that the operator is forcing the position commanded by the *Pilot controller*. The master controller tries to push the operator into the right x position.

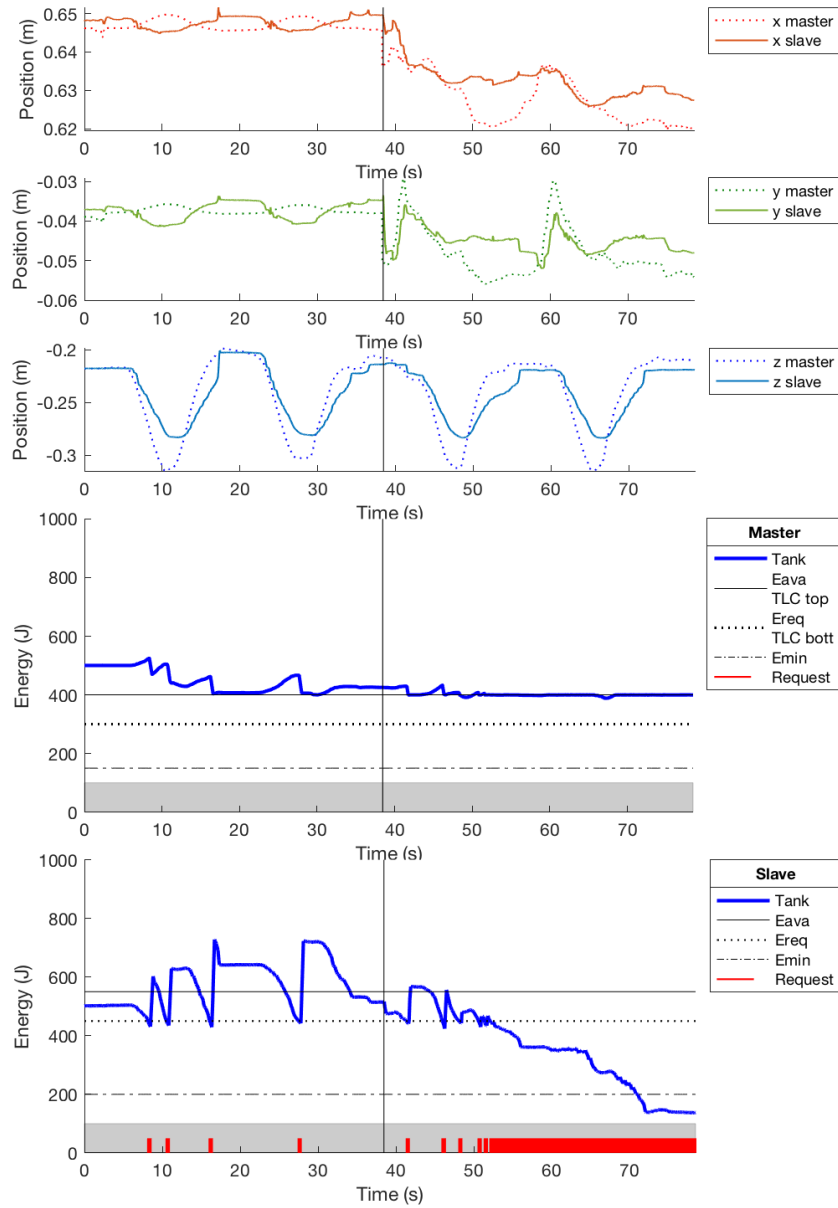


Figure 6.13: Position tracking with 90° insertion approach. P-P control architecture with 0.2s RTT delay.

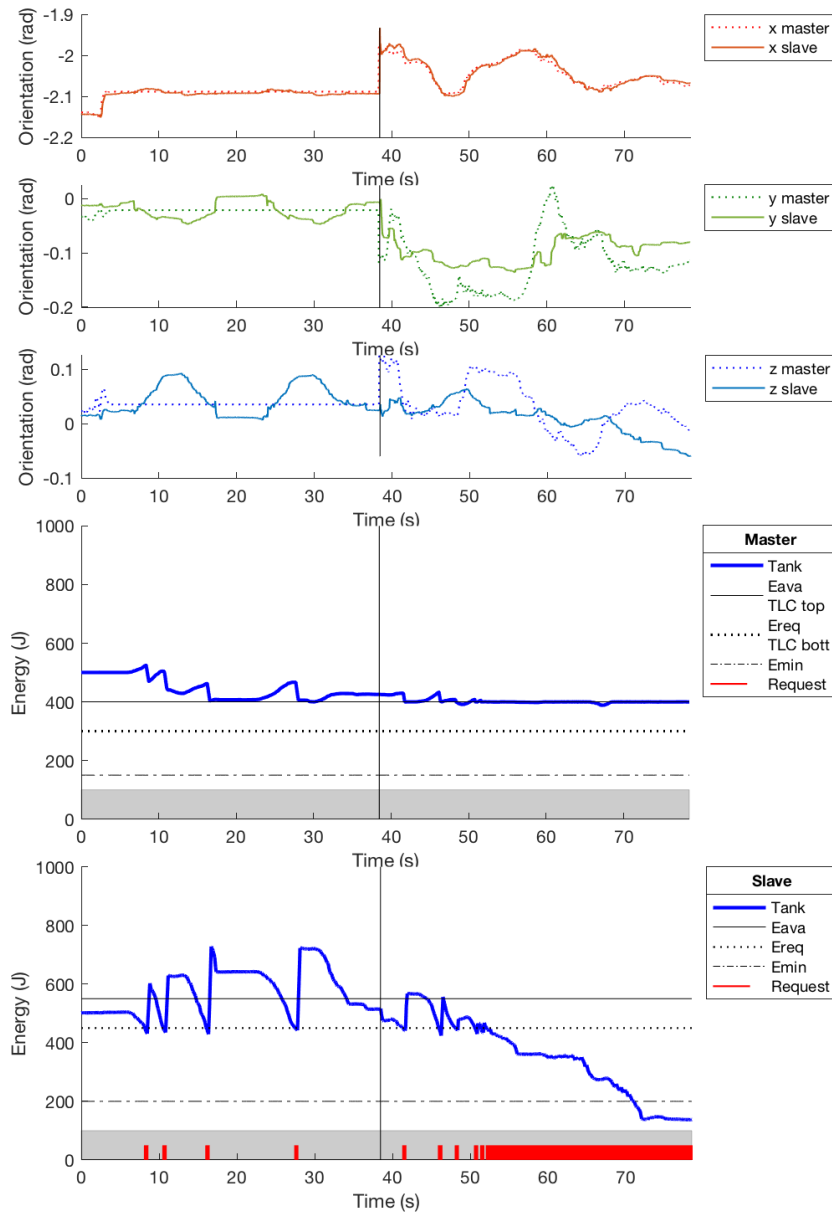


Figure 6.14: Orientation tracking with 90° insertion approach. P-P control architecture with 0.2s RTT delay.

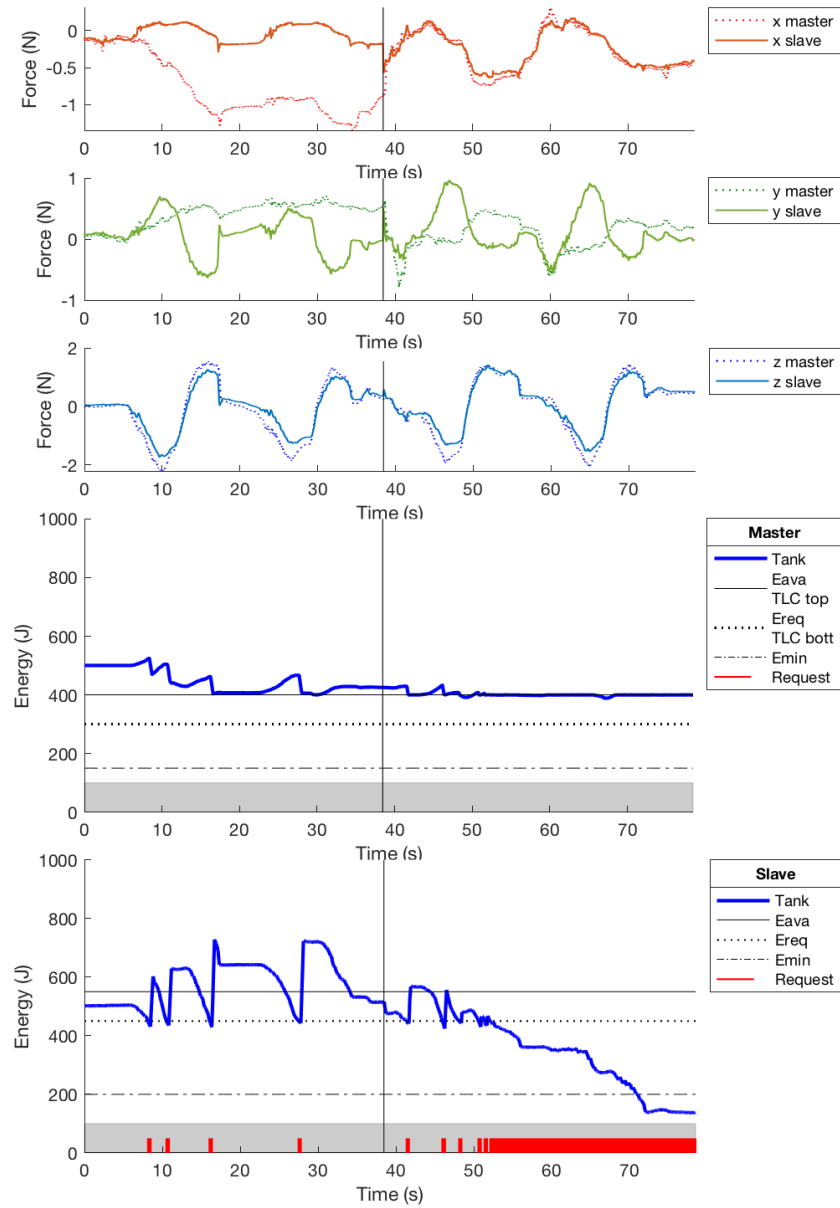


Figure 6.15: Force tracking with 90° insertion approach. P-P control architecture with 0.2s RTT delay.

Insertion with 45° approaching angle

In this test (Figures 6.16 to 6.18) the first two punctures have been done within the *Pilot Mode* and the other two with the standard controller. The test is the delayed version of the one with 45° insertion previously commented. The change of controller at time 40s is highlighted by a vertical line.

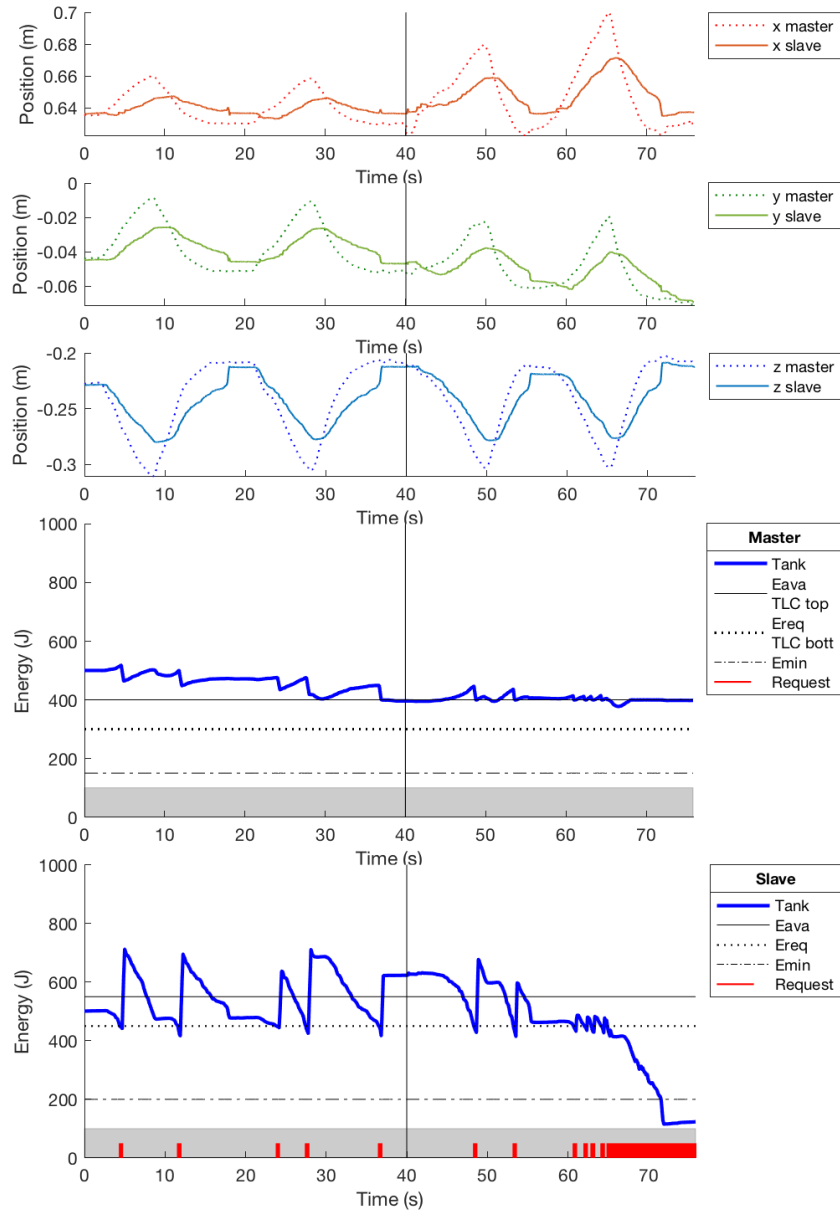


Figure 6.16: Position tracking with 45° insertion approach. P-P control architecture with 0.2s RTT delay.

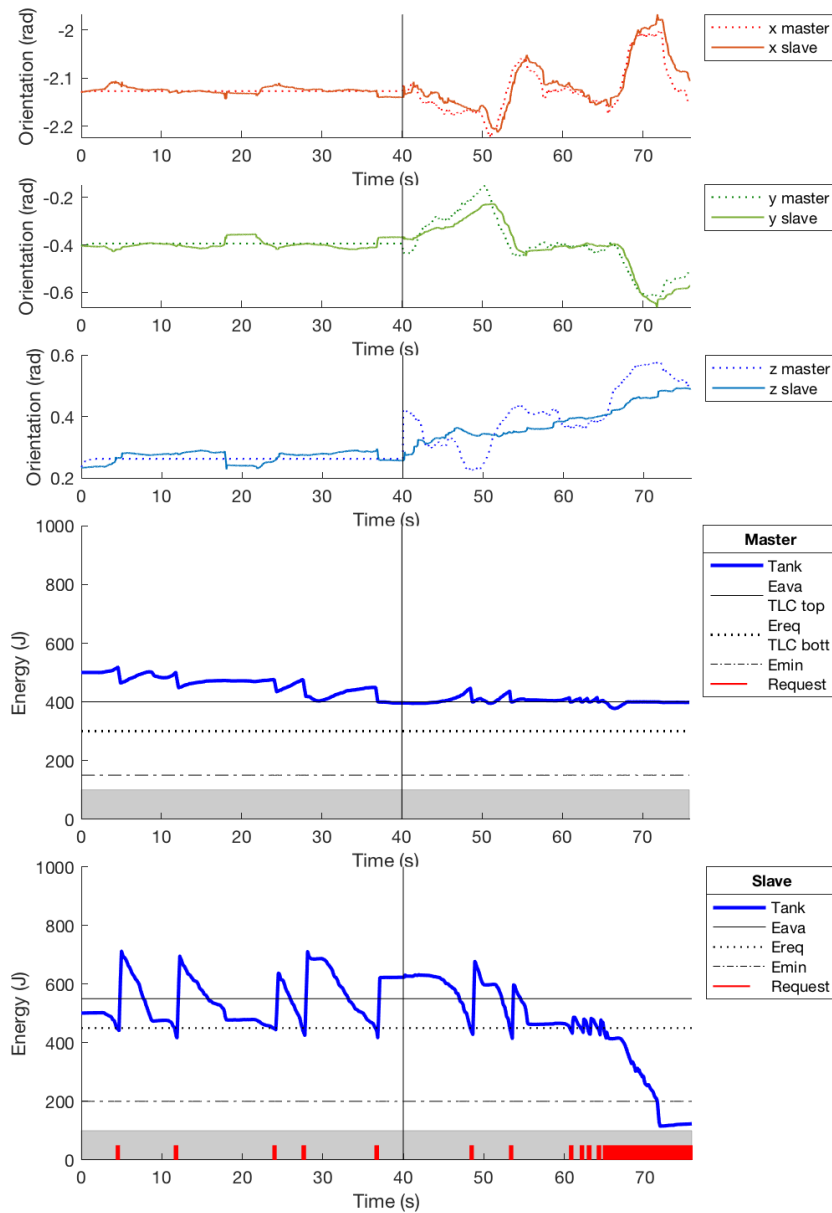


Figure 6.17: Orientation tracking with 45° insertion approach. P-P control architecture with 0.2s RTT delay.

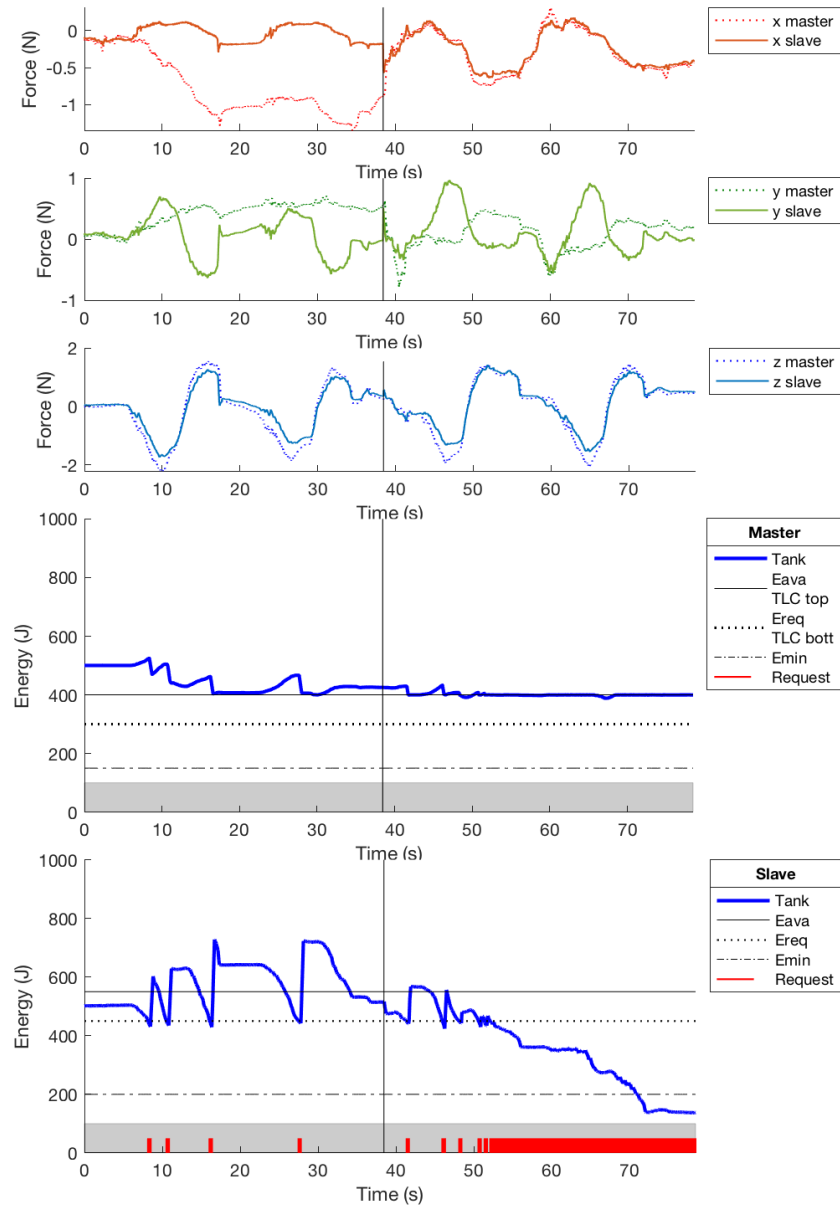


Figure 6.18: Force tracking with 45° insertion approach. P-P control architecture with 0.2s RTT delay.

		Slave	Master	Master _{pilot}
Position PD	$K_{p_{pos}}$	500.0		50.0
	$K_{d_{pos}}$	5.0	0.15	0.15
Orientation PD	$K_{p_{ang}}$	0.0		0.0
	$K_{d_{ang}}$	0.06	0.0	0.0
Force Gain	K_f		0.5	0.5
Passivity Layer	\bar{T}	1000.0	1000.0	
	T_{ava}	550	400	
	T_{req}	450	300	
	$T_{TLC_{top}}$		400	
	$T_{TLC_{bot}}$		300	
	ε_{top}	200	150	
	ε_{bot}	100	100	
	K_{TLC}		0.07	
Scale Factor (α/γ)		1/6	6.0	

Table 6.3: System's parameters for the Position-Force architecture

6.2 Position-Force

The last set of experiments are on the Position-Force teleoperation architecture. The experimental setup has been tuned with the parameters showed in Table 6.3 which are described in Sections 4.1.3 and 3.6.2. Because of the P-F architecture, the force commanded at master side is scaled by the K_f gain. As done with P-P architecture, we choose to show the slave interaction force in the master reference frame scaled by K_f .

6.2.1 Without Delay

Free motion

The free motion test (Figures 6.19 to 6.21) shows the behaviour of the system when no interaction of the slave robot with the tissue occurs.

In Figure 6.19 we can see a good position tracking between the two manipulators. The orientation tracking, as shown in Figure 6.20, is less precise than expected. This is due to the limits of the slave robot discussed in Section 6.1.1.

The energy balance in the system is assured through the constant damping at master side explained in Section 4.3.2. The master is able to provide enough energy to the slave without draining its tank ss shown in Figure 6.21.

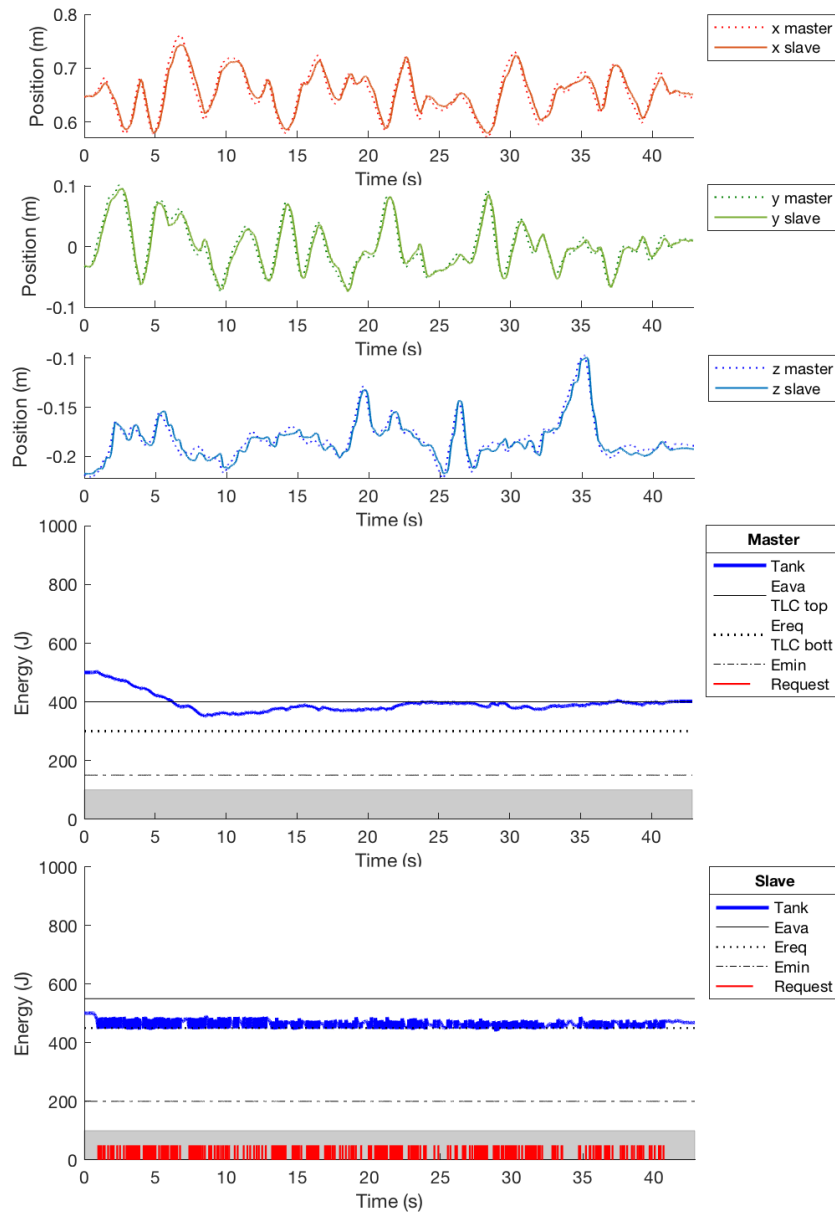


Figure 6.19: Position tracking in free motion. P-F control architecture without delay.

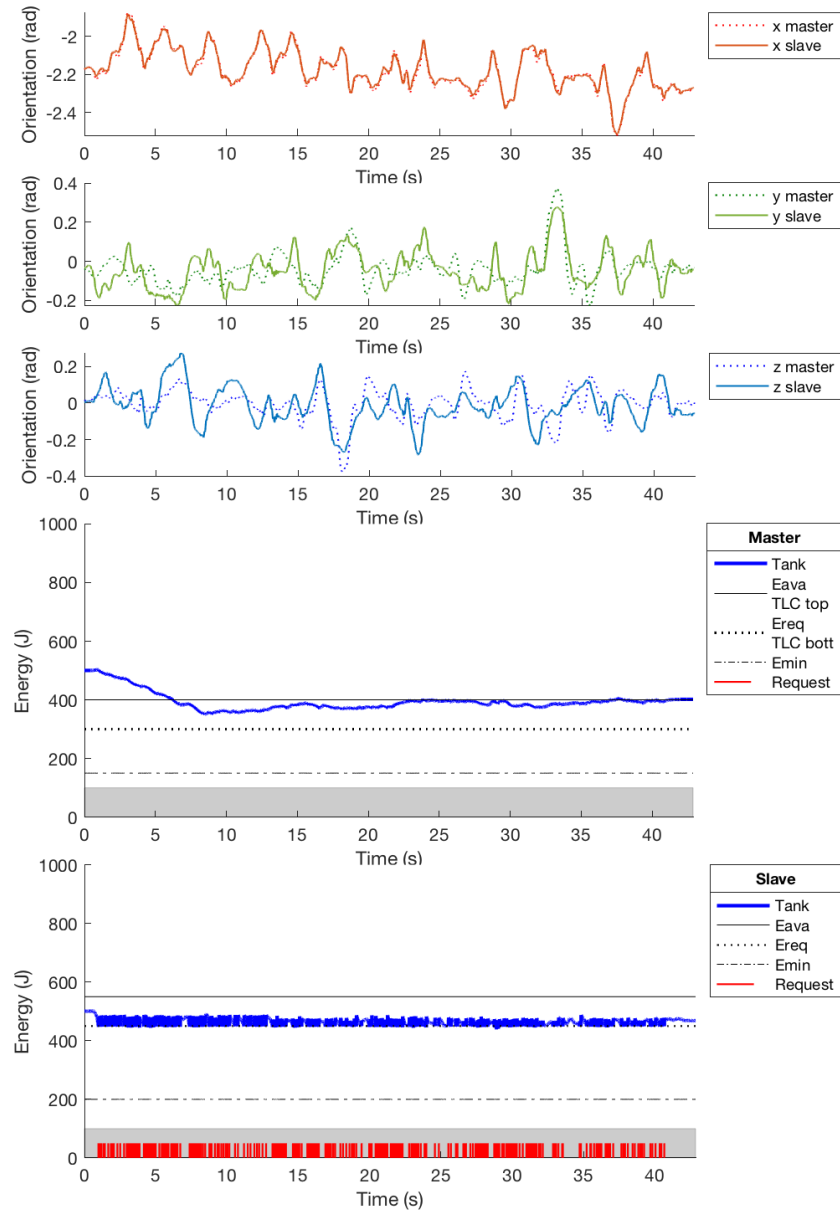


Figure 6.20: Orientation tracking in free motion. P-F control architecture without delay.

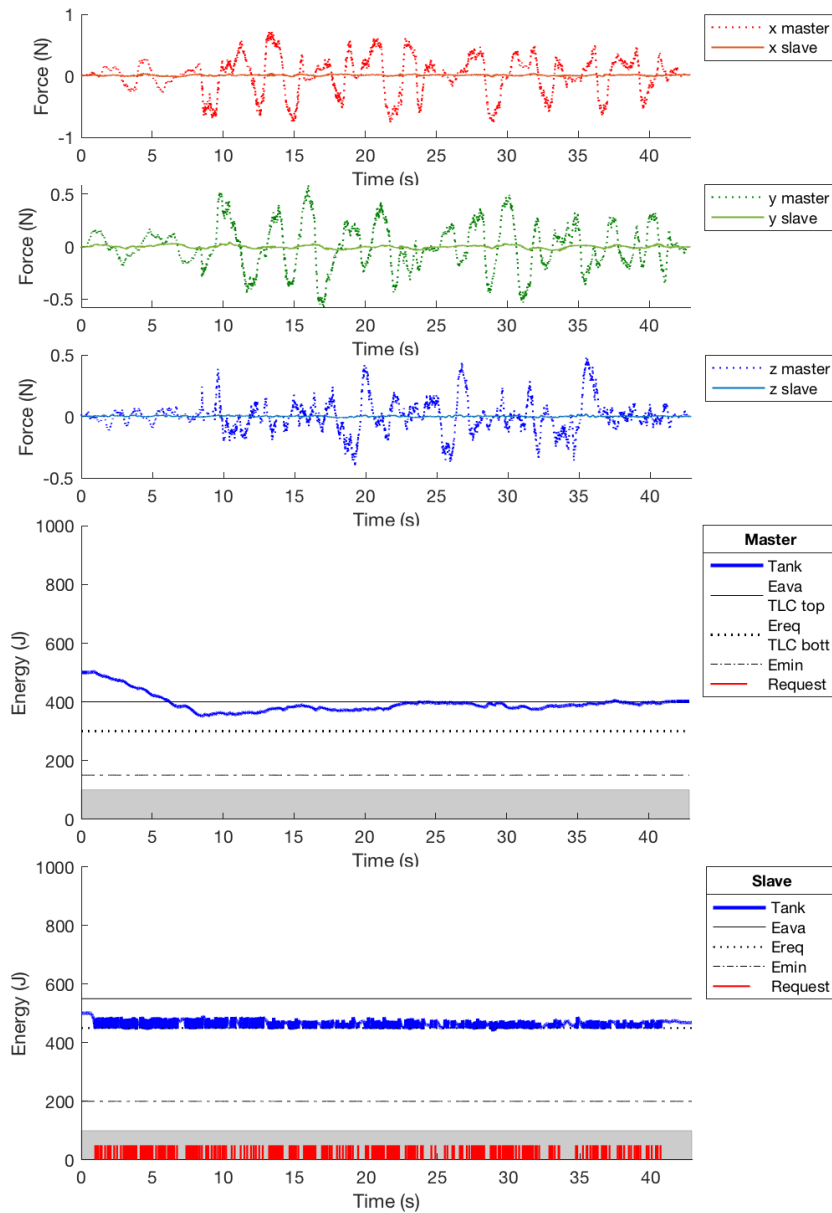


Figure 6.21: Orientation tracking in free motion. P-F control architecture without delay.

Insertion with 90° approaching angle

In this test (Figures 6.22 to 6.24) the first puncture have been executed with the standard controller and the other two within the *Pilot Mode*. The change of controller at time 20.0s is highlighted by a vertical line.

In the first puncture we can see some unwanted movements due to the reaction force exerted on the needle shaft by the phantom tissue when the needle advance varying its orientation. We previously discussed this behaviour in Section 6.1.1.

The component of that force that implies a translation is felt by the operator who try to correct the behaviour. However the lack of actuation on the orientation gives only a partial feedback.

Due to the tissue constraints the operators reaction easily produces an excessive movement that has to be balanced again. This undesired behaviour could be compensated with the *Pilot controller* that preserves the force feedback along z . The *Pilot controller* for the P-F teleoperation architecture is explained in Section 4.3.2.

The forces on $x - y$ at the slave can be explained due to the errors in position and orientation. On the master these forces are due to the violation of the virtual trajectory constraints by the operator. What we can notice is the very good tracking of the force feedback provided in z due to nature of the architecture.

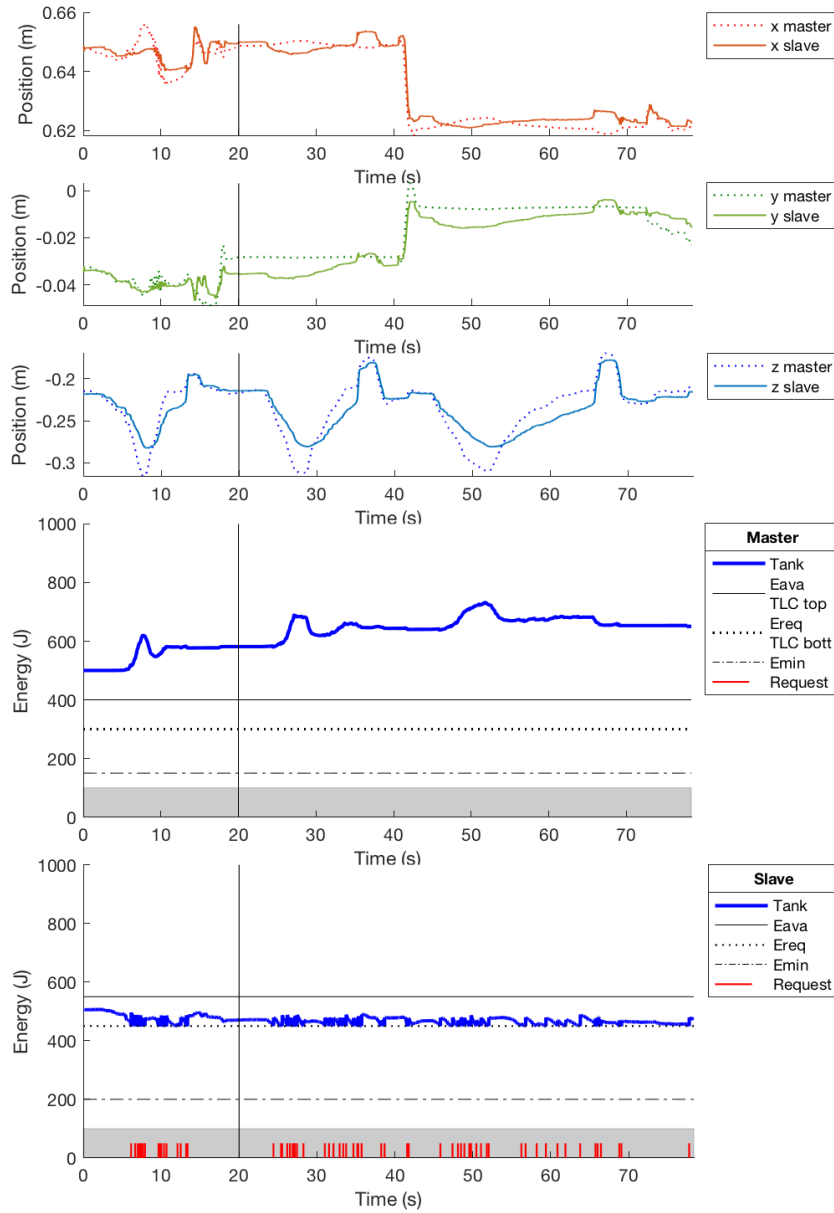


Figure 6.22: Position tracking with 90° insertion approach. P-F control architecture without delay.

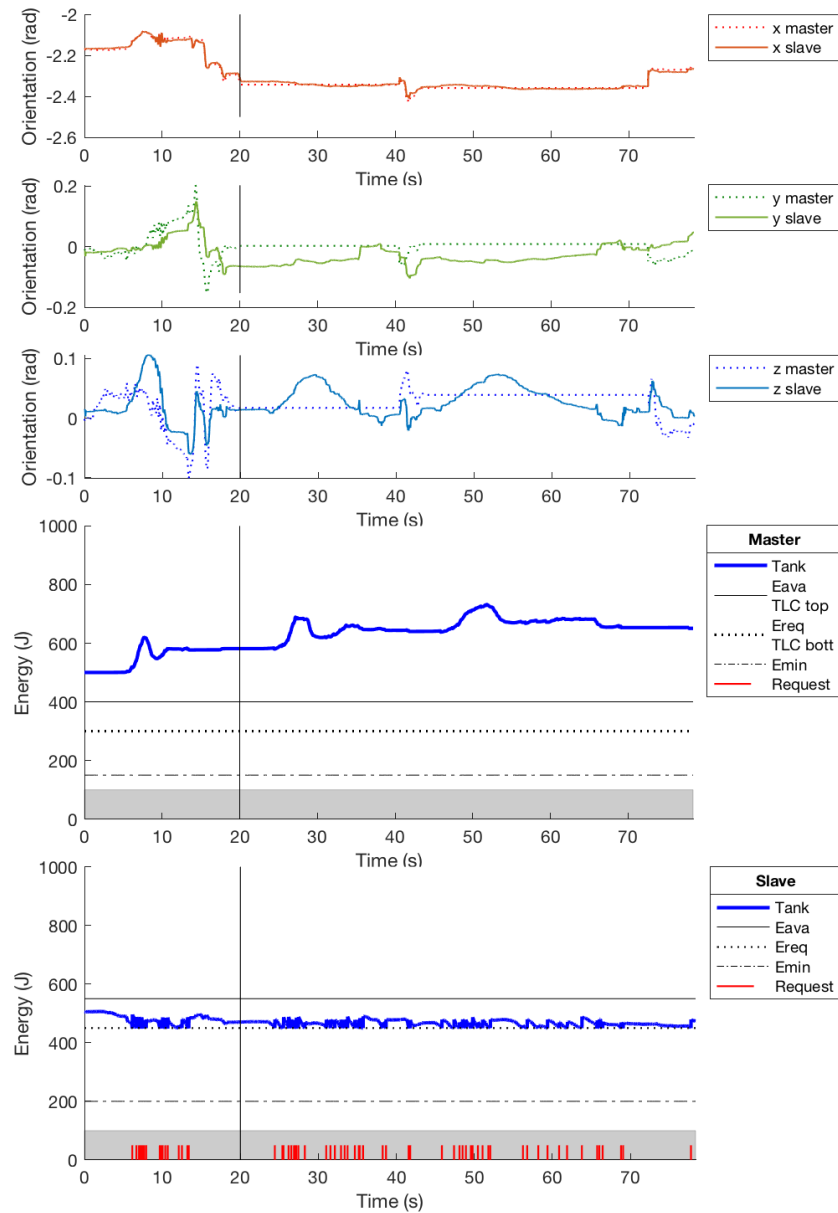


Figure 6.23: Orientation tracking with 90° insertion approach. P-F control architecture without delay.

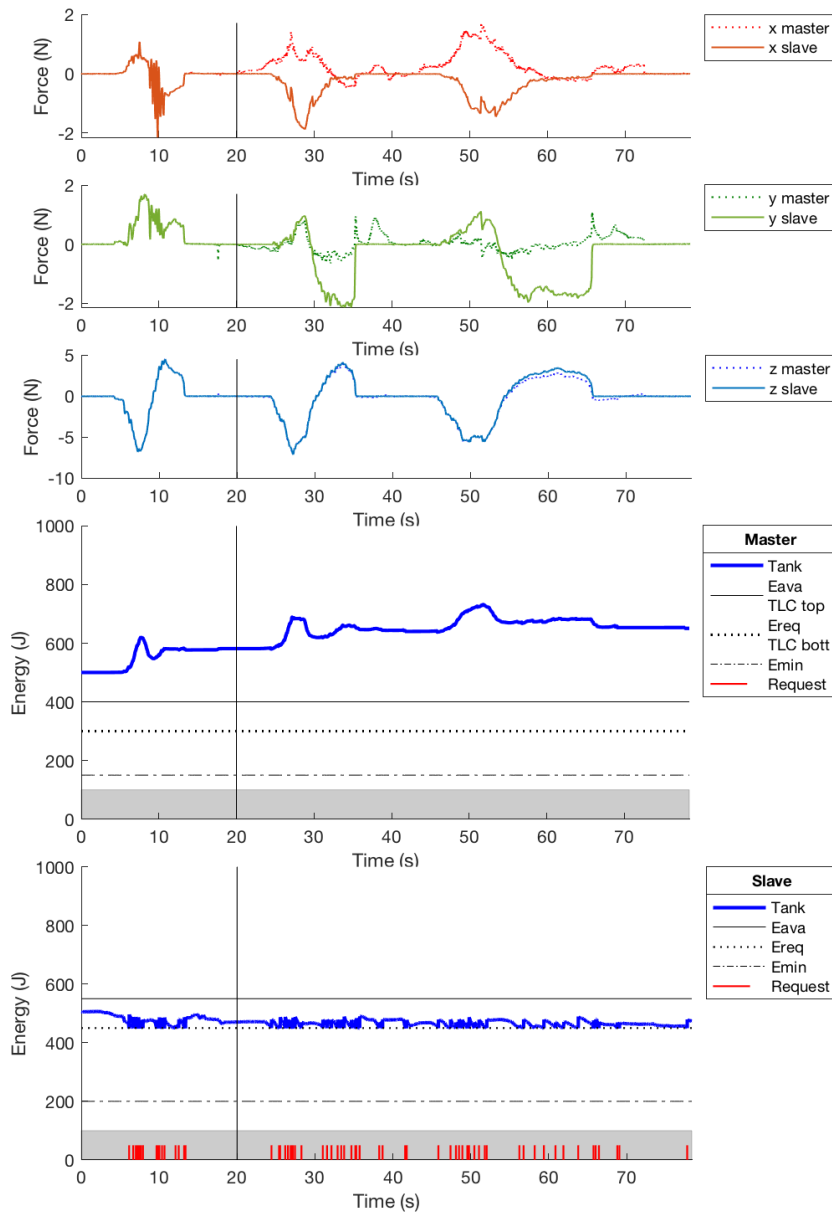


Figure 6.24: Force tracking with 90° insertion approach. P-F control architecture without delay.

Insertion with 45° approaching angle

In this test (Figures 6.22 to 6.24) the first puncture has been done within the *Pilot Mode*, the other with the standard controller. The change of controller at time 23.3s is highlighted by a vertical line. In this test both the punctures have been executed accurately.

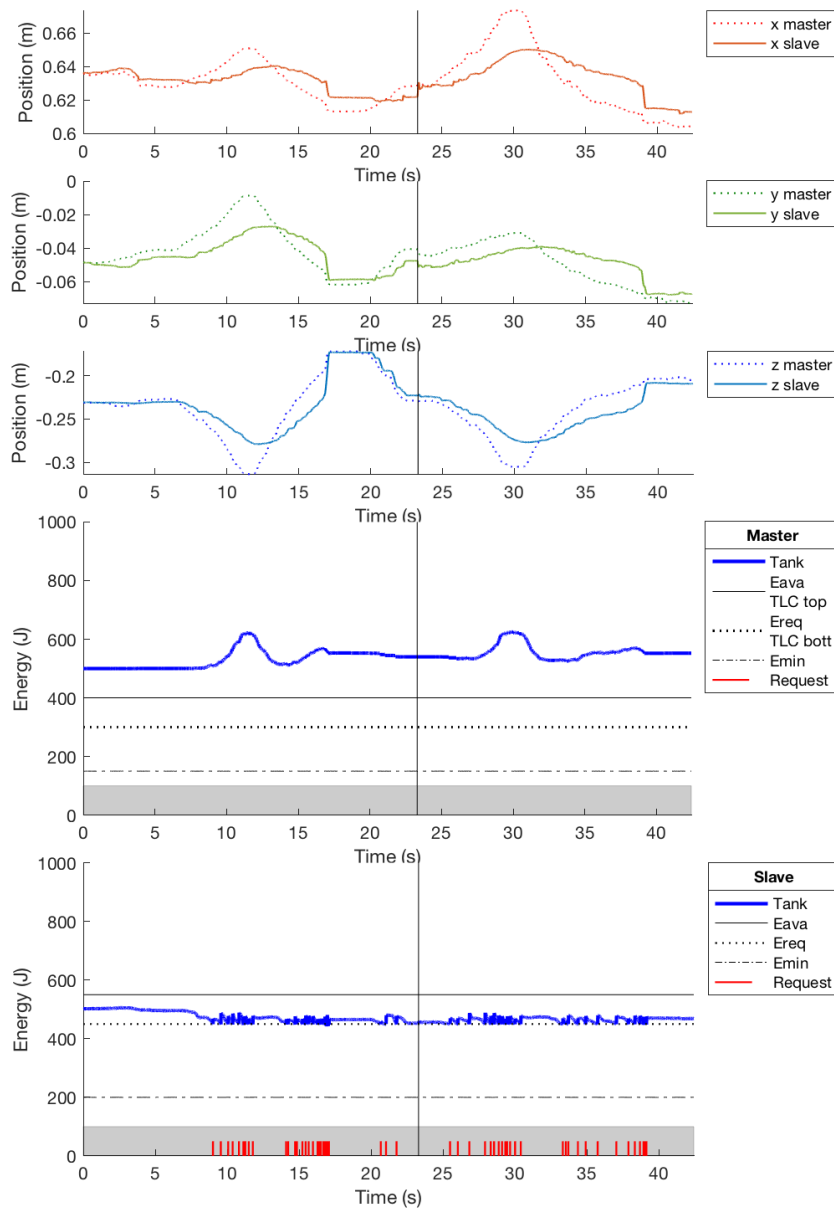


Figure 6.25: Position tracking with 45° insertion approach. P-F control architecture without delay.

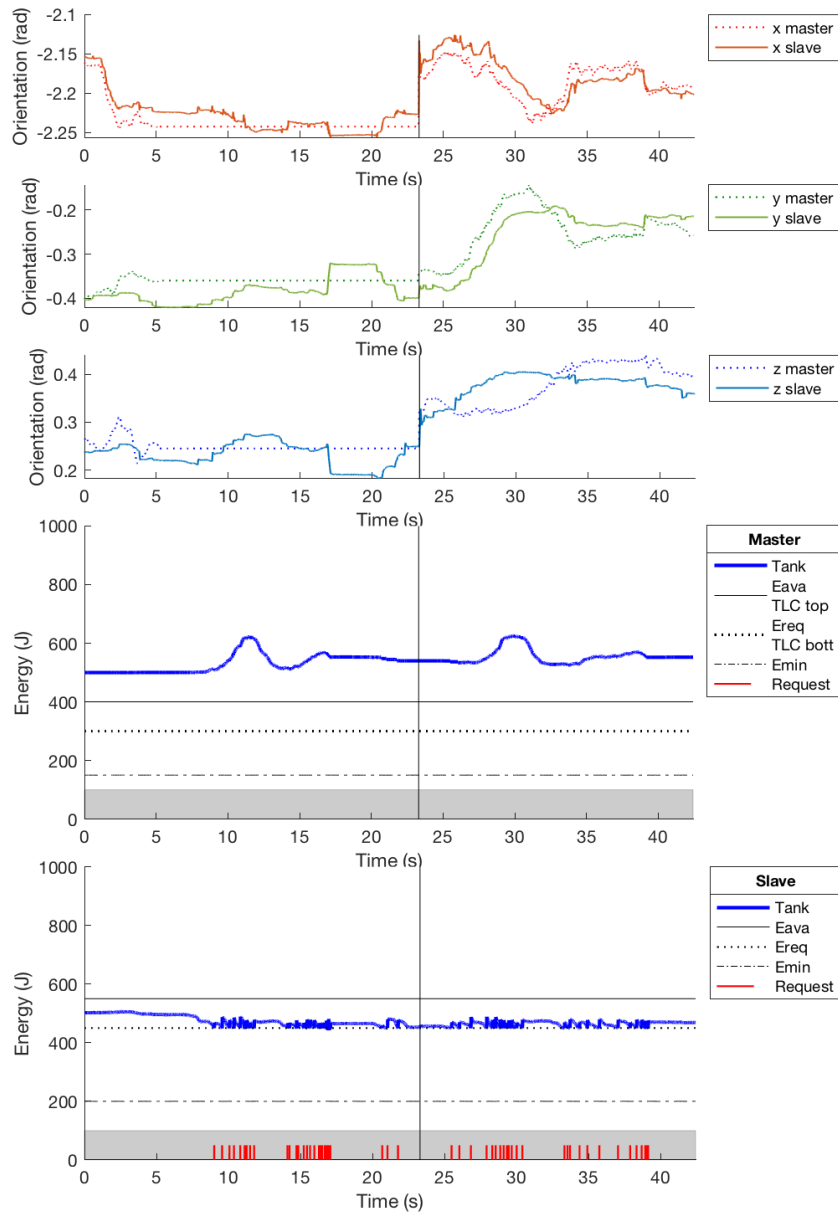


Figure 6.26: Orientation tracking with 45° insertion approach. P-F control architecture without delay.

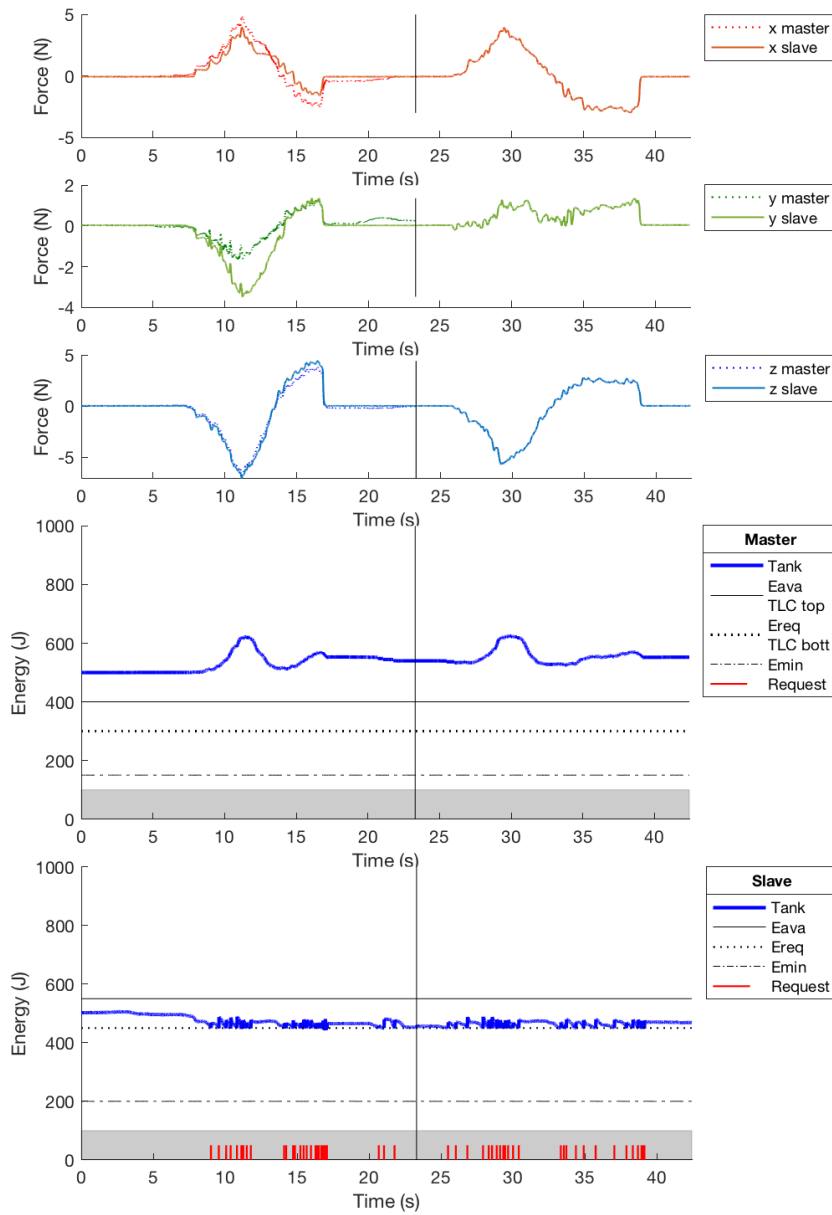


Figure 6.27: Force tracking with 45° insertion approach. P-F control architecture without delay.

6.2.2 Constant Delay

Free motion

The free motion test has been repeated introducing a constant delay into the communication channel (Figure 6.28 to 6.30). The system's energy behave as described in the delayed P-P architecture.

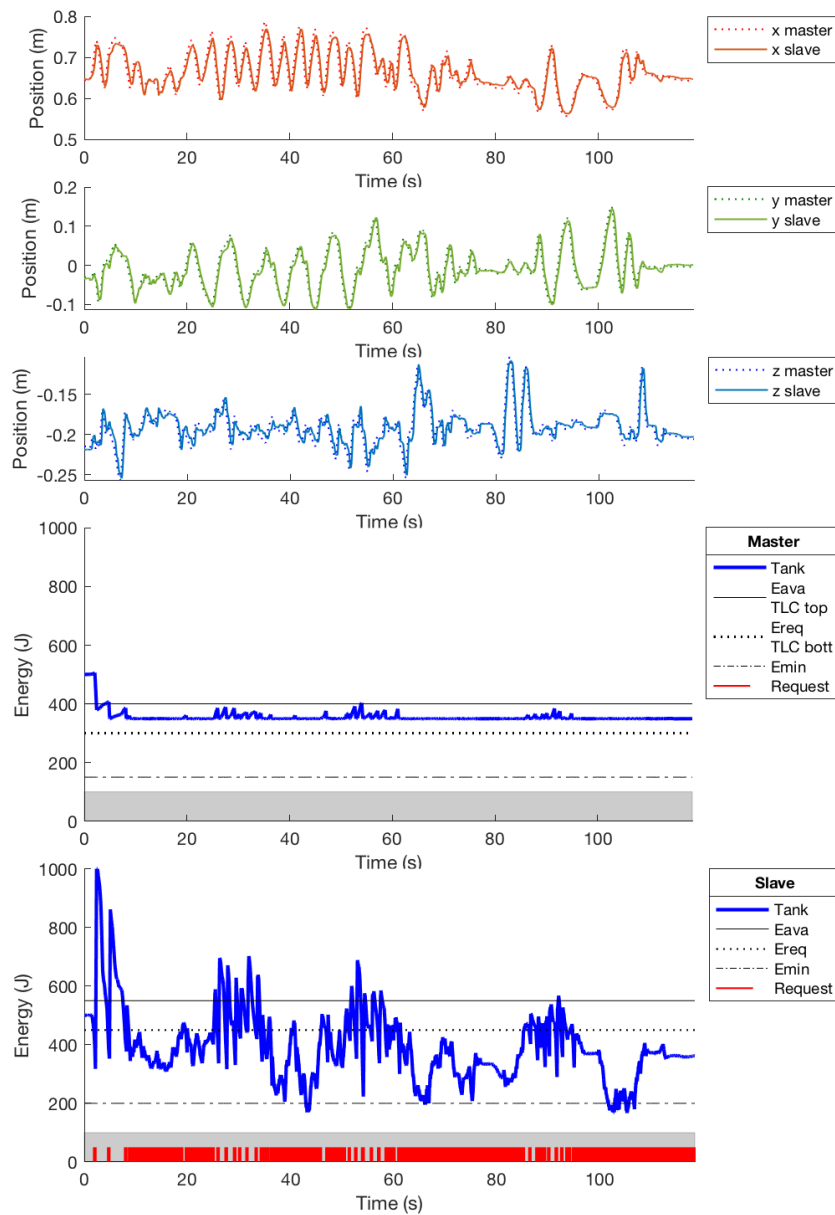


Figure 6.28: Position tracking in free motion. P-F control architecture with 0.2s RTT delay.

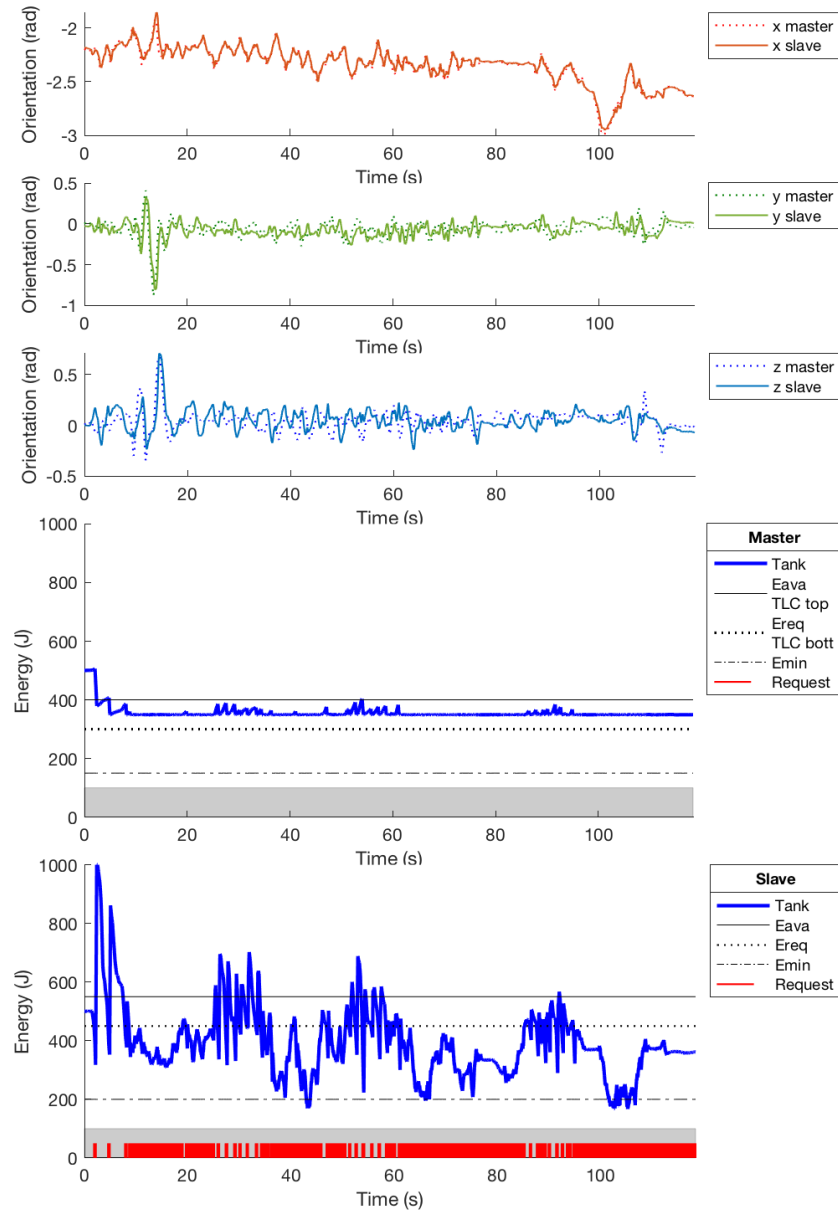


Figure 6.29: Orientation tracking in free motion. P-F control architecture with 0.2s RTT delay.

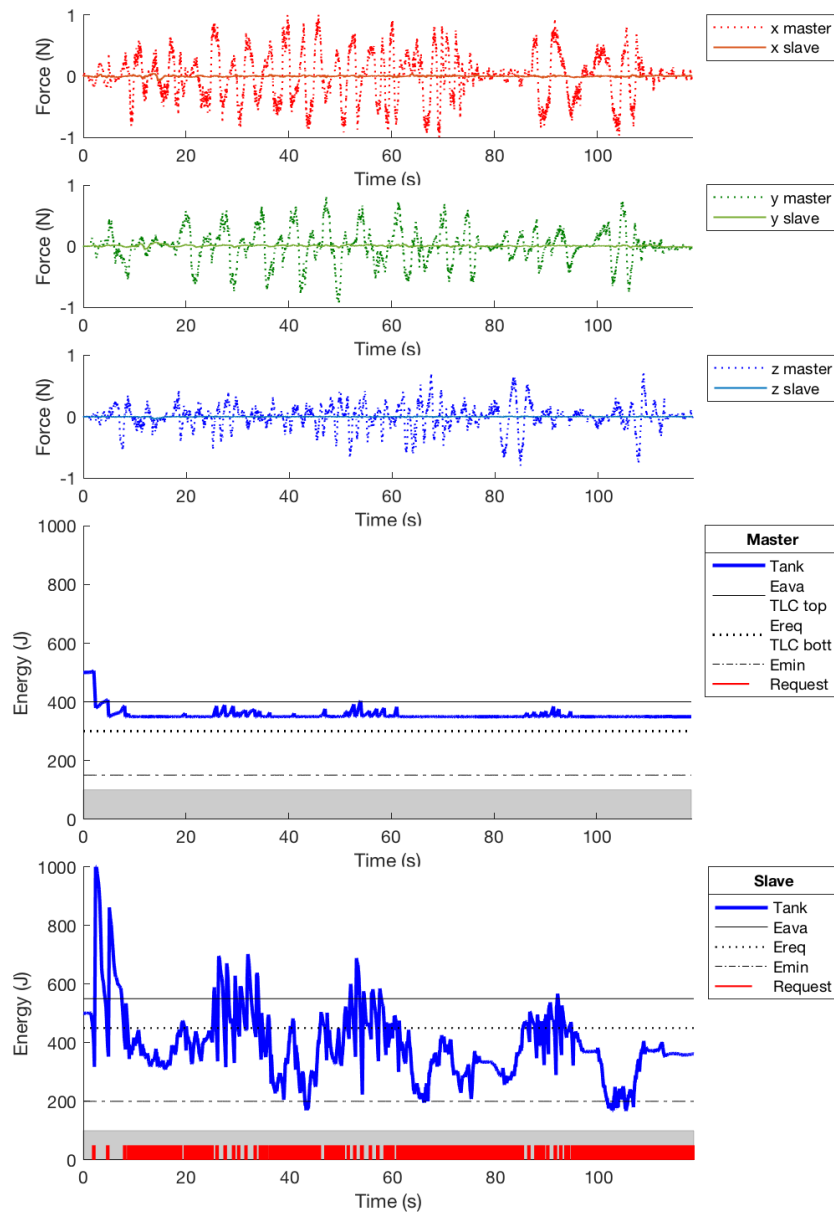


Figure 6.30: Force tracking in free motion. P-F control architecture with 0.2s RTT delay.

Insertion with 90° approaching angle

In this test (Figure 6.31 to 6.33) the first puncture has been done within the *Pilot Mode*, and the other two with the standard controller. The change of controller at time 43.5s is highlighted by a vertical line.

Notice here how the problem of operator reaction is amplified when the *Pilot controller* is disabled: both the master and the slave lost their energy due to the instability of the system.

This is a clear intervention of the Two-Layer passivity layer. In fact the main reason of the energy drop in the previous cases was the energy leakage in the system due to extra amount of energy required by the slave when performing the puncture varying the orientation.

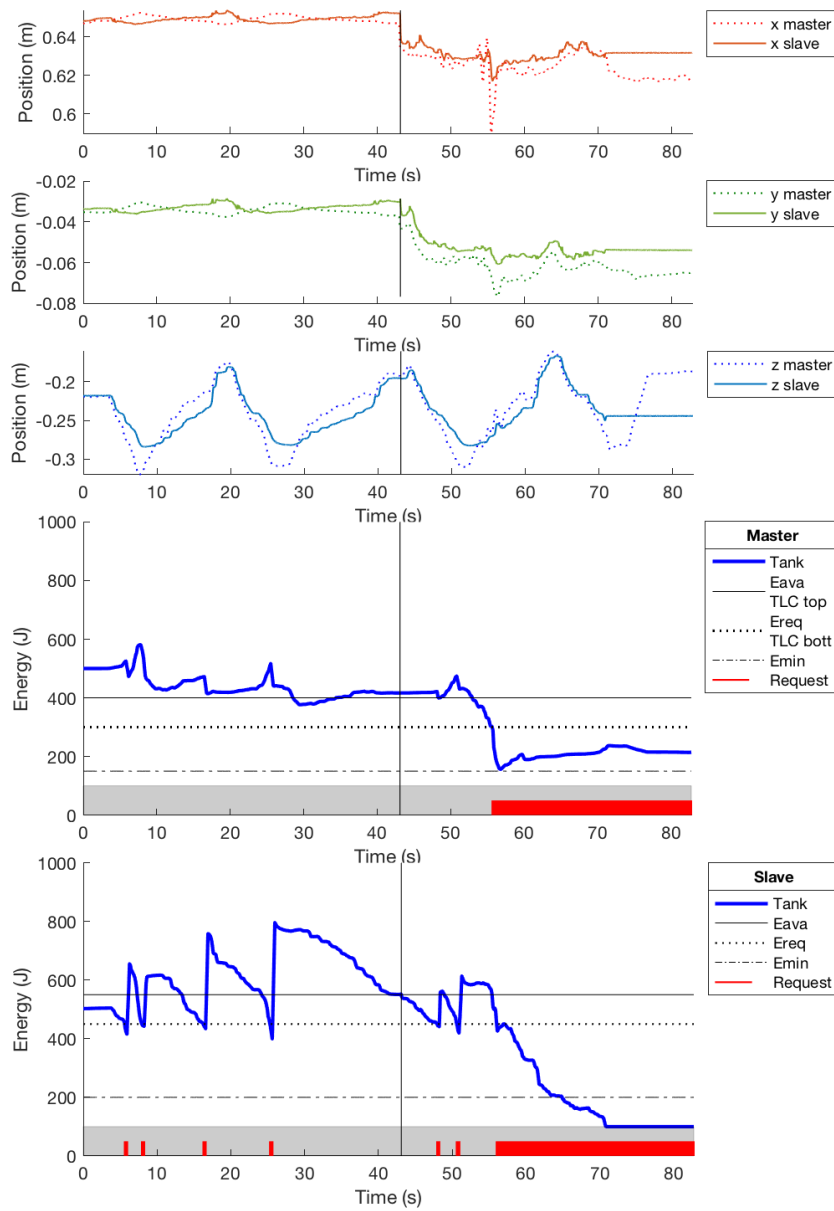


Figure 6.31: Position tracking with 90° insertion approach. P-F control architecture with 0.2s RTT delay.

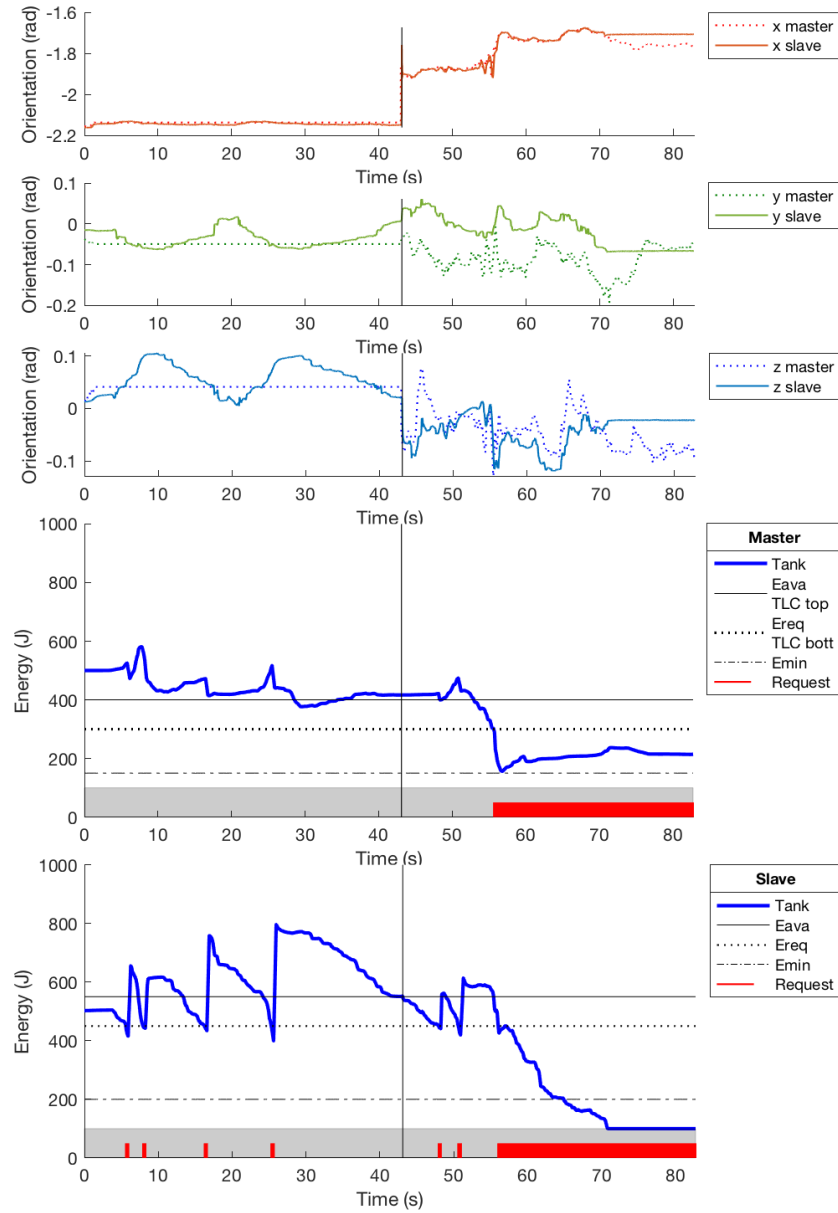


Figure 6.32: Orientation tracking with 90° insertion approach. P-F control architecture with 0.2s RTT delay.

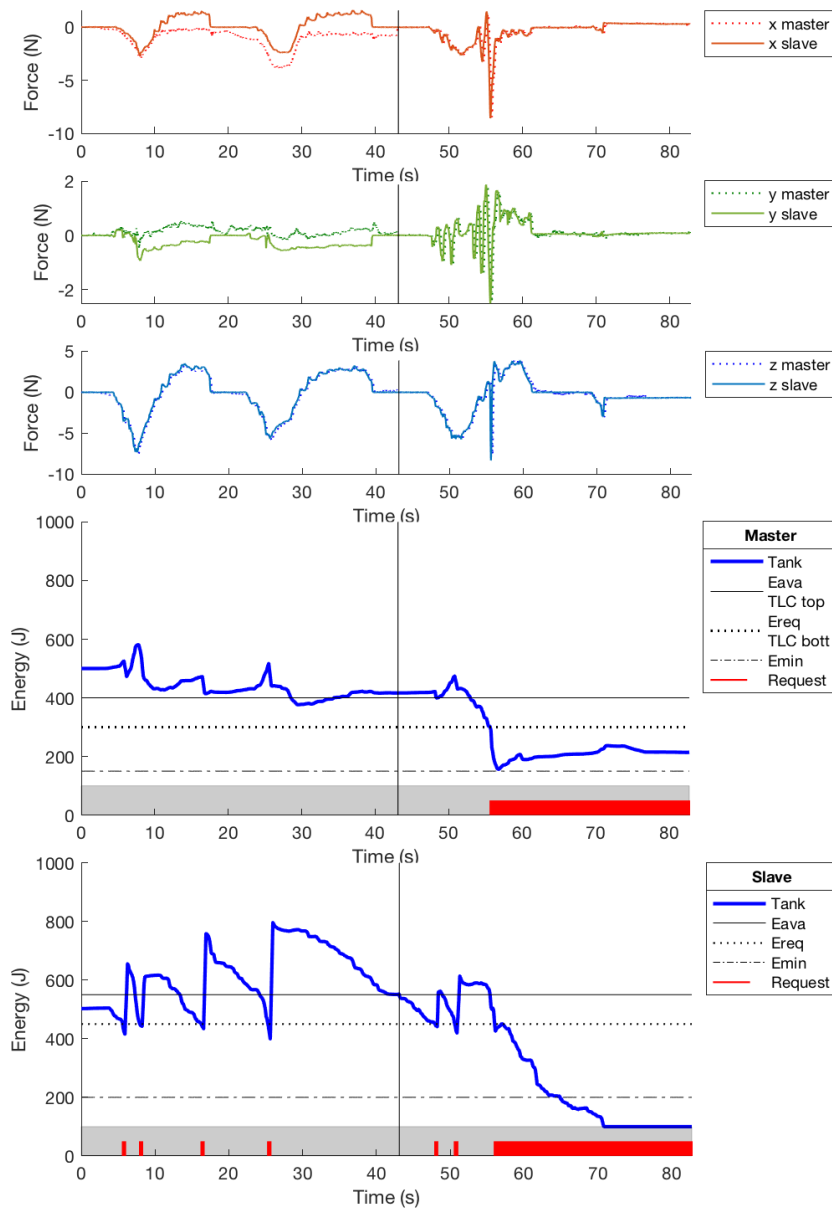


Figure 6.33: Force tracking with 90° insertion approach. P-F control architecture with 0.2s RTT delay.

Insertion with 45° approaching angle

In this test (Figure 6.34 to 6.36) the first two punctures have been done within the *Pilot Mode*, and the other two with the standard controller. The change of controller at time 50s is highlighted by a vertical line.

The instability in the second puncture causes energy draining in the whole system which is close to the passivity layer intervention. The instability is managed by the operator meaning that holds steadily the master manipulator dissipating the energy. Thanks to the operator intervention the interaction forces are balanced by and the velocity at the end effector are not so high. Without the operators reaction, the passivity layer would have intervened.

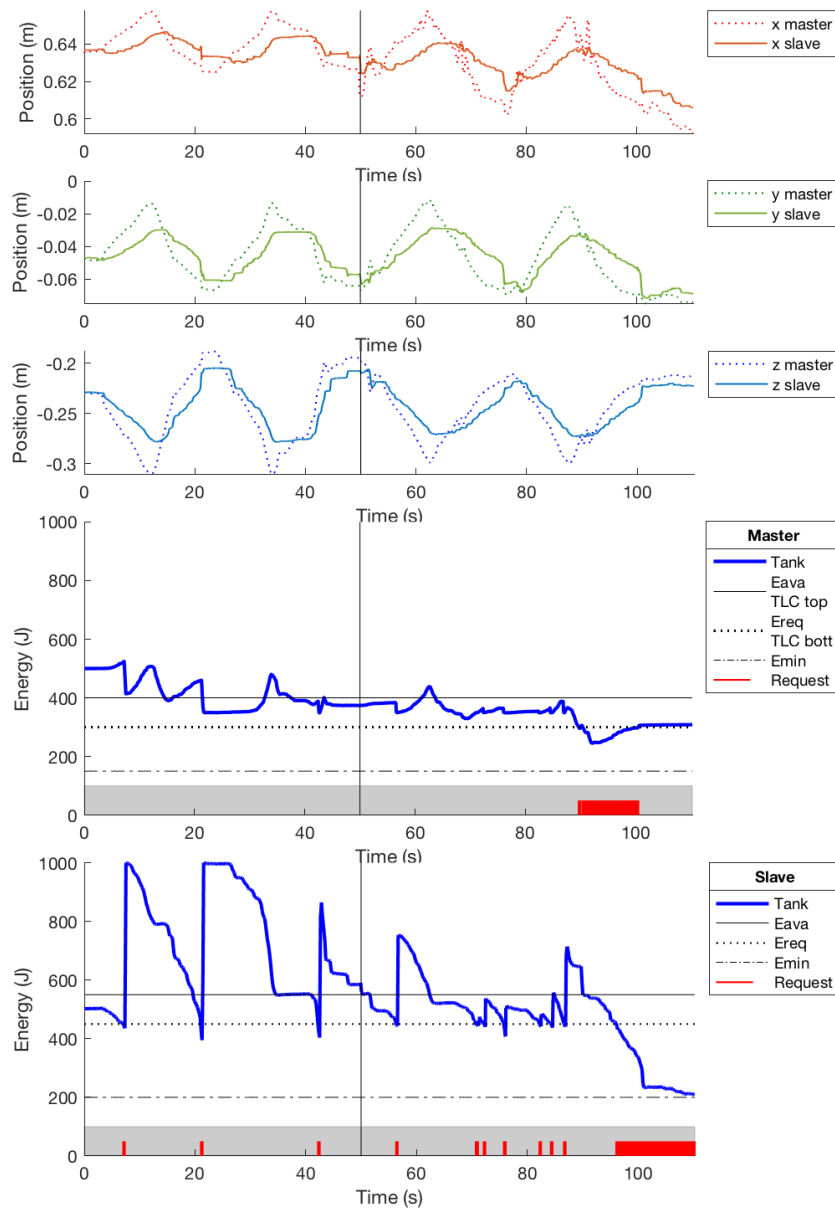


Figure 6.34: Position tracking with 45° insertion approach. P-F control architecture with 0.2s RTT delay.

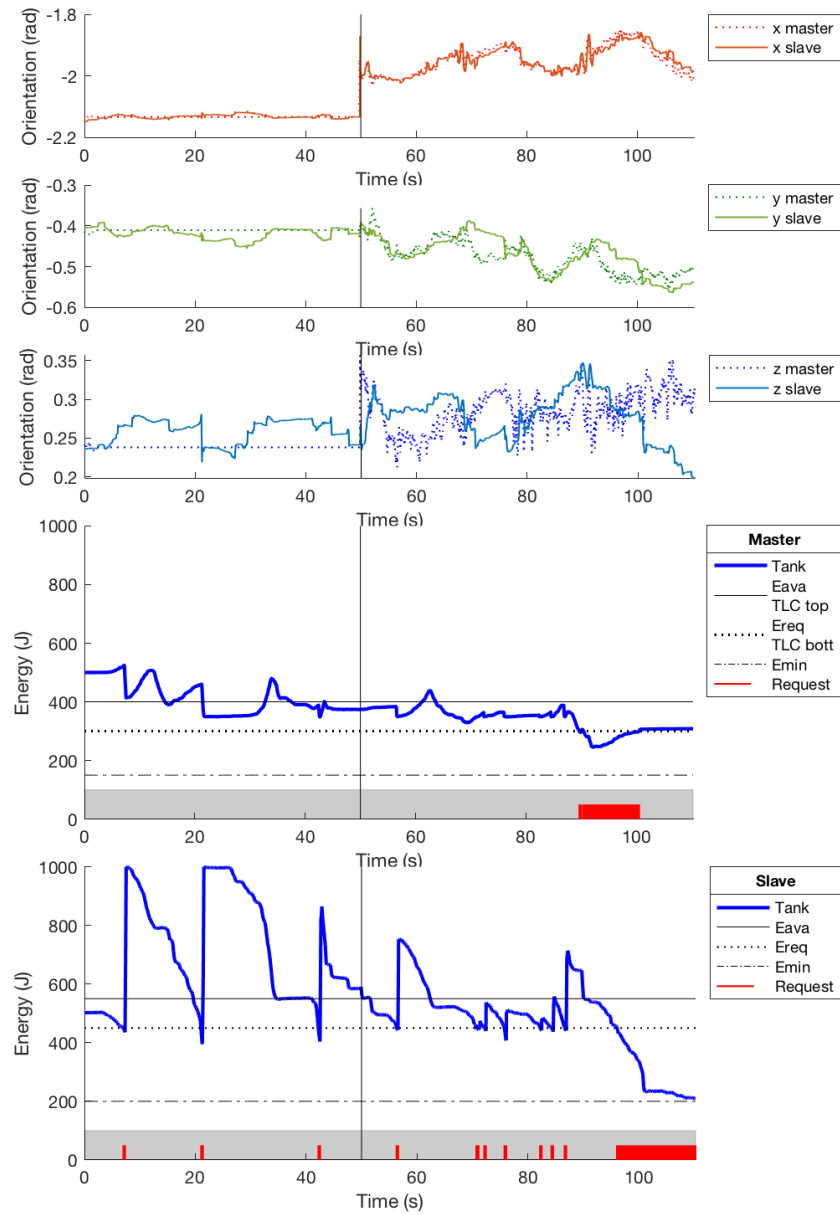


Figure 6.35: Orientation tracking with 45° insertion approach. P-F control architecture with 0.2s RTT delay.

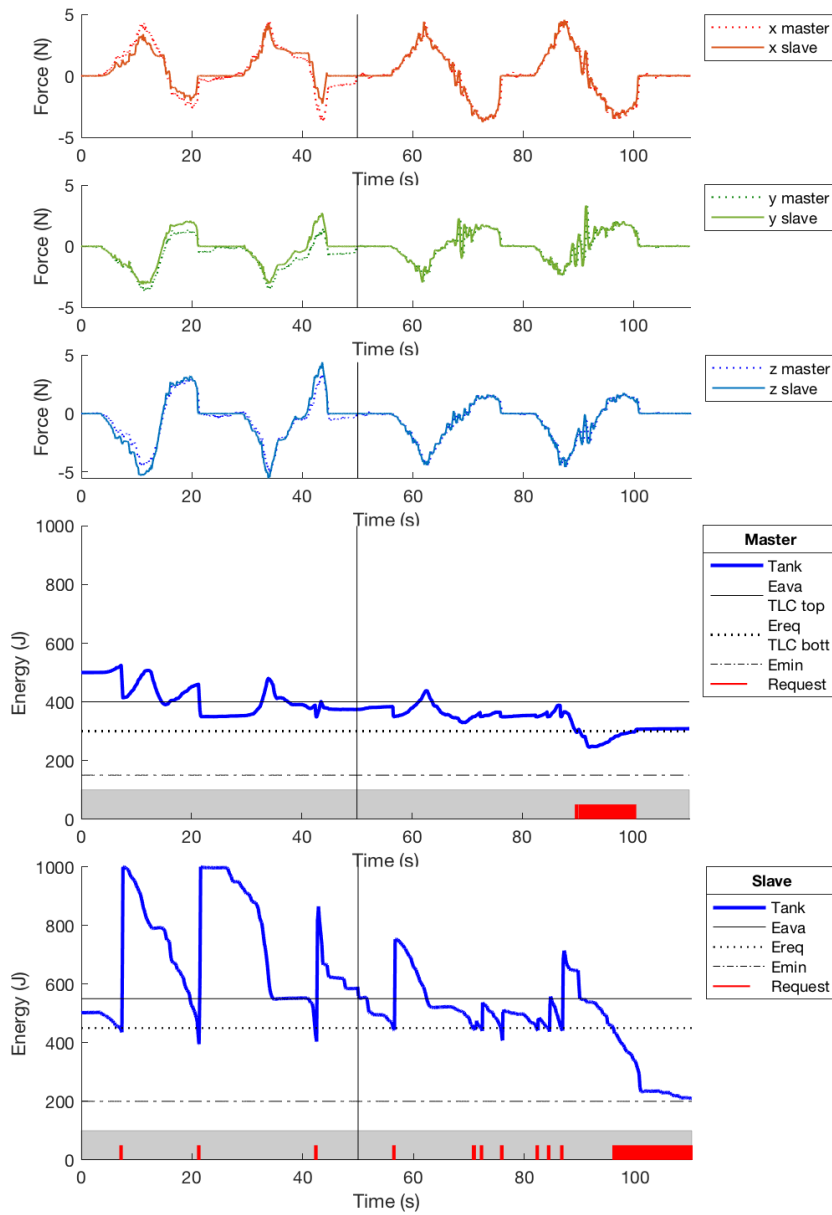


Figure 6.36: Force tracking with 45° insertion approach. P-F control architecture with 0.2s RTT delay.

6.3 Discussion

The tuning of the Two-Layer has been kept as much as possible constant among all the experiments. Its not the preferred way to show the results because we can not show its best performance in each testing scenario, but we believe that with this choice can show the flexibility of the our system and better understand its limits with the purpose of enhance it in a near future.

The P-P architecture seems not to be the proper teleoperation architecture for the needle insertion procedure:

- The force feedback is estimated on the tracking error and is not due to the real interaction force. This means that the operator feels an apparent inertia when controlling the end-effector due to the values of both $K_{p_{pos}}$ at master and slave sides.
- This inertia, if not to high, gives the feeling of handling the instrument, but when its effects become more prominent e.g. due to delays in the channel, it enhances the operators fatigue.
- A high perceived inertia negatively affects the level of transparency in the system by making less clear the difference between the free motion movement and the tissue insertion.

The P-F architecture is clearly the preferred architecture to address such procedure:

- The force feedback is due to the real interaction force thus we can reach higher degrees of transparency.
- The lower stability of the P-F architecture is managed by the Two-Layer algorithm.
- When performing the insertion with the *Pilot controller* we can also reach an high level of transparency by keeping the fundamental feedback along z .

Focusing on the Two-Layer framework we can also obtain better result if we tune it differently for each testing scenario. We can made the following considerations on the basis of our experience while tuning the system:

- To better manage the problem of delays we can act reducing the power rate. This helps because we can send less extra energy because of the RTT that the system needs to stop the energy flow.
- Between the two architectures the effects of energy leakage are different and more prominent in the P-P architecture. This suggest that a slight higher value for the Scale Factor is required for the P-P architecture. This will help in the procedures performed without the *Pilot controller* in which the energy draining in the slave tank is due to a more prominent energy leaking, a side effect of our setup that does not allow the orientation feedback.
- The effects of instability and the corresponding intervention of the two layer are shown in the 90° insertion with delay with the P-F architecture (Section 6.2.2). Here the energy drops down both at master and slave side so that the system does not move any more.
- The other example of instability, shown in the 45° insertion with delay with the P-F architecture (Section 6.2.2), suggests that in the P-F architecture the *passivity margin* of the system should be decreased. With a smaller passivity margin we would have seen the intervention of the passivity layer despite the dissipation due to the operator firmly holding the master console.

Conclusions and future works

In this thesis a teleoperation architecture has been presented to address the issue of providing kinaesthetic feedback in remote percutaneous procedures such biopsy.

The inclusion of a virtual guiding mode for a more precise insertion is only one of the possible solution for augmenting the performance and exploiting such a system.

For such kind of system the problem of delay is usually not addressed due to the presence of a dedicated connection between the master console and the slave robot. The proposed teleoperated architecture has been tested with positive results even in a constant delayed network.

A future, extension of this work could be the test on a time-vary delayed network with packet loss and/or packet retransmission.

For an evaluation of the setup architecture more closer to th clinical case, the criablation needle could be mounted and tested: this will require a retuning and possibly a re-shaping of the slave controller.

The substitution of the master console with a 6-DoF model, as the Phantom Premium 1.5, will enable the full potentiality of the implemented architecture with no extra effort.

With this physical change, a future work could be the evaluation of the system performance in a full bilateral configuration.

Another future improvement could be to take into account the dynamical model of the two manipulators, expressed in task space. This should reduce the need for scaling the energy between them and could enable a more suitable control strategy at the slave side for the puncturing task such as the impedance control.

Bibliography

- [1] www.github.com/fsuarez6/phantom_omni.
- [2] www.ros.org.
- [3] Robert J. Anderson and Mark W. Spong. Bilateral Control of Teleoperators with Time Delay. *IEEE Transactions on Automatic Control*, 34(5):494–501, 1989.
- [4] Federica Ferraguti, Nicola Preda, Auralius Manurung, Marcello Bonfe, Olivier Lambercy, Roger Gassert, Riccardo Muradore, Paolo Fiorini, and Cristian Secchi. An Energy Tank-Based Interactive Control Architecture for Autonomous and Teleoperated Robotic Surgery. *IEEE Transactions on Robotics*, 31(5):1073–1088, 2015.
- [5] Michel Franken, Stefano Stramigioli, Sarthak Misra, Cristian Secchi, and Alessandro MacChelli. Bilateral telemanipulation with time delays: A two-layer approach combining passivity and transparency. *IEEE Transactions on Robotics*, 27(4):741–756, 2011.
- [6] Ian Goodfellow, Yoshua Bengio, and Aaron Courville. *Deep Learning*. MIT Press, 2016. <http://www.deeplearningbook.org>.
- [7] Dale A. Lawrence. Stability and Transparency in Bilateral Teleoperation. *IEEE Transactions on Robotics and Automation*, 9(5):624–637, 1993.
- [8] D Lee and M W Spong. Passive Bilateral Teleoperation With Constant Time Delay. *IEEE Transactions on Robotics*, 22(2):269–281, 2006.

- [9] Dongjun Lee and Ke Huang. Passive-set-position-modulation framework for interactive robotic systems. *IEEE Transactions on Robotics*, 26(2):354–369, 2010.
- [10] Rogelio Lozano, Bernard Brogliato, Olav Egeland, and Bernhard Maschke. *Dissipative Systems Analysis and Control*. Springer-Verlag London, 2000.
- [11] Sebastian Ruder. An overview of gradient descent optimization algorithms., 2016. cite arxiv:1609.04747Comment: Added derivations of AdaMax and Nadam.
- [12] Olga Russakovsky, Jia Deng, Hao Su, Jonathan Krause, Sanjeev Satheesh, Sean Ma, Zhiheng Huang, Andrej Karpathy, Aditya Khosla, Michael Bernstein, Alexander C. Berg, and Li Fei-Fei. ImageNet Large Scale Visual Recognition Challenge. *International Journal of Computer Vision (IJCV)*, 115(3):211–252, 2015.
- [13] Bruno Siciliano and Oussama Khatib. *Springer Handbook of Robotics*. Springer-Verlag, Berlin, Heidelberg, 2007.